ABSTRACT

Title of thesis: ANALYSIS OF THE EFFECTS OF NON-SUPINE SLEEPING POSITIONS ON THE STRESS, STRAIN, DEFORMATION AND INTRAOCULAR PRESSURE OF THE HUMAN EYE

Peter A. Volpe, Master of Science, 2014

Thesis directed by: Dr. Alison B. Flatau
Department of Aerospace Engineering

This thesis presents analytical models, finite element models and experimental data to investigate the response of the human eye to loads that can be experienced when in a non-supine sleeping position. The hypothesis being investigated is that non-supine sleeping positions can lead to stress, strain and deformation of the eye as well as changes in intraocular pressure (IOP) that may exacerbate vision loss in individuals who have glaucoma. To investigate the quasi-static changes in stress and internal pressure, a Fluid-Structure Interaction simulation was performed on an axisymmetrical model of an eye. Common Aerospace Engineering methods for analyzing pressure vessels and hyperelastic structural walls are applied to developing a suitable model. The quasi-static pressure increase was used in an iterative code to analyze changes in IOP over time.

ANALYSIS OF THE EFFECTS OF NON-SUPINE SLEEPING POSITIONS ON THE STRESS, STRAIN, DEFORMATION AND INTRAOCULAR PRESSURE OF THE HUMAN EYE

by

Peter A. Volpe

Thesis submitted to the Faculty of the Graduate School of the
University of Maryland, College Park in partial fulfillment
of the requirements for the degree of
Master of Science
2014

Advisory Committee:
Professor Alison B. Flatau, Chair
Dr. Mary L. Bowden
Professor Sung W. Lee

Acknowledgments

Much thanks to the National Science Foundation for providing the funding to conduct this research (Proposal #: 1337502), specifically program manager Ted A. Conway. I would like to thank all of those at the University of Maryland, College Park with providing me with the opportunity and means to conduct this research. Specifically I would like to thank my advisor Dr. Alison Flatau for her support and guidance through this project as well as my thesis committee members Dr. S.W. Lee and Dr. Mary Bowden for their input and guidance. I would like to acknowledge and give thanks to Dr. Harry Quigley, MD and his team at Johns Hopkins Medical Center for their insight and collaboration. I appreciated all of the assistance from the COMSOL Multiphysics support team whom offered helpful advice for successful simulations, specifically Dr. Supratik Datta. I must also thank those in the University of Maryland AeroSmart research group and the Aerospace Engineering department. Their support has meant very much to me throughout the project. Finally, I would like to thank my friends and family for their continued love and support throughout my journey.

Table of Contents

List of Tables

List of Figures

List of Abbreviations

F_{out}	Total Aqueous Humor Outflow Rate
F_{uveo}	Uveo-scleral Aqueous Humor Outflow Rate
C_t	Aqueous Humor Flow Facility through the Trabecular Meshwork
β	Fiber angle
λ	Principle Stretch
I_i	Principle Invariant
Ψ	Strain Energy Density Function
Ψ_{iso}	Isotropic Strain Energy Density Function
Ψ_{aniso}	Anisotropic Strain Energy Density Function
E	Green-Lagrange Strain Tensor
C	Right Cauchy-Green Tensor
J	Determinant of the Deformation Gradient Tensor
K	Friedenwald's Coefficient of Ocular Rigidity
R	Electrical Resistance
ρ	Material Resistivity
IOP	Intra-ocular Pressure
IVP	Intra-venous Pressure
FSI	Fluid Structure Interaction
FEA	Finite Element Analysis

Chapter 1: **Introduction**

1.1 Complex Pressure Vessels

The field of aerospace engineering is filled with numerous examples of pressure vessels. Many aerospace structures experience both internal and external loads paired with complicated fluid flow conditions. These various factors provide for complex systems with both discrete and distributed loads applied with a wide range of magnitudes and combinations. Studying the variations of forces on a structure is important for understanding the applications and limitations of every aerospace structure.

An aircraft fuselage is pressurized at high altitudes to maintain a comfortable atmosphere for passengers. Pressurization systems utilize forced air inflow to keep the interior at an appropriate pressure. This system constantly changes the pressurization for various phases of flight and aircraft altitudes. At the same time, this pressure vessel must withstand external distributed and discrete loads stemming from airflow, wind gusts, wing loading, and general dynamic events. These simultaneous loads cause constant changes to the stress and strain state in the fuselage. The combination of fluctuating internal pressure loads and dynamic external loads makes an aircraft fuselage a complex pressure vessel.

Another aerospace engineering pressure vessel would be an aeronautical balloon. High altitude weather balloons must be pressurized with low density fluid in order to achieve lift. Such a balloon experiences internal pressure associated with the fluid needed to cause buoyant forces greater than the forces of gravity acting on the system. The pressure within the balloon and forces on the walls of the balloon will vary depending on altitude and other external forces such as wind related effects. Understanding the effects of the changing internal pressures and the different external forces on the structure of the balloon are important for characterizing its capabilities.

A very well known example of a pressure vessel is the famous International Space Station, or ISS. The ISS is a massive structure that is inhabited by up to six astronauts for many months at a time. Creating a habitable environment in the harsh elements of space requires adequate circulation and pressurization of the air inside. The nearly 30,000 cubic feet of air inside of the ISS must be pressurized to atmospheric levels of 14.7 psi and maintained there while also having proper filtration and circulation. The lack of external pressure and frequent thermal cycling associated with near earth orbit means the ISS structure is always highly stressed. Proper analysis of the ISS as a complex pressure vessel is needed to ensure that these loads never lead to catastrophic failures.

The case of a complex pressure vessel under extreme loads is that of a submarine. Similar to the ISS, a submarine has to maintain habitable conditions in very harsh environments. This requires maintaining an internal pressure of 14.7 psi with proper air filtration and circulation. However, unlike the ISS an underwater

submarine has to withstand tremendous external forces associated with the hydrostatic pressure. The average depth of the ocean floor is roughly 14,000 feet at which the external pressure is over 400 times standard atmospheric pressure. Being able to withstand these external forces without affecting the internal conditions is vital for proper function of a submarine. This represents yet another complex pressure vessel with potential for life threatening catastrophe.

There are many similar dynamic pressure vessel systems that naturally occur in the world, but one particularly important and not fully understood system is the human eye. Similar to aerospace structures, an eye must maintain a particular internal pressure for its specific functions. In the case of airplanes, submarines and the ISS, the inflow of air must be regulated to control the internal pressure relative to the external pressure conditions. This is similar to the eye since to keep the correct distance between the lens at the front of the eye and the retinal wall at the back of the eye, internal pressure must be regulated in response to various internal and external changes. The rubber material in high altitude weather balloons has a particular response to the variety of forces, which relates to an eye in the sense that ocular wall structures consist of similarly behaving non-linear material. Studying the way an eye is impacted by changes in internal and external conditions can be related back to several aerospace structural applications.

Within the eye the regulation of the internal pressure is very important for maintaining the proper health and function. Eyes are naturally pressurized fluid filled vessels that circulate fluid to regulate pressure and nourish the internal components. This internal fluid pressure is linked directly to the stress and strain in the

ocular walls. As the fluid volume in the eye increases, the ocular walls stretch and become increasingly stressed. The stress in the walls applies a force on the external boundaries of the fluid region inside causing an increase in fluid pressure. This is the case for any thin walled spherical pressure vessels which follows the relationship seen in Equation 1.1 where σ is the stress in the wall, p is the internal pressure, R is the radius and t is the wall thickness. Any changes to the pressure inside of the eye will always accompany changes in wall stress.

$$\sigma = \frac{p \cdot R}{2 \cdot t} \tag{1.1}$$

1.2 The Eye as a Pressure Vessel

This thesis focuses on an analysis of the eye as a pressure vessel under varying external load states. The intraocular pressure, IOP, that is normally present within the eye, is primarily caused by the resistance to fluid outflow. Ocular fluid enters and inflates the eye until the internal fluid pressure is great enough to overcome the outflow resistance. When the rates of inflow and outflow of ocular fluid are equal, the eye has reached a steady-state IOP which is typically about 15 mmHg (0.29 psi) for a healthy eye (with a normal range of 10 to 21 mmHg (0.19 to 0.4 psi) between individuals). This pressurization is important for maintaining the structure and shape of the eye. An internal pressure keeps the eye inflated and the shape roughly constant allowing for proper visual focal lengths to be maintained, thus ensuring the

clearest possible vision [2]. In a normally functioning eye the rate of fluid outflow is regulated to maintain a healthy IOP level.

When an eye loses the ability to properly regulate the internal pressure, potentially dangerous conditions may develop. Glaucoma is a disease that is associated with progressive vision loss due to damage to ocular nerves. This disease is directly responsible for much of the vision loss throughout the world [3]. Specific light-sensing nerve cells known as ganglion cells transmit visual information from the retina to the optic nerve connected to the brain. These ganglion cells pass through the walls of the eye on their way to the optic nerve. The stress in the ocular wall due to the IOP applies transverse stress to the ganglion cells as they pass through the wall. In individuals with glaucoma, this stress is great enough to cause damage to these cells. When IOP remains at detrimental levels, more ganglion cells are damaged and vision is gradually lost. Therefore it is in the best interest of individuals with glaucoma to take measures to keep IOP as low as possible while maintaining the ability to focus.

The initial inspiration for this study came from observations by an individual who has glaucoma. In order to reshape the cornea and improve daily vision the individual regularly used Orthokeratology, or Ortho-K, contact lenses while sleeping. Following nights spent sleeping on their right side, i.e. in a non-supine position, it was noticed that significant Ortho-K lens misfit issues in their right eye developed over night. This misfit development suggested that ocular deformation occurs during non-supine sleeping positions. It also happens that this individual has asymmetric glaucoma damage primarily in their right eye. Upon discovery of the correlation

between deformation induced Ortho-K lens misfit issues and glaucoma-related vision loss, the individual hypothesized that spending the night in a non-supine sleeping position can aggravate the conditions that cause glaucoma. Since one would want to mitigate the number of harmful factors that might contribute to glaucoma damage, it is important that the possibility of non-supine sleeping positions contributing to damage be investigated thoroughly.

The function of this research is to investigate the effects of non-supine sleeping positions on IOP as well as stress, strain and deformation of the eye. Every person has their own opinion on what sleeping positions are the most comfortable. It is not uncommon for people to spend a portion of their time sleeping in a non-supine position. Non-supine sleeping positions are positions of being on one's side or stomach and they often result in the face being partially compressed into a pillow or mattress. When someone is in a non-supine position, the weight of their head results in a pressure to both the pillow and the face of the individual. The weight of a typical human head is roughly 10 lbs and a single side of a typical adult human head that might be in contact with a pillow would be roughly 8 inches by 6.5 inches with an area of roughly 52 square inches. This means that the weight of an individual's head would cause a pressure of 9.93 mmHg (0.192 psi) across the side of their face in contact with the sleeping surface. A human face has various protrusions and cavities that would cause a variation in applied pressure, however it is reasonable to assume that all regions of the face experience a pressure of roughly 10.3 mmHg (0.2 psi) while someone is in a non-supine sleeping position (the compliance of the pillow will also help distribute the load evenly). The goal of this research is to investigate

the impact of this load on the IOP and the stress, strain and deformation of the eye in contact with a pillow and the potential impact on glaucoma related damage.

The possible reasons for what would cause an increase to the IOP of an individual in a non-supine sleeping position must be determined. The primary reason is due to the physical external load that is being applied to a fluid filled object. When a fluid filled structure such as the eye has an external load applied to it, there is an increase in the internal pressure of the fluid. The amount in which the pressure increases is dependent on the amount of pressure applied and the make up of the structure itself.

An increase in the IOP during non-supine sleeping positions may also be due to an increase in the intravenous pressure, IVP, in the blood vessels in and around the eye. It is entirely possible that the IVP may also increase when a load is applied to the entire region of the face and eye since a blood vessel is also a fluid filled structure. In order for the eye to receive the proper nutrients, the ocular fluid known as aqueous humor, located mostly in the anterior chamber of the eye, must be circulated over time. The aqueous humor has a constant inflow rate and a variable outflow rate that is a function of the current IOP inside of the eye among other factors [4]. Of these other factors affecting the outflow rate is the current IVP. Depending on the level of IVP change, a variety of IOP responses can occur. Since the outflow regulatory system depends on the pressure gradient between the current IOP and IVP values, the change in one relative to the other dictates the response of the outflow rate and will alter the aqueous humor equilibrium and steady-state IOP.

Lastly, an increase in the IOP during non-supine sleeping positions could also be associated with a decrease in the fluid outflow capacity of the eye. One of the factors affecting the outflow rate of the aqueous humor is the flow facility out of the physical fluid outlets. Loading the eye will cause some level of deformation which can disrupt the amount of fluid able to exit the eye. Once again, a change in outflow rate will affect the aqueous humor equilibrium and result in a change to the steady-state IOP. This study aims to investigate the impact of these phenomena on the response of the human eye during a situation of external loading.

1.3 Investigation

Originally the goal was to build a single simulation that would investigate the quasi-static increase in IOP and the transient IOP response due to the loading associated with non-supine sleeping positions all at once. Due to difficulties integrating the analytical relationships into a single simulation, it was decided to investigate the quasi-static increase in IOP in a different manner than the transient changes to IOP. The simulations for this research were divided into two main stages: COMSOL Multiphysics Fluid-Structure Interaction (also known as FSI) simulations and MATLAB iterative codes.

The COMSOL Multiphysics software was used to investigate how much an external load would increase the IOP alone without yet considering the effects of the fluid exchange across the boundaries of the eye. The information gained from this FSI simulation was then used in a MATLAB code to simulate the change in

IOP over time as a result of the fluid exchange. This code uses various known pressure volume relationships to link the changes in IOP to the changes in ocular fluid volume. The changes to ocular fluid volume can be determined using the current aqueous humor inflow and outflow rates. The whole process is iterated to build a time dependent model of how the IOP changes over time. These two simulations build the base for the model of how the eye reacts to a sudden external loading. Additional simulations were conducted in order to investigate the likelihood of deformation based changes in IOP. In the end, a comprehensive picture of how the eye would respond to different scenarios will be built.

In addition to the investigation into the mechanics using computer simulations, an experimental procedure aimed at studying this phenomena was conducted in collaboration with physicians at Johns Hopkins Medical Center in Baltimore, Maryland. Currently in the world of ophthalmology, the standard methods for measuring IOP all require contact with the patient's eye by a technician with an instrument. In the investigation here, the patient's eye of interest is nestled into a pillow to simulate a non-supine sleep position which makes it impossible to measure the IOP using any of the standard methods. Therefore, a new approach is needed. This approach requires the use of a new technology known as the SENSIMED Triggerfish® contact lens. This lens utilizes a set of strain gauges to measure the changes in strain on the surface of the eye. This strain is caused by changes in ocular volume and there is a direct link between this change in ocular volume and the change in the IOP. Therefore, this Triggerfish contact lens provides a method of inferring changes in IOP in a non-invasive manner. Patients both with and without glaucoma will have these

Triggerfish lenses placed on their eye and will go through a simulated sleep study under the supervision of physicians at Johns Hopkins Medical Center. This simulated sleep study procedure includes periods of both supine and non-supine sleeping positions. These results will help form a picture of what is happening inside of an actual patient's eye.

By combining the theoretical modeling with the results of the simulated sleep study, the goal is to build a picture of what is occurring when an external load associated with non-supine sleeping is applied to the eye and to understand the associated risks. Furthering the understanding of the implications of sleeping in non-supine positions will greatly help in developing mitigation techniques to avoid further potential damage.

1.4 Organization of Thesis

The focus on this project was to develop a finite element model that would properly simulate the changes in pressure vessel stress, strain, internal pressure and deformation under localized external loads. To develop this model a review of the structure and fluid properties of the eye as a pressure vessel is presented in Chapter 2. Chapter 3 describes the experimental procedures that were conducted to estimate typical loads in a non-supine sleeping position, as well as an experiment designed to simulate a real-world fluid filled pressure vessel with localized loading. Chapter 4 discusses the FSI modeling to investigate the quasi-static change in fluid pressure and stress, strain and deformation of the eye under external loading. Chapter 5

discusses the utilization of the findings from the FSI model to build a time dependent picture of the fluid pressure of the eye in various scenarios. Chapter 6 introduces the findings of the simulated sleep study and offers a comparison with the results of the modeling. Chapters 7 and 8 feature a summarizing discussion as well as future directions for similar research. And finally, the appendices contain additional information on the Triggerfish technology as well as an in-depth discussion of the modeling procedures.

Chapter 2: **Literature Review**

The first step of the investigation is to gain an understanding of the human eye itself. This starts with the basic ideas behind how the eye works. Objects in the world reflect light off of their surface that is scattered into various directions upon reflection. Some of the reflected light rays have a trajectory towards an individual's eye. These light rays enter the cornea of the eye and pass through the aqueous humor, optical lens and vitreous humor until they reach the retina which contains light-sensing nerve cells. By adjusting the size of the pupil (the hole in the center of the iris) and the shape and position of the lens, the light can be properly focused [5]. The retina converts the incoming light rays into nerve signals to be transmitted to the brain. While this is a vastly simplified description, it is a basic overview of how the eye allows for sight.

2.1 **The Structure of the Eye**

2.1.1 Structural Components and Dimensions of the Human Eye

Before any discussion of the complex functions of the eye can begin, it is important to fully understand the components and dimensions that make up a

typical human eye. The majority of this knowledge was acquired from *Eugene Wolff's Anatomy of the eye and Orbit* [6]. Starting from the exterior and working inwards, the eye sits in what is known as an orbit. The orbit is a rounded cavity in the anterior portion of the human skull. Inside of this orbit are six individual muscles that stabilize and redirect the eyes line of sight. These muscles are: the medial and lateral rectus (which control movement about the transverse axis), the superior and inferior rectus (which control movement about the vertical axis) and the superior and inferior oblique (which control movement about the line of sight axis, and prevent the eye from retracting into the rear of the orbit) [6]. This set of ocular muscles keeps the eye in the correct location and allows for all of the ocular movements necessary for efficient sight.

The next component is the wall of the eye itself. This set of outer layers encapsulates all of the ocular components and provides the primary structure for the eye. This outer wall can be split up into three major regions which can be seen as part of Figure 2.1. The first being the cornea, which is located in the extreme anterior portion of the globe. It has a smaller radius of curvature then the rest of the globe and therefore it appears as a bump off the front of the eye. Upon microscopic inspection it includes layers such as the epithelium, Bowman's Membrane, Stroma, Descemet's Membrane and Endothelium [6]. However, the ocular model used in this research will consider all of the layers as one. The next major region is the limbus. This region is essentially a transition zone between the cornea and the third major region of the ocular wall, the sclera. Upon inspection, and as seen in Figure 2.1, the posterior portion of the globe is actually made up a several layers. These layers

include the retina, choroid and sclera. However, since this research only needs to replicate the structural characteristics of the ocular wall, this will also be considered as one single layer. These three regions make up the ocular wall of the human eye.

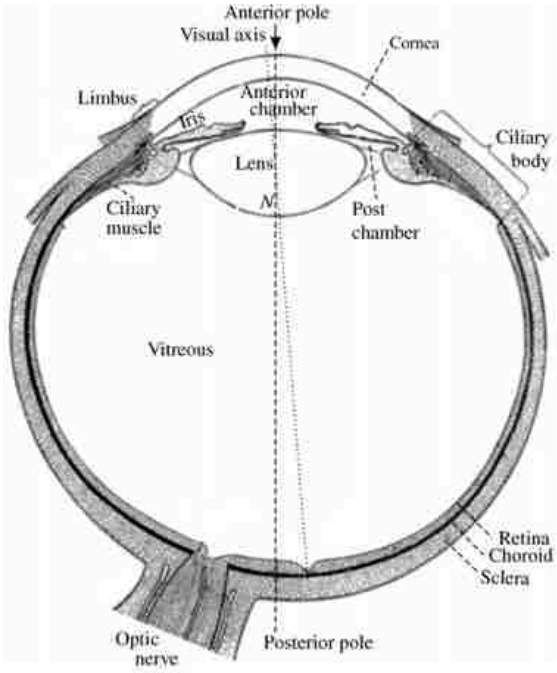

Figure 2.1: *Components of the Human Eye (Image from References [6] and [7])*

The remaining components of the eye are not as vital to the simulation because they do not add an appreciable amount of support when compared to the outer walls. These components include the ciliary body, iris, lens and the ciliary zonules. These components form a barrier across the eye that provides some lateral stiffness which helps prevent the eye from flattening. The barrier is also important because it divides the eye into two regions that contain different fluids. The anterior chamber and the anterior portion of the posterior chamber contain the aqueous humor which delivers nutrients to the surrounding components. This fluid is secreted out of the ciliary

body near the ciliary zonules, and flows past the ocular lens and around the iris until it reaches the trabecular meshwork and Schlemm's canal in the region between the base of the iris and the limbus where it then exits the eye into the episcleral veins. The remaining portion of the posterior chamber contains the vitreous humor which is a gel-like substance meant to help maintain the overall shape of the eye while allowing for the light rays to still reach the retina.

In order to build an accurate model, it is important to know the relative dimensions of these components to one another. In the real world the eye is not quite a true sphere, however it is very close. For a typical human eye, the anteroposterior diameter of the globe is 24 mm, the vertical diameter is 23 mm and the horizontal diameter is 23.5 mm [6]. The exterior boundary of the sclera (which makes up the majority of the globe) can be considered as an ellipse with an anteroposterial radius of 12 mm and a lateral radius of 11.75 mm. The thickest point of the sclera is 1 mm thick located at the extreme posterior wall and the thinnest is 0.55 mm thick located at the extreme lateral wall. The most anterior portion of the sclera has a thickness of 0.8 mm just before transitioning into the limbus [8]. The limbus acts as a smooth transition zone between the different properties and dimensions of the cornea and sclera. The cornea is located on the anterior portion of this globe connected to the anterior portion of the sclera via the limbus. The exterior boundary of the cornea has a radius of curvature of 7.8 mm with a center point located 5 mm anterior to the center of the globe [9]. The portion of the cornea directly adjacent to the limbus has a thickness of 0.66 mm and the anterior most portion of the cornea has a thickess of 0.52 mm, as seen in Figure 2.2.

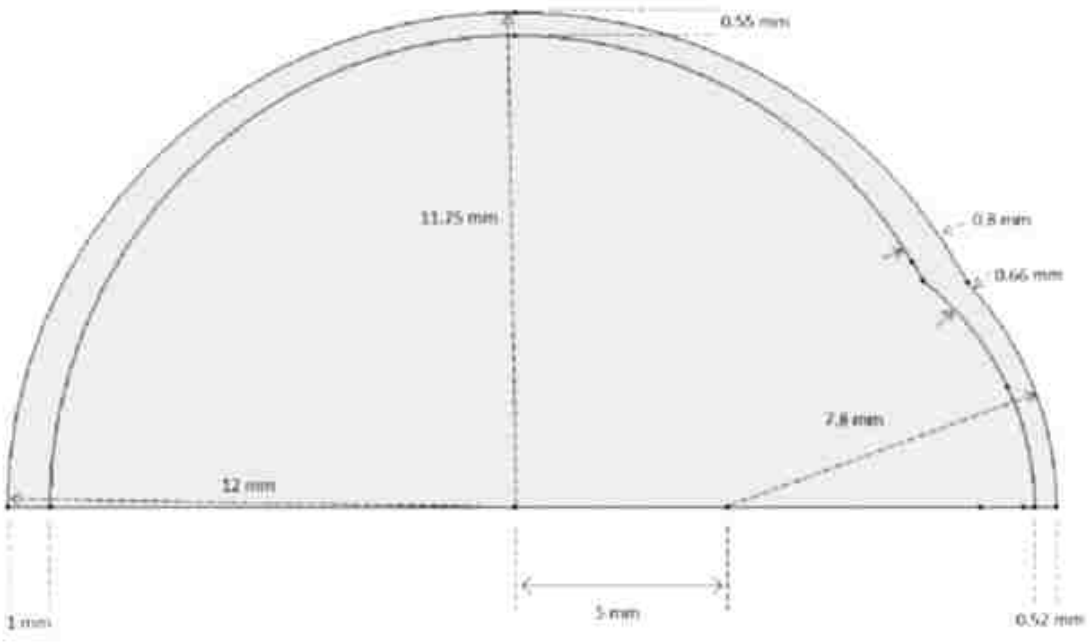

Figure 2.2: *Dimensions of the Corneo-Scleral Shell*

Inside the eye, there is the lens, iris, ciliary body and zonules. The anterior surface of the lens has a curvature of about 10 mm and the posterior surface has a radius of curvature of about 6 mm. The center of the anterior surface is located about 3 mm behind the back of the cornea [6]. The iris and ciliary body are fundamentally connected. The purpose of the ciliary body is to act as a connecting base for the lens as well as a portal for aqueous humor to enter the eye. The purpose of the iris is to control the amount of light that penetrates into the lens from the anterior chamber. The pupil is the circular opening created by the iris to control the light penetration. In a typical human, the pupil has a diameter of 5 to 8 mm [10] and it will vary depending on lighting conditions. Finally, the lens and the ciliary body are connected by what are called ciliary zonules. These fiber-like objects act as a

barrier between the two fluid regions of the eye and hold the ocular lens in place. The ciliary body will use the ciliary zonuales to re-position and reshape the lens to focus incoming light rays. All of these components can be seen in Figure 2.3.

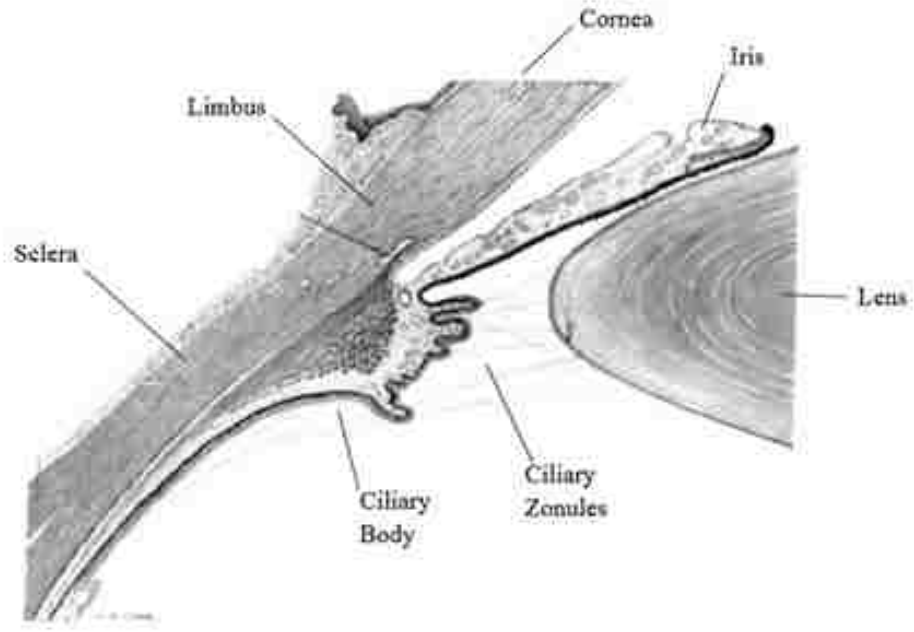

Figure 2.3: *The limbic region of the eye (Images from Reference [6])*

2.1.2 Flow Characteristics

Now the understanding of the physical components and geometry that make up the eye must be combined with their functions with respect to the problem at hand. The eye contains two different fluids within its borders. The aqueous humor is circulated from the anterior portion of the posterior chamber and into the anterior chamber of the eye (the region next to and in front of the lens, up until the back of the cornea). The vitreous humor is located in the remaining portion of the posterior

chamber of the eye (the region behind the lens and ciliary zonules). Both fluids are there to provide ocular rigidity as well as nourish the various components inside the eye. Empirical formulas must be determined to describe the flow of the aqueous humor into and out of the eye. From the text *Adler's Physiology of the Eye* [4], equations and constants can be assigned to the flow characteristics.

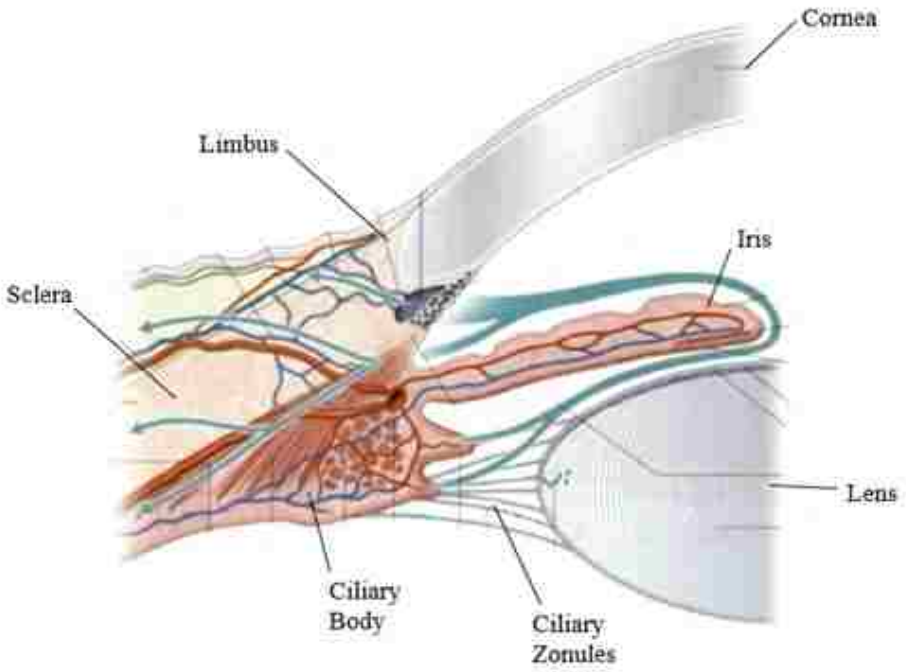

Figure 2.4: *Aqueous humor flow through the anterior chamber (Image from Reference [4])*

The aqueous humor, which provides nutrients to the lens and cornea, is produced in the region of the ciliary body known as the ciliary process. From there, the aqueous humor flows in front of the lens and into the anterior portion of the anterior chamber. After flowing around the iris, the fluid travels towards the trabecular meshwork and out through the Schlemm's canal which are located in the limbus

region of the outer wall. This flow path can be seen in Figure 2.4. In a normal, healthy human eye, the IOP reaches a steady-state value around 15 mmHg. This steady-state value is reached when the pressure inside of the eye is at a sufficient level to overcome outflow impedance and force fluid out of the eye at the same rate in which it is entering the eye from the ciliary body.

The rate in which aqueous humor is entering a normal human eye is roughly 2.5 μL per minute. Three distinct processes contribute to the production and inflow of the aqueous humor: diffusion, ultrafiltration and active secretion. The diffusion occurs internally between the stages of aqueous humor production. The ultrafiltration and active secretion are responsible for transferring the aqueous humor from reservoirs inside the ciliary body into the fluid chambers. Under a relatively normal range of conditions, the active secretion consists of 80-90% of the aqueous humor inflow and is considered to be pressure independent in this range. On the other hand, the ultrafiltration component will decrease with increasing IOP. However, this change in inflow has a very small effect on the total inflow. In fact, it is noted that any decrease in the inflow rate will simply appear as an increase in the outflow rate for all intents and purposes (and is hence known as pseudofacility of inflow) [4]. Therefore the aqueous humor inflow rate is considered as independent of the IOP and can be assumed as constant under the range of conditions that are being studied here. This means that the eye will reach steady state when the outflow rate matches 2.5 μL per minute. The dynamic properties of the aqueous humor outflow can be reasonably approximated using the empirical relationship given in Equation 2.1.

$$F_{out} = C_t(IOP - IVP) + F_{uveo} \tag{2.1}$$

Equation 2.1 characterizes the outflow rate of the aqueous humor out of the anterior chamber of the eye [4]. The trabecular meshwork outflow facility, C_t, represents the ease in which the flow can exit through the trabecular meshwork. The uveo-scleral outflow rate, F_{uveo}, makes up the second half of the outflow equation and it is independent of IOP changes in the range of values that are experienced in this research. Therefore, the rate of outflow of aqueous humor is dependent on the values of the flow facility, intra-ocular pressure and the intravenous pressure. The eye will continue to be in a transient phase until the conditions allow for the inflow and outflow rates to reach equilibrium.

On the other hand, the vitreous humor circulates via diffusion through the posterior ocular walls. This diffusion does not have any variation as a function of IOP. The main purpose of the vitreous humor is to act as a transparent medium that gives rigidity to the eye. Therefore the vitreous humor flow is not a factor in an investigation into the effects of non-supine sleeping positions on IOP [4].

2.2 Material Properties and Flow Characterization

For more specific information on details of the function and theory behind the eye, several key papers are highlighted and discussed in this section.

2.2.1 Hyperelastic Model for Arterial Wall

In recent years, it has been found that a hyperelastic (also known as Green-elastic [11]) material theory has many advantages for modeling of biological tissue. The advantage of characterizing a material as hyperelastic is that one needs only define a strain energy density function for that material in order to determine the stress-strain relationship. Many materials do not follow the behavior of ordinary linear elastic material so their material properties can not be categorized in the same way. Using the strain energy density function can allow for these non-linear materials to be appropriately modeled. In the case of a hyperelastic material, the stress can be determined by utilizing Equation 2.2. This equation states that the strain energy density function, $\Psi(\lambda)$, is a function of the principal stretches of the material, λ_i.

$$Stress = S(\lambda) = \frac{\delta \Psi(\lambda)}{\delta \lambda} \tag{2.2}$$

The work done by Dr. Gerhard Holzapfel beginning with his paper in 1997, *Biomechanical behavior of the arterial wall and its numerical characterization* [12], discusses how the walls of an artery can be appropriately modeled as a biphasic hyperelastic material. This work was based off of previous work done by Y.C. Fung in 1979 [13]. In the case of an artery, the walls are composed to two distinct layers, the media and the adventitia. Both of these layers consist of two phases, the isotropic media and an-isotropic fibers. The isotropic portion of each layer can be modeled using existing hyperelastic material theory, in this case a Neo-Hookean

material. However, a new strain energy density function must be determined for the an-isotropic fiber portion of the composite. The following was proposed:

$$\psi = \psi_{iso} + \psi_{aniso} \tag{2.3}$$

with

$$\psi_{iso} = c_1(I_C - 3) \text{ and } \psi_{aniso} = c_2(\exp(Q) - 3) \tag{2.4}$$

where c_1 and c_2 are material constants, I_C is the first principle invariant of the right Cauchy-Green tensor, and Q represents a quadratic function of the Green-Lagrange strain tensor such as seen in Equation 2.5.

$$Q = a_1 E_1^2 + a_2 E_2^2 + 2a_4 E_1 E_2 \tag{2.5}$$

where a_1 and a_2 are dependent on the fiber directions [12, 13]. In subsequent years this material definition was refined to a form requiring only material properties and principle invariants [14]. The new form of the strain energy density functions can be seen as Equations 2.6 and 2.7.

$$\bar{\psi}_{iso}(\bar{I}_1) = \frac{c}{2}(\bar{I}_1 - 3) \tag{2.6}$$

$$\bar{\psi}_{aniso}(\bar{I}_4, \bar{I}_6) = \frac{k_1}{2k_2} \sum_{i=4,6} \left\{ \exp[k_2(\bar{I}_i - 1)^2] - 1 \right\} \tag{2.7}$$

Equation 2.6 defines the strain energy density for the isotropic portion of each layer and it is represented here as a Neo-Hookean hyperelastic material. Variable

c represents a stress-like material parameter and variable $\bar{I}_1$ is the first principle invariant of the right Cauchy-Green tensor, which is a function of the principles stretches, λ_i. Equation 2.7 defines the an-isotropic portion of each layer and it represents the strain energy stored in the collagen fibers of the artery. Variable k_1 is a stress-like parameter and variable k_2 is a dimensionless parameter that must be determined from known data. Variables $\bar{I}_4$ and $\bar{I}_6$ are additional invariants that describe the fibers of the media and adventitia layers of the artery. These invariants are defined using Equations 2.8 to 2.11.

$$\bar{I}_{4j} = A_{1j} : \bar{C} \text{ and } \bar{I}_{6j} = A_{2j} : \bar{C} \tag{2.8}$$

for which

$$A_{1j} = a_{01j} \otimes a_{01j} \text{ and } A_{2j} = a_{02j} \otimes a_{02j} \tag{2.9}$$

where

$$[a_{01j}] = [0, \cos(\beta_j), \sin(\beta_j)]^T \tag{2.10}$$

$$[a_{02j}] = [0, \cos(\beta_j), -\sin(\beta_j)]^T \tag{2.11}$$

where $j = M, A$ for media or adventitia, respectively. Variable β_j is the angle between the fibers for that layer. Equations 2.6 and 2.7 are now fully defined and can be used to characterize the material model for a human artery. Now this model

needs to be adapted to fit the properties of the human eye, which behaves in a very similar manner.

2.2.2 Adaptation to Ocular Wall

Several researchers have undertaken the task of attempting to characterize the walls of the human eye based on the strain energy density function introduced for a human artery. The material definition used in this work is introduced in Lanchares et al. [1] which combines with ideas from several papers into a unified set of equations and parameters to model the eye. The work is based off of the ideas proposed by Alastrué et al. [15] and is similar to the work done by Pandolfi et al. [16]. The definition proposed by Alastrué et al. starts off by defining the overall free energy equation form as follows:

$$\psi(C) = \psi_{vol}(J) + \bar{\psi}(\bar{C}, M, N) \tag{2.12}$$

where the term $\psi_{vol}(J)$ describes the energy associated with the volumetric response and the term $\bar{\psi}(\bar{C}, M, N)$ describes the energy associated with the isochoric response. The volumetric strain energy density function used in this model was introduced by Gardiner et al. [17]. Gardiner et al. discussed modeling of human medial collateral ligaments which share properties with the eye. The proposed volumetric strain energy density function can be seen as Equation 2.13.

$$\psi_{vol} = \frac{1}{D}(\ln J)^2 \tag{2.13}$$

where $1/D$ is a penalty coefficient related to the bulk modulus and J is the determinant of the deformation gradient tensor, F. The isochoric portion of the material definition is described using the definitions introduced by Pandolfi et al. [16] and Holzapfel [14]. This definition of the ocular wall models the isotropic-isochoric matrix portion as a Mooney-Rivlin material [11] and the anisotropic-isochoric fiber portion as previously defined in Equation 2.7. This results in an isochoric strain energy density function as seen in Equation 2.14.

$$\begin{aligned}\psi_{isochoric} =& \frac{C_1}{2}(\bar{I}_1 - 3) + \frac{C_2}{2}(\bar{I}_2 - 3) \\ &+ \frac{k_1}{2k_2}\left\{\exp[k_2(\bar{I}_4 - 1)^2] - 1\right\} + \frac{k_3}{2k_4}\left\{\exp[k_4(\bar{I}_6 - 1)^2] - 1\right\}\end{aligned} \tag{2.14}$$

where C_1 and C_2 are material properties of the matrix and k_1, k_2, k_3, and k_4 are material properties of the fibers. In order to determine the values of the constants that fit this material definition, non-linear regression method was performed on experimental stress-strain data of the cornea that was gathered by Hoeltzel et al. [18]. The material properties of the sclera were iteratively adjusted to fit data presented by Buzzard [19]. The resulting properties as presented in Lanchares et al. [1] are shown in Table 2.1.

Table 2.1: Material Properties of the Eye Wall [1]

Material	$C_1(MPa)$	$D(MPa^-1)$	$C_2(MPa)$	$k_1(MPa)$	k_2	$k_3(MPa)$	k_4
Cornea	0.1	1e-5	0.0	0.234	29.917	0.234	29.917
Limbus	0.1	1e-5	0.0	0.234	29.917	0	0
Sclera	35	1e-5	-32	0	0	0	0

This set of coefficients considers the cornea to have two sets of fibers (oriented in different directions), the limbus to have one set of fibers and the sclera to consist of only matrix material. The ocular walls can be accurately modeled using this material definition as laid out in Lanchares et al. [1].

2.2.3 Pressure vs. Volume relationship

The next important subject to review is the pressure versus volume relationship within the eye. In order to link instantaneous pressure events (such as a sudden loading) to the transient response, it is important to understand this particular relationship. A paper written by Van der Werff et al. [20] introduces the various pressure volume relationships that have been developed over the years. This section will review and discuss the differences between the various relationships and their impact on the research. All of these relationships correlate the change in ocular fluid volume, ΔV, to the IOP before and after that change in volume, P_1 and P_2 respectively. The first relationship that is introduced in the paper is the relationship developed by Friedenwald and can be seen as Equation 2.15.

$$\Delta V = \frac{1}{K} \log \left(\frac{P_2}{P_1} \right) \tag{2.15}$$

where K is known as Friedenwald's coefficient of ocular rigidity and has a value of 0.0215 $\mu L^{-}1$. While this relationship has been a long lasting standard, some feel it is not completely accurate due to the fact that the coefficient of ocular rigidity , K, appears to decrease as the IOP increases. However, this would not

be of great concern when studying the eye over a limited range of pressures. The next relationship that is discussed in the paper is the McBain's pressure volume relationship. This relationship can be seen as Equation 2.16.

$$\Delta V = a\left[P_2^b - P_1^b\right] \tag{2.16}$$

where the variable a has a value of 29.38 and variable b has a value of 0.356 (all volume units in this section are given in microliters and all pressure units are in millimeters of mercury). The next equation is the Holland et al. equation which can be seen as Equation 2.17.

$$\Delta V = a\left[(P_2 - c)^b - (P_1 - c)^b\right] \tag{2.17}$$

where the variable a has a value of 2.779, variable b has a value of 0.611 and variable c has a value of 10.71. The next three relationships all have the same form, however they have different coefficient values. The equation form can be seen as Equation 2.18.

$$\Delta V = a \ln\left(\frac{P_2 + b}{P_1 + b}\right) \tag{2.18}$$

For the McEwen et al. equation, the variable a has a value of 45.45 and variable b has a value of 9.55. For the Woo et al. equation, the variable a has a value of 62.5 and variable b has a value of 8.1. And for the Hibbard et al. equation, the variable a has a value of 50.0 and variable b has a value of 12.0. The final pressure versus volume relationship discussed in Van der Werff et al. [20] was the relationship that

was first introduced in this paper, known as the cube root ocular rigidity function. This relationship can be seen as Equation 2.19.

$$\Delta V = a\left(P_2^{\frac{1}{3}} - P_1^{\frac{1}{3}}\right) \tag{2.19}$$

A recreation of Figure 2 from the Van der Werff et al. [20] paper can be seen as Figure 2.5. This plot illustrates the changes in IOP corresponding to changes in fluid volume for the various pressure volume relations presented previously. The Friedenwald and Woo relationships are labeled so that they may be referred to later on.

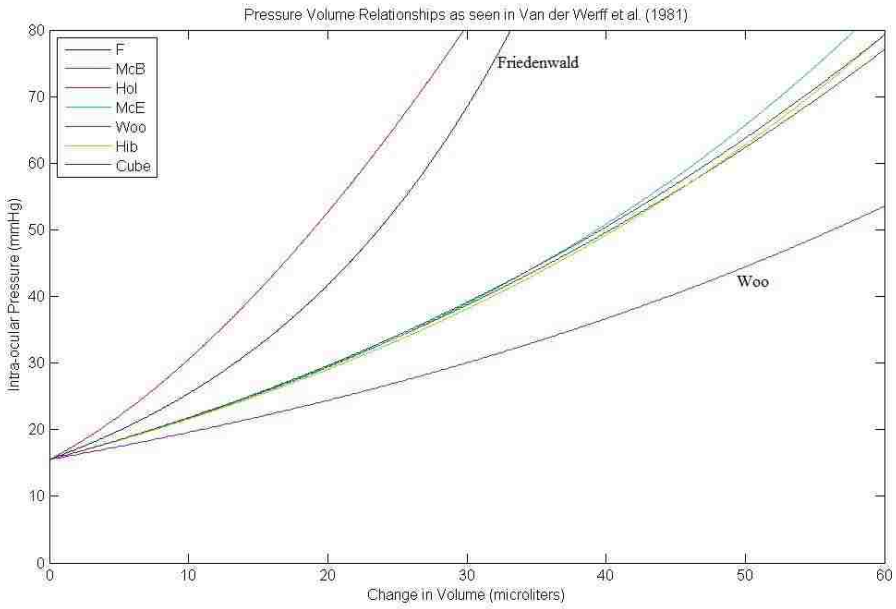

Figure 2.5: *Pressure Volume Relationships from Van der Werff et al. [20]*

The Friedenwald and Holland relationships are the two lines seen above of all of the other relationships in Figure 2.5. For these two cases, a large pressure

difference is associated with a small change in volume and vice versa. The line below all of the other relationships represents the Woo relationship. For the Woo relationship, a small change in pressure is associated with a large change in volume, making it the opposite case of the Friedenwald and Holland relationships. If the goal is to model an eye with a high level of responsiveness to changes in ocular volume, then the Friedenwald or Holland relationships would better represent that and the opposite case for the Woo relationship. The remaining pressure volume relationships correspond to the McBain, McEwen, Hibbard and the cube root formulas. They represent relationships that have average responsiveness to changes in pressure. In Chapter 5, there will be a discussion of which relationship is most appropriate for the modeling done in this research.

2.2.4 Honan Intraocular Pressure Reducer

There is a device known as the Honan intraocular pressure reducer that has a purpose just as its name suggest, to temporarily reduce an individual's IOP. The device consists of a Honan balloon (a semi-rigid, unidirectional inflatable cylinder), a head strap and an inflation pump and gauge connected to the balloon with rubber tubing. The device works by strapping it to the head of the patient so that the balloon is in place over their eye. Air is then pumped into the balloon to apply pressure to the anterior surface of the eyelid. Initially, this loading causes a drastic increase in IOP which triggers the eye's natural pressure regulating system. In order to compensate for the increase in pressure, the eye evacuates fluid at an

increased rate until the pressures drop back down to appropriate levels (utilizing the pressure volume relationships as previously introduced). This is accurately modeled by Equation 2.1. Upon the removal of the device after some time, the IOP instantaneously falls to a significantly lower value in comparison to the steady-state value due to the decrease in overall ocular fluid volume while the Honan balloon was applied (once again due to the pressure volume relationship). For a period of time following the removal of the external load, the IOP is lower than normal allowing for certain surgical procedures to be done. Several similar approaches are employed pre-operatively to lower IOP. This well known mechanism of applying an external pressure to lower IOP lead to significant scepticism over the proposed hypothesis that a sleep position might induce potentially damaging stress, strain and/or IOP levels.

A study of the IOP while the Honan device was applied to eyes and the resulting pressure response following the removal of the device was conducted by Ernest et al. [21]. It was shown that the IOP values in a cadaver eye under Honan device loading ranged from 60 mmHg up to 180 mmHg over the full range of gauge readings (gauge readings range from 5 to 30 mmHg). Normal healthy human IOP values are around 15 mmHg which means that the external load applied by the Honan device causes a great increase to IOP while under load. After the balloon was applied for 30 minutes at a gauge reading of 30, the immediate post-removal IOP had a value of roughly 7 mmHg, much lower than the average IOP of 15 mmHg. Over the course of 20 to 25 minutes, the IOP slowly rose back to steady-state values creating a window of low pressure conditions conducive to certain surgical

procedures [21]. The phenomena experimentally measured by Ernest et al. is highly related to the focus of this research.

2.2.5 Outflow from the Eye

It is also important to understand the structure of the aqueous humor outflow canals. A discussion of these components and their functions as well as computer simulations of the flow of the aqueous humor through the anterior chamber was performed by Villamarin et al. [22]. The aqueous humor is formed in the anterior portion of the posterior chamber by the ciliary body at a rate of 2-3 $\mu L/min$. The fluid flows past the posterior portion of the iris until it passes through the pupil into the anterior chamber. From the anterior chamber, there are two outflow options: 1) through the trabecular meshwork or 2) through the uveoscleral pathway. The trabecular meshwork is a multi-layered lattice structure that provides resistance to flow egress and therefore helps maintain ocular pressure. The uveoscleral outflow consists of the aqueous humor being absorbed via diffusion into the anterior iris and base of the ciliary body. This outflow pathway makes up somewhere between 5-40% of the total aqueous humor outflow depending on age [23]. After exiting the anterior chamber, the aqueous humor passes into the Schlemm's canal and the collecting channels which are linked to the episcleral veins. There are about 25-30 of these outflow channels with a diameter of approximately 120 μm [24]. From here the aqueous humor diffuses into the bloodstream and away from the eye. The flow vectors and approximate geometry can be seen in Figure 2.6 which is part of the

published simulation results by Villamarin et al [22]. The general dynamics of the fluid is dependent on the direction of gravity, as shown by Figure 2.6. However, in both cases, it is easy to see how the fluid is able to circulate nutrients to the boundaries of the anterior chamber and then exit the chamber before being replaced with fresh aqueous humor to keep the eye adequately pressurized and nourished.

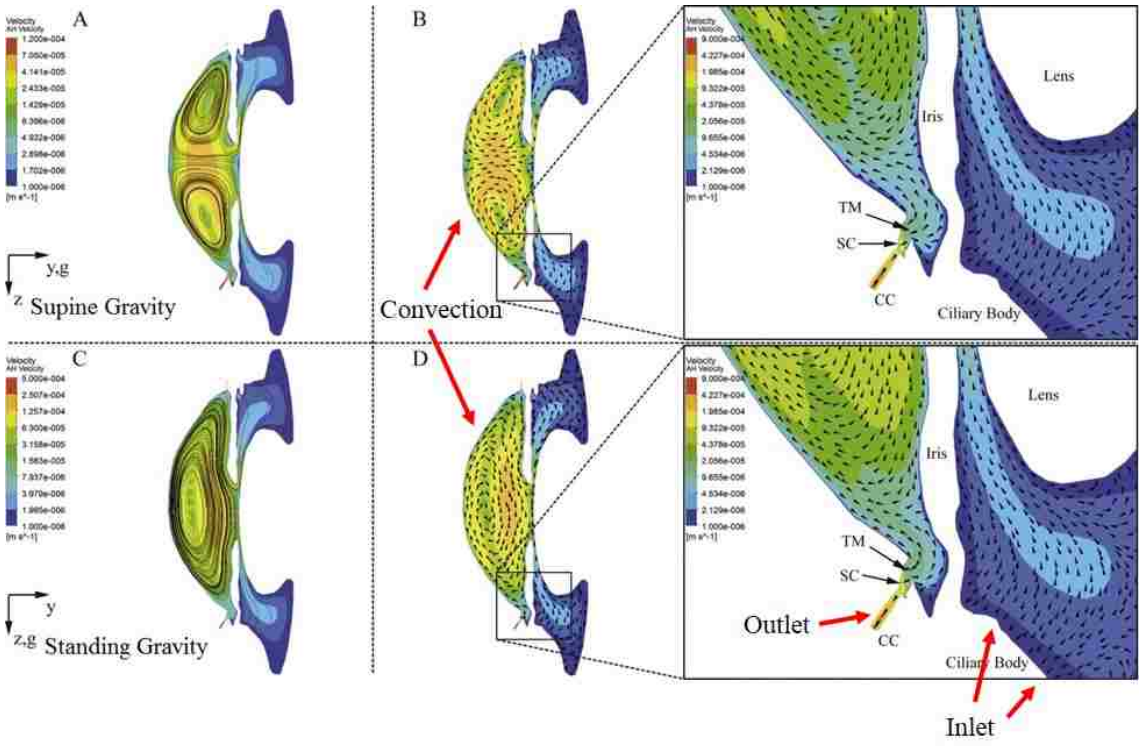

Figure 2.6: *Aqueous humor flow as simulated by Villamarin et al. (Image from Reference [22])*

Chapter 3: **Measurements**

3.1 **Eye Load**

3.1.1 Pressure Device

The hypothesis for this research was developed following initial observations of Ortho-K lens misfits leading to blurry vision after nights spent sleeping partially in non-supine positions. Starting from that hypothesis only, it is important to investigate every single aspect of the problem in order to gain a complete overview of what is occurring. This means that an important first step is to figure out exactly what pressure is applied to the eye when a person is sleeping in a non-supine position. To measure this, a device was built that would be able to measure the pressure between the eye lid of a subject and the sleeping surface that their face is in contact with.

The device consists of a standard 9 inch diameter (when inflated) rubber party balloon that is attached to a tube fitting and rubber hoses connected to a digital air manometer (Dwyer, Series 476A) and a sphygmomanometer bulb pump. The digital manometer had an accuracy of 0.001 psi. The assembled device can be seen in Figure 3.1. Resting a face into a pillow or other sleeping surface will generate

pressure against the portion of the face in contact. If the balloon is placed in between the patients eye and the sleeping surface, this pressure will now be applied to the top and bottom surfaces of the barely inflated balloon which will increase the pressure of the air inside.

Figure 3.1: *Device created to measure the pressure on the eye*

Any changes to the air pressure inside of the balloon will also occur to the air located throughout the tubing. These pressure changes will be picked up by the digital manometer connected to the tubing. The purpose of the sphygmomanometer bulb pump is to provide a means of adjusting the quantity of air inside of the entire system. Inflating the balloon with too much air will artificially increase the pressures felt between the eye and the pillow. Therefore it is important to have a very small amount of air in the balloon, making it as thin as possible.

3.1.2 Procedure

The goal is to capture measurements of the pressures that a person might experience while naturally sleeping. In order to mimic natural sleep, it is important to build an environment that closely resembles one's bed. As a result, a full sized fold-able twin sized bed was purchased for the sole purpose of measuring the load on the eyes while sleeping partially face down. Using a full sized twin bed in combination with several types of pillows allows for a sleeping environment very close to reality for many subjects.

For the gathering of this data, after securing IRB approval, a number of volunteers were gathered to participate in the measurement. Each individual was allowed to choose the pillow most like what they would naturally sleep with. The bed would be set up in a comfortable location with the patient lying in a non-supine position with their face in the pillow as naturally as possible. Beforehand, the sphygmomanometer bulb valve was opened so that all the air can be let out of the balloon. The balloon was then placed under one of the eyes of the patient while the valve was kept in the open position. Once the balloon was comfortably placed, the valve was closed and very small increments of air were pumped into the now closed system until the subject announced that they could just start to feel the added pressure of the balloon. In order to alleviate any added pressure due to the presence of that air, the valve was momentarily opened and then closed, letting out a small volume of air and making the balloon again unnoticed by the subject. Now the system was

entirely closed and it has just enough air to transfer the pressure from the balloon to the manometer without artificially affecting the measurement.

Once the balloon has the proper amount of air inside the closed system, the subject is asked to re-position themselves to a non-supine position that they might naturally sleep in during the night. As they position themselves, the balloon is centered comfortably on their closed eye. After they have settled into the pillow, the steady-state pressure measurement is recorded. The subject is then asked to re-position themselves in any other comfortable non-supine position they might naturally sleep in and the measurement is repeated. The re-positioning and measuring then occurs a third and final time. At this point, three measurements have been gathered for this patient corresponding to slightly different non-supine positions. The patient is then asked to repeat this same process using a specific soft pillow that contains a low volume of feathers. The second half of these measurements are taken to investigate if the softness of the sleeping surface impacts the value of the pressure measurement.

3.1.3 Results

The results of the measurements can be seen in Table 3.1.

The average pressure measurement for all of the subjects using their choice in pillow was 9.76 mmHg (0.189 psi), using the softer pillow was 8.77 mmHg (0.170 psi) and the overall average of all of the measurements was 9.26 mmHg (0.179 psi). The predicted external load discussed in Chapter 1 was 9.93 mmHg (0.192 psi) which has

Table 3.1: Measurements of the Eye Load

Subject #	Stiff Pillow Average Load in mmHg (psi)	Soft Pillow Average Load in mmHg (psi)
1	13.10 (0.253)	8.45 (0.163)
2	7.29 (0.141)	9.89 (0.191)
3	12.86 (0.249)	8.05 (0.156)
4	6.52 (0.126)	11.17 (0.216)
5	9.02 (0.175)	6.29 (0.122)
Average:	**9.76 (0.189)**	**8.77 (0.170)**

a percent error of 7.26% from the average of all of the measurements. The results of these measurements do not show any distinct correlation between the stiffness of the pillow and the measured pressure load. While the overall average for the stiffer pillows was slightly higher than the overall average for the softer pillow, this was only the case for 3 of the subject averages. It is important to remember that the patient positioning was subjective and there may be many differences between how any one individual might position themselves in a non-supine sleeping position. What this experiment shows is that the external pressure applied to the eye falls within the range of 6.3 mmHg to 13.1 mmHg (0.12 to 0.25 psi) with an average close to 10.3 mmHg (0.2 psi) when sleeping in a non-supine position.

3.2 Fluid Filled Balloon

3.2.1 Purpose

It is advantageous to be able to conduct real world experiments to partially or completely verify the phenomena being researched. Unfortunately, this can be difficult when conducting research on biological systems. It is not easy to obtain nor work with any enucleated eyes, whether human donor or animal, to run pressure measuring experiments on. Therefore it is necessary to come up with other ways of simulating a loaded fluid object similar to an eye. For this research, it would be helpful to have a deformable fluid-filled pressure vessel that can be tested in a manner similar to what the eye experiences during non-supine sleeping positions. The pressure vessel could be fit with a pressure measuring device and an external load could be applied to the exterior of the pressure vessel and the resulting changes in internal pressure could be monitored.

3.2.2 Apparatus

The solution to this was to pressurize an ordinary rubber party balloon with water while attached to tubes leading to a digital fluid manometer. This device can be seen in Figure 3.2. Water can be injected into the system through the open end of the third tube using an ordinary plastic syringe until water has entered every cavity and the balloon has reached its maximum inflation pressure. Standard rubber balloons such as this have a peak inflation pressure very early in the inflation

period [11]. Once this peak inflation pressure is reached, the internal pressure does not continue to rise. Therefore only a certain level of initial internal pressure can be obtained.

Figure 3.2: *Device created to simulated a loaded fluid filled deformable pressure vessel such as the eye*

3.2.3 Procedure

Once the tubes have been connected and secured to one another, the system must be filled with water and all of the air must be evacuated. With the balloon at the bottom of a sink and the open ended tube in the air, water is inserted into the system until the balloon is pressurized and the water is spilling out of the open tube. At this point, the tubes are manipulated to help any remaining air pockets rise to the top and exit the system through the opening. The system is then topped off with water and plugged shut so that it becomes a closed system filled with water

only. At this point the pressure gauge should read some pressure associated with the inflation pressure of the balloon. This pressure is the simulated initial IOP of the pseudo-eye. Now the device can be taken to a flat surface where every component of the system is placed at the same height to nullify the effects of gravity on the system. At that point, an external load can be applied to the balloon and the pressure changes can be recorded.

For the experiment carried out here, a normal U.S. quarter dollar coin (diameter $\approx$ 1 inch) was taped to a sequentially increasing number of standard aluminum washers. Use of the quarter allowed for complete and repeatable contact area between the balloon and the applied weight. Whereas the larger washer diameter would overhang off of the balloon depending on the balloon's degree of flatness. The fluid pressure both before and after each load was recorded. The procedure was conducted with the balloon on a hard counter top as well as on a soft glove in order to investigate the effects of the surface condition on the pressure change.

3.2.4 Results

The results of this experiment can be seen in Table 3.2. Note that the pressures are given in units of mmHg because this is the unit typically associated with IOP.

The plot of the change in fluid pressure in mmHg versus the applied pressure in psi can be seen as Figure 3.3. The increase in internal fluid pressure follows an almost linear trend throughout the loadings. As expected, the pressure increase was greater for the case of the balloon on the hard table top versus a softer surface. In

Table 3.2: Measurements of the Fluid Filled Balloon Experiment

Surface	Applied Pressure (mmHg)	Initial Pressure (mmHg)	Final Pressure (mmHg)	Pressure Change (mmHg)	Percent Change
Counter Top	4.87	9.72	10.71	0.99	10.10
Counter Top	8.93	9.83	11.53	1.70	17.37
Counter Top	13.15	9.83	12.57	2.74	27.89
Counter Top	17.14	9.83	13.76	4.03	41.05
Soft Surface	4.87	9.93	10.29	0.36	3.65
Soft Surface	8.93	9.72	11.02	1.30	13.30
Soft Surface	13.15	9.77	12.15	2.38	24.34
Soft Surface	17.14	9.72	13.55	3.83	39.36

the work done by Ernest et al., tests on enucleated eyes showed that peak pressures are higher when the eyes rest on a hard surface in comparison to a somewhat softer ocular orbit [21]. While the soft glove does not accurately recreate the conditions inside the orbit, it does highlight the difference in pressure change between the two resting surfaces.

Remember that the pressure being applied to the eye during a non-supine sleeping position is approximately 10.3 mmHg (0.2 psi). Looking at the results from the balloon test in Figure 3.3, an external pressure around 10 mmHg (0.2 psi) results in a roughly 2 mmHg increase in fluid pressure inside of the balloon. It is important to remember that a rubber balloon filled with water sitting on a counter-top is very different than a human eye in the orbit. A rubber balloon represents a significantly more elastic structure than the fiber reinforced walls of the eye. The main goal of

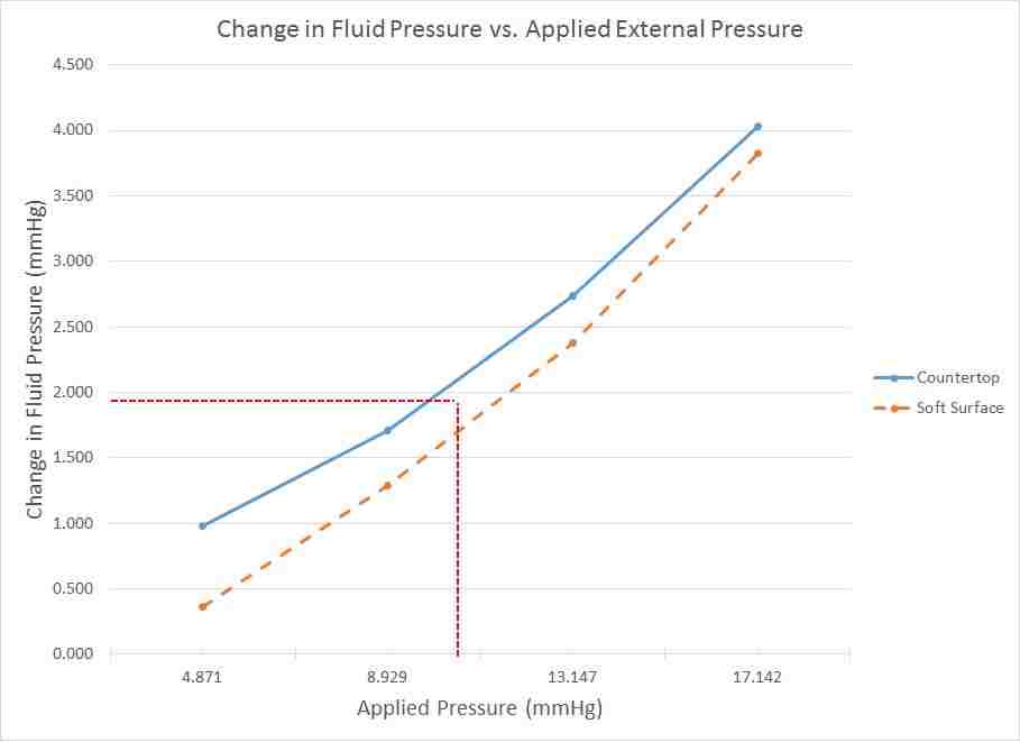

Figure 3.3: *Results of the Balloon Experiment*

this experiment was to investigate the relative impact of external loads on internal fluid pressure as well as the impact of the underlying surface on the pressure changes.

Chapter 4: **COMSOL Simulations**

It is already known that some level of pressure is being applied to the exterior portion of the eye but what remains unknown is what happens inside of the eye itself. Originally, the goal was to build a single comprehensive simulation that would incorporate both the external loading and the variation in fluid flow over time. However, difficulties integrating the known analytical relationships of the fluid flow and pressure volume relationships was encountered. Therefore, as mentioned earlier, the approach to simulating the eye under external loading was split up into two main components: 1) a fluid-structure interaction, FSI, finite element simulation, and 2) an iterative numerical computing code. In this chapter, which addresses the FSI simulation, the eye is treated as a completely closed fluid filled pressure vessel. This assumption is valid because the FSI simulation occurs over a span of time less than what the eye would need to begin to dynamically respond to the changing conditions. The iterative code introduced later will then use known empirical relationships to address the dynamic response. With an approximate total ocular fluid volume of roughly 6500 μL and an equilibrium fluid flow rate of 2.5 μL per minute, only 0.002% of the fluid is replaced during the three second simulations, a very small amount. The purpose of the FSI simulation is to determine the impact of the external load on

the initial internal fluid pressure before this fluid exchange comes into effect. This chapter contains a discussion of the model used to investigate this and the impacts of the results.

4.1 Geometry of Model

The first important aspect of any model is the geometry of the structure being simulated. For this research, the modeling was done using COMSOL Multiphysics 4.4. The advantages of this software is that it allows for many different types of physics modules to be mixed together to create unique and very specific solutions to complex problems. This research utilizes the FSI module as well as the hyperelastic material feature to construct and analyze the eye in an environment similar to the real world. An axisymmetrical version of the model was chosen to simplify the complexities of the simulations and utilize the natural symmetry of the eye. When adding a third dimension to the model, a much greater number of elements must be meshed as well as a much larger number of variables solved for with each iteration. Since the simulation being done is time dependent, it was decided that it would be more efficient to use a two-dimensional axisymmetrical model without losing significant accuracy to the simulations. Another example of a two-dimensional axisymmetrical model of the eye can be seen in Mudry et al. [25].

First, recall the components of the eye that need to be modeled here. The outer wall of the eye is the principle load-bearing component and it consists of three distinct regions: the cornea, the limbus and the sclera. As previously mentioned

in Chapter 2, these regions can be split up into further smaller microscopic layers. However it is not necessary for the model to contain such microscopic detail. The goal here is to capture the macroscopic behavior of the ocular wall as a whole. This can be done by using the material definition as laid out in Lanchares et al. [1] and the hyperelastic materials feature inherent within the COMSOL Multiphysics software. In reality the eye is sitting inside of the ocular orbit with six muscles attached to the sclera to control eye movement and location. Brief consideration was given to modeling the individual muscle attachment regions as fixed boundary conditions however this poses unnecessary difficulties for an axisymmetrical model. Instead, an orbit shaped region of fatty tissue was built around two-thirds of the outside boundary of the sclera. This is meant to represent the rigid nature of the ocular orbit while allowing for some compliance to mimic the soft tissue and muscles lining the orbit. Inside of the ocular globe are four main solid components: the iris, the ciliary body, the ciliary zonules and the lens. These four components are all connected and span the anterior portion of the globe which provides for a certain level of additional lateral stiffness. The final components to mention are the two fluids: the aqueous humor found in the anterior chamber and the anterior portion of the posterior chamber and the vitreous humor found in the remaining region of the posterior chamber. These ten components are what makes up the model used here in these simulations.

As mentioned in the discussion of *Eugene Wolff's: Anatomy of the Eye and Orbit* in Chapter 2, the dimensions used for the ocular wall can be seen in Figure 2.2. This figure shows that the exterior scleral region of the globe has an anthroposterior

radius of 12 mm and a lateral radius of 11.75 mm. The posterior wall of the sclera is the thickest portion of the ocular wall with a thickness of 1 mm. At the midpoint of the globe along the sclera, the wall thins to a thickness of 0.55 mm only to increase to a value of 0.8 mm at the most anterior portion of the sclera. Then begins the transitional region to the cornea, known as the limbus. No specific measurements for the limbus are given but it represents a roughly 1 mm long region of the ocular wall in between the sclera and the cornea. The cornea has a thickness of 0.66 mm just after the limbus and a thickness of 0.52 mm at its forward most point at the most anterior point in the globe. However the cornea does not have the same radius of curvature as the sclera. Instead it is a bulge off the front of the eye with a radius of curvature of 7.8 mm centered 5 mm anterior to the scleral radial center. These dimensions culminate in the ocular wall structure seen in Figure 2.2.

The lens is suspended by the ciliary zonules attached to the ciliary body to form the barrier between the two fluid regions. The anterior surface of the lens has a radius of curvature of 10 mm and is located approximately 3 mm behind the posterior surface of the cornea. The posterior surface of the lens has a radius of curvature of 6 mm. The ciliary body on the other hand does not have a rigidly defined set of dimensions. A rough idea of the shape can be seen in Figure 2.3. It is difficult to capture the subtle intricacies inherent to the ciliary body but for the purposes of this research those details are not important. The final component is the ciliary zonules. This consists of fibers whose main purpose is to connect the ciliary muscle (part of the ciliary body) to the lens and to complete the fluid barrier. This

was simply modeled as a thin wall spanning the gap between the ciliary body and the lens. Figure 4.1 shows the geometry as it was built in COMSOL Multiphysics.

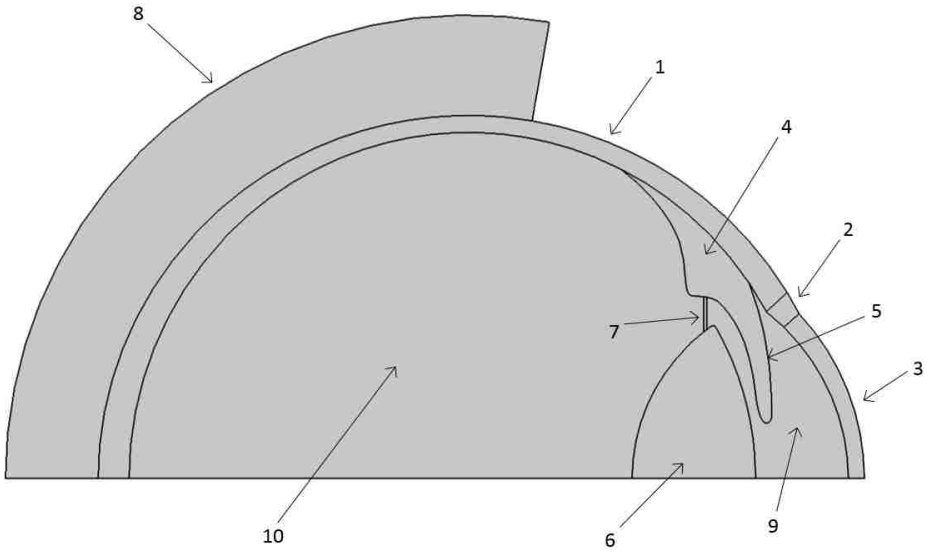

Figure 4.1: *Computer Model Geometry, 1) Sclera, 2) Limbus, 3) Cornea, 4) Ciliary Body, 5) Iris, 6) Lens, 7) Ciliary Zonules, 8) Fatty Tissue Orbit 9) Aqueous Humor and 10) Vitreous Humor*

4.2 Material Properties

Equally as important as portraying accurate geometry of the eye is defining the material properties in an appropriate manner. In the case of studying the effects of loading on a pressure vessel, the material properties of the walls of the vessel are of great importance to the accuracy of the model. Often in engineering, load bearing materials are able to be defined as linear meaning they have a specific modulus of elasticity and a Poisson's ratio. However, due to the non-linear nature of the behavior of the ocular wall structure, a non-conventional approach must be taken to

describe that material. In this case, it is most appropriate to describe the walls as a hyperelastic material. A hyperelastic material is often used to describe rubber-like material as well as biological tissue. What is unique and useful about a hyperelastic material is that it is principally defined by the strain energy density function of a material. The strain energy density is the work required to cause a specific amount of strain. More accurately, it is represented by the area under an instantaneous stress-strain curve [26]. An in-depth introduction into the strain energy density of the ocular wall can be found in Chapter 2. The equations and parameters used in this model for the cornea, limbus and sclera are the same as those found in Lanchares et al. [1].

The remaining material properties are not as vital to the accuracy of the simulations because those components contribute less structural support in comparison to the the ocular wall. Because of this, a less rigorous approach was used for assigning those material properties. The connection between the ciliary body, iris and sclera do not have visible discrete boundaries. For that reason, the material properties of the sclera were simply applied to the ciliary body and iris as well. It is reasonable to assume that the material properties are rather similar to begin with and the ciliary body does not have a major structural role aside from keeping the lens in place. As done by Power [9], the lens was assumed to be essentially rigid. As an approximation to what a transparent light focusing object might be made up of, the lens was given properties close to that of ordinary glass. In reality the lens is an organic material that changes shape to focus light and would behave somewhat differently than glass, however in this model the contribution of the lens is to be

part of the chain of three components (cilary body, ciliary zonules and lens) that span the anterior portion of the globe and provide additional lateral stiffness.

The last solid structural components to assign material properties to are the exterior fatty tissue orbit and the supportive ciliary zonules. The fatty tissue orbit was assigned linear elastic values that would model it as nearly incompressible soft human tissue [9]. Since the ciliary zonules are meant to simply connect the ciliary body and the lens and create a fluid boundary between the aqueous and vitreous humor, the same fatty tissue material properties were assigned to a thin ciliary zonule region.

The only components left to assign material properties to are the aqueous and vitreous humors. These components are the fluids that make up the vast majority of the ocular volume. The aqueous humor has properties very close to that of water with the added ability to provide nutrients to the inner components of the anterior chamber [27]. The vitreous humor takes up about 80 % of the globe and contains more than 99 % water [4]. However the vitreous humor has a viscosity about 2 to 4 times that of water. [28]. Therefore the density will be assumed to be that of water and the viscosity will be considered to be three times that of water. The material properties used for all of the components in the model can be seen in Table 4.1.

4.3 Fluid Structure Interaction Model

Once the dimensions and material properties are determined, it is time to build the actual simulation model in COMSOL Multiphysics. To avoid including

Table 4.1: Material Properties for the FSI Model

Component	Description	Density (kg/m^3)	Viscosity ($Pa \cdot s$)	Modulus of Elasticity (MPa)	Poisson's Ratio
Sclera	Hyperelastic	1400	N/A	N/A	N/A
Limbus	Hyperelastic	1400	N/A	N/A	N/A
Cornea	Hyperelastic	1400	N/A	N/A	N/A
Ciliary Body	Hyperelastic	1400	N/A	N/A	N/A
Iris	Hyperelastic	1400	N/A	N/A	N/A
Lens	Linear Elastic	2000	N/A	50e3	0.4
Orbit	Linear Elastic	999	N/A	0.047	0.4
Ciliary Zonules	Linear Elastic	999	N/A	0.047	0.4
Aqueous Humor	Fluid	1000	1e-3	N/A	N/A
Vitreous Humor	Fluid	1000	3e-3	N/A	N/A

an overflow of details in the main body of this paper, the complete discussion of the detailed simulation settings can be found in Appendix B. Figure 4.1 is a view of exactly how the geometry appears in the software. Following the construction of the geometry as previously described, the parameters to be used in the simulation need to be entered. The parameters are a list of every single numerical constant or initialized variable that will be needed for the simulation. This includes material properties, geometric features and initialized variables among other things. Following the definition of all of the parameters, the various equations used to determine the hyperelastic material behavior must also be defined as COMSOL variables. A full description of these definitions are given in Appendix B.

In order for the simulation to converge smoothly over time, the exterior load was applied as a ramp function over 0.5 seconds with smooth transitioning added to the end of the ramp. Using a ramp function is an alternative to applying the load impulsively at time equal to zero. The abrupt nature of the latter approach could

make iterating to a converged solution more difficult. Additionally, the 0.5 second range from no external load to full external load is analogous to an individual re-positioning and settling their head over a 0.5 second period, a reasonable assumption.

Once the parameters, variables and functions are defined, the settings within the FSI module node can be defined. This includes assigning the material properties to various components and applying the boundary conditions to appropriate regions. As previously discussed, the model consists of three hyperelastic materials, two linear elastic materials and two fluids. An in depth description of how to assign these materials is given in Appendix B.

To mimic the conditions inside of the ocular orbit, a layer of fatty tissue was built into the model to represent the intra-orbital tissues. Now in order to represent the rigid wall of the orbit itself, the outer boundary of the fatty tissue region will be set as a fixed constraint. This represents an eye that is immobile similar to the behavior of the eye during the majority of the time when someone is sleeping.

Lastly, the external and internal pressures need to be defined as boundary loads. The initial IOP is set as a boundary load over every internal surface of the eye. This value is there to set the initial conditions inside the eye before the loading is added. The external load was applied as a boundary load to the anterior surface of the cornea and limbus by utilizing the ramp function that was defined earlier to simulate loads similar to those presented in Table 3.1. By multiplying the ramp function by the value of the external load (values ranging from 5-15 mmHg (0.1-0.3 psi) were used), the loading itself follows the shape of the ramp function and in effect the load will be progressively applied over the first 0.5 seconds of simulation.

At this point, everything for the fluid-structure interaction has been fully defined and all that is left is meshing and setting up the study steps. COMSOL Multiphysics has a helpful feature known as a physics-controlled mesh. The software will build a mesh that is appropriate for the physics of the model according to a specific level of element density. In this case, normal element sized physics controlled mesh was selected and generated. This generated the mesh as it is seen in Figure 4.2.

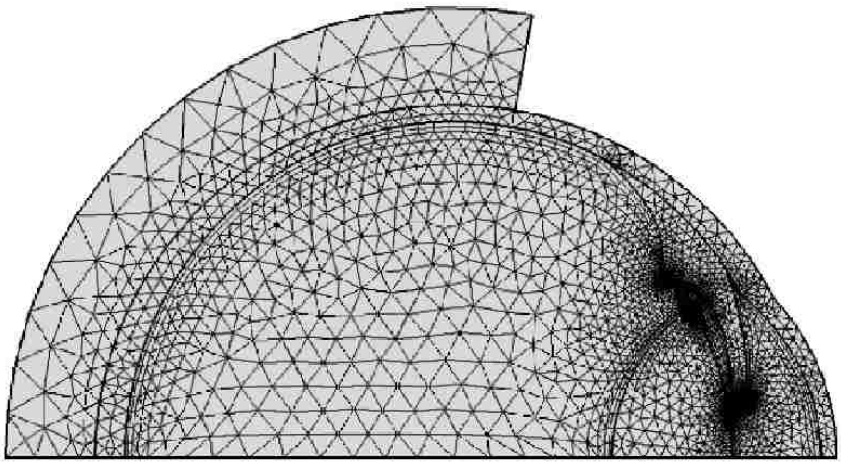

Figure 4.2: *Software derived element mesh for the model*

The software returned a warning message stating that a finer mesh than the one specified was used in certain regions. This finer mesh was used along the wall boundaries as well as near the rounded corners of the ciliary body, iris and lens. The finer portion of the mesh can be seen more clearly in Figure 4.3. To simplify the mesh and avoid the increased mesh density at the lateral point on the lens (just anterior to the ciliary zonules), a more rounded boundary could have been used here, similar to that seen in Figure 2.3.

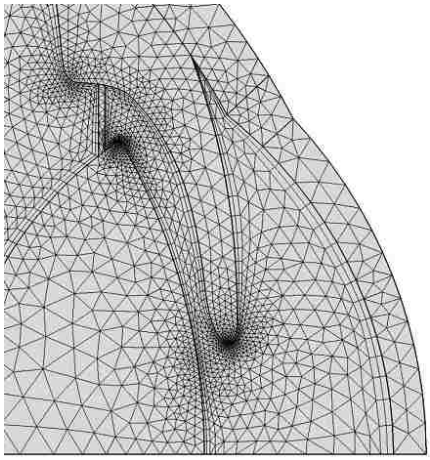

Figure 4.3: *Finer mesh for the anterior chamber*

The types and number of elements used in this physics controlled mesh can be seen in Table 4.2.

Table 4.2: Mesh Elements

Triangular Elements	4542
Quadrilateral Elements	498
Edge Elements	421
Vertex Elements	19
Total Elements	5040

The last items to be set up before the model can be run are the study definitions. For this model, two studies will have to be run sequentially. The first is a stationary study in order to set up the initial IOP. This is an important step to include in order for the results to show the change in pressure from a specific starting pressure. Without this step, all of the changes in pressure from the loading would occur from a starting pressure of zero, which is unrealistic. Now the fact that a ramp function was used for the external load becomes even more useful, due to

the fact that the ramp function is a function of time. During the stationary study, time is set to zero, and therefore the internal IOP load is active and the external load is not active during this phase. The second study is a time dependent study that now marches the model ahead through time greater than zero. The time range for the simulation was set to 3 seconds at 0.1 second intervals. After adjusting the study settings as described in Appendix B, the simulation is ready to compute.

4.4 **Results**

4.4.1 Intraocular Pressure

The investigation starts by looking into the initial change in IOP corresponding to several different external loading values. As discussed in Chapter 3, the load measurements yielded averages that spanned from 6.3 mmHg (0.12 psi) to 13.1 mmHg (0.25 psi). To investigate how the response would change over this range of external loading values, simulations were conducted for external loads of 5.2, 10.3, and 15.5 mmHg (0.1, 0.2 and 0.3 psi respectively) on a model with an initial IOP value of 15 mmHg. The results of these simulations over a three second time span can be seen plotted in Figure 4.4 and summarized in Table 4.3. The three second time span was chosen so that the simulation could stabilize for 2.5 seconds after the loading was complete.

As the value of the external load increases, so does the change in the internal fluid pressure. The relationship between these two values is almost linear. Going from an external load of 5.2 mmHg to 10.3 mmHg (0.1 psi to 0.2 psi) resulted in

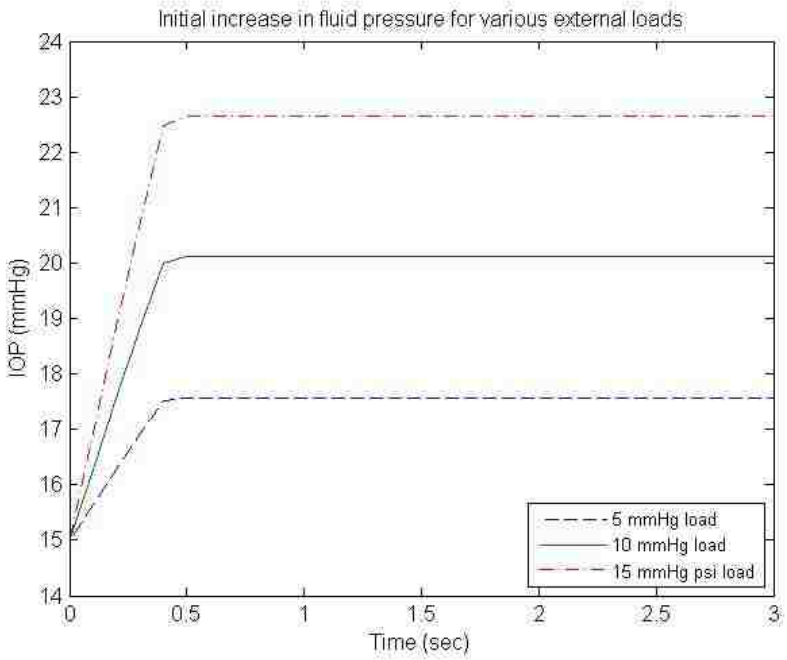

Figure 4.4: *Pressure vs. Time for various external loads*

Table 4.3: Simulation Results for Various External Loads from Initial IOP of 15 mmHg

External Load (mmHg)	Change in Internal Pressure (mmHg)	Percent Change from 15 mmHg
5.2	2.57	17.1%
10.3	5.12	34.1%
15.5	7.65	51.0%

an additional increase in IOP of 2.55 mmHg. Going from an external load of 10.3 mmHg to 15.5 mmHg (0.2 to 0.3 psi) resulted in an additional increase in IOP of 2.52 mmHg (almost the same as the previous case but slightly less). These results suggest that higher facial loads will cause roughly proportionally higher quasi-static increases to IOP.

As mentioned in the set up of the model, any initial pressure can be initialized for the model by changing the value of the initial pressure parameter in the model builder. The next set of simulations that were run calculate the pressure over a three second time span with starting IOP values of 10, 15, 20 and 25 mmHg for an external load of 10.3 mmHg (0.2 psi). This pressure range was chosen because it represents the range of IOPs that are seen with the vast majority of healthy and glaucoma affected eyes. The result of these simulations were compiled into a single plot and can be seen as Figure 4.5.

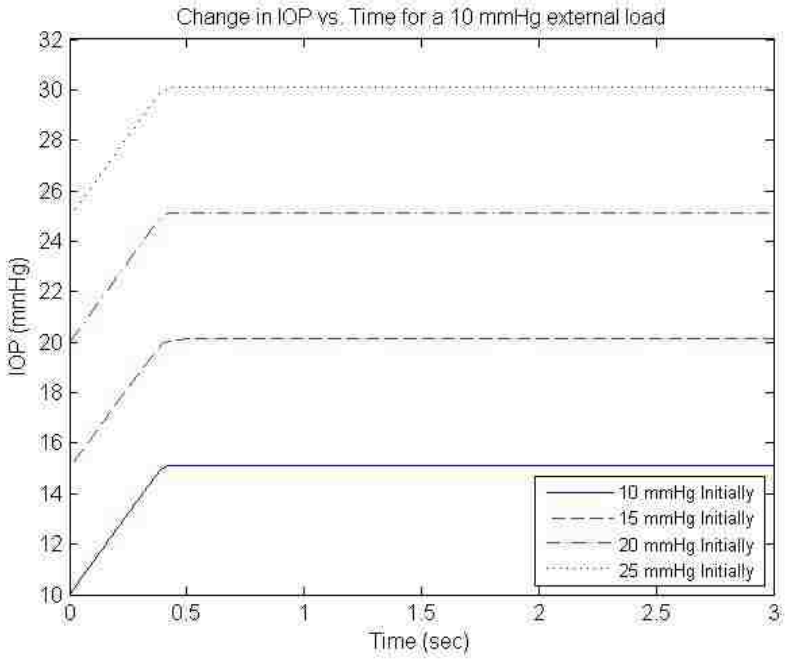

Figure 4.5: *Pressure vs. Time during FSI simulations for starting pressure 10, 15, 20 and 25 mmHg for a 10.3 mmHg (0.2 psi) load*

The resulting pressure increases were slightly different depending on the starting pressure, however not by a significant amount. The average pressure increase when a 10.3 mmHg (0.2 psi) load is applied to the cornea and limbus of the ocu-

lar model was found to be 5.125 mmHg. The resulting pressure increases in these simulations can be found in Table 4.4.

Table 4.4: Simulation Results with Original Properties

Initial Internal Pressure (mmHg)	Change in Internal Pressure (mmHg)	Percent Change
10	5.12	51.2%
15	5.12	34.1%
20	5.13	24.7%
25	5.13	20.5%

These results suggest that as a subject rolls onto their face during a night's sleep and applies a load of 10.3 mmHg (0.2 psi) to the anterior portion of their eye, the pressure inside of the eye will increase by just more than 5 mmHg. This is 33% increase in IOP considering a normal healthy eye only has an IOP of approximately 15 mmHg.

These simulation results represent the pressure increase when using the hyperelastic material parameters exactly as laid out in Lanchares et al. [1]. Those material parameters considered the sclera to be a matrix absent of fibers. While those parameters were determined using a iterative data fit, in reality the sclera does have stiff collagen fibers as well. Therefore two additional cases were simulated to examine the sensitivity to these material properties. For case two, the limbus properties were applied to the sclera, giving it some fibrous properties and increasing the wall stiffness. In the third material properties case study, the corneal properties were used in all three regions and the ocular wall fiber angles were set to 45 degrees,

increasing the wall stiffness further. The latter case has uniform properties across all three regions of the ocular wall. The resulting internal pressures for all three cases with an initial IOP of 15 mmHg and external load of 10.3 mmHg (0.2 psi) applied to the exterior boundary of the cornea and limbus are summarized in Table 4.5 and are plotted in Figure 4.6.

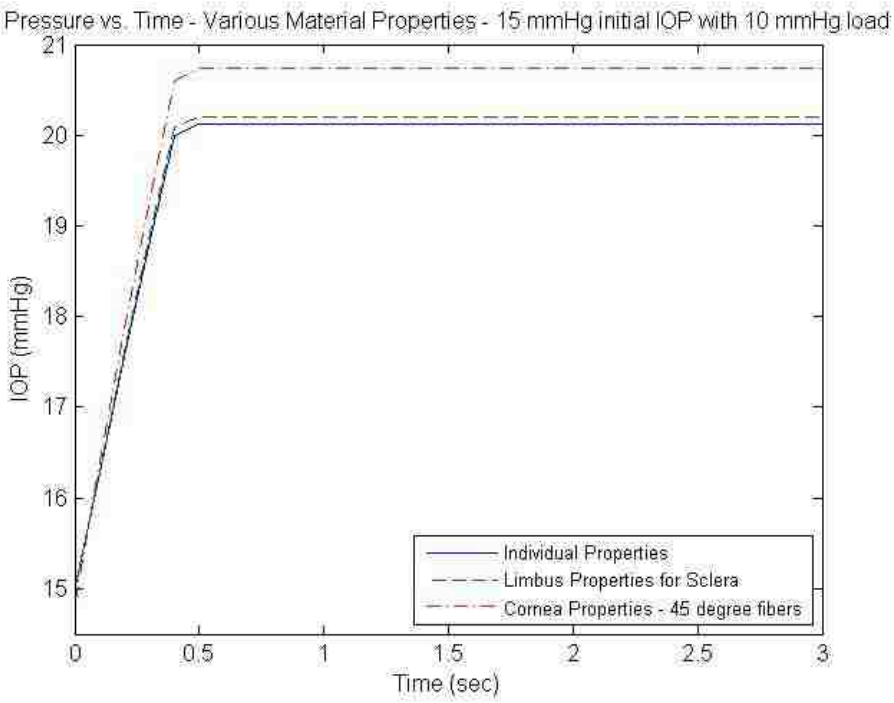

Figure 4.6: *Pressure vs. Time for various ocular wall material properties with 15 mmHg initial IOP and a 10.3 mmHg (0.2 psi) external load*

Table 4.5: Simulation Results with Sclera and Limbus Matching at 15 mmHg

Material Properties	Change in Internal Pressure (mmHg)	Percent Change from Initial IOP
Original Properties at 15 mmHg	5.12	34.2%
Sclera and Limbus matching at 15 mmHg	5.21	34.7%
Uniform Properties at 15 mmHg	5.91	39.4%

The pressure increase when the sclera is given limbus properties was 0.09 mmHg greater than when the original individual material properties are used. For the case when all three ocular wall regions have uniform cornea properties, the pressure increase was 0.79 mmHg greater than when the original individual properties are used and 0.70 mmHg greater than when the sclera is given limbus properties.

In conclusion, these simulations show that the pressure increase to an eye with an initial IOP of 15 mmHg under an external pressure of 10.3 mmHg (0.2 psi) on the anterior region of the ocular wall will result in an increase to IOP by about 5-6 mmHg. Since the simulations using the properties laid out in Lanchares et al. [1] yielded an average pressure increase of 5.13 mmHg, this is the increase that is used in the iterative code portion of the simulations.

4.4.2 Stress and Strain

As described in Chapter 1, the internal pressure of a pressure vessel is directly associated with the stress and strain in the structures walls. In the case of glaucoma related damage, the stress in the ocular wall is the true cause of the damage of the vital ganglion light-sensing nerve cells. As the IOP inside of the eye increases, the stress in the walls also increases and can eventually lead to the death of these cells. This increasing stress also indicates increasing strain within the walls. Figure 4.7 shows the simulated stress in the eye both before and after the applied external loading.

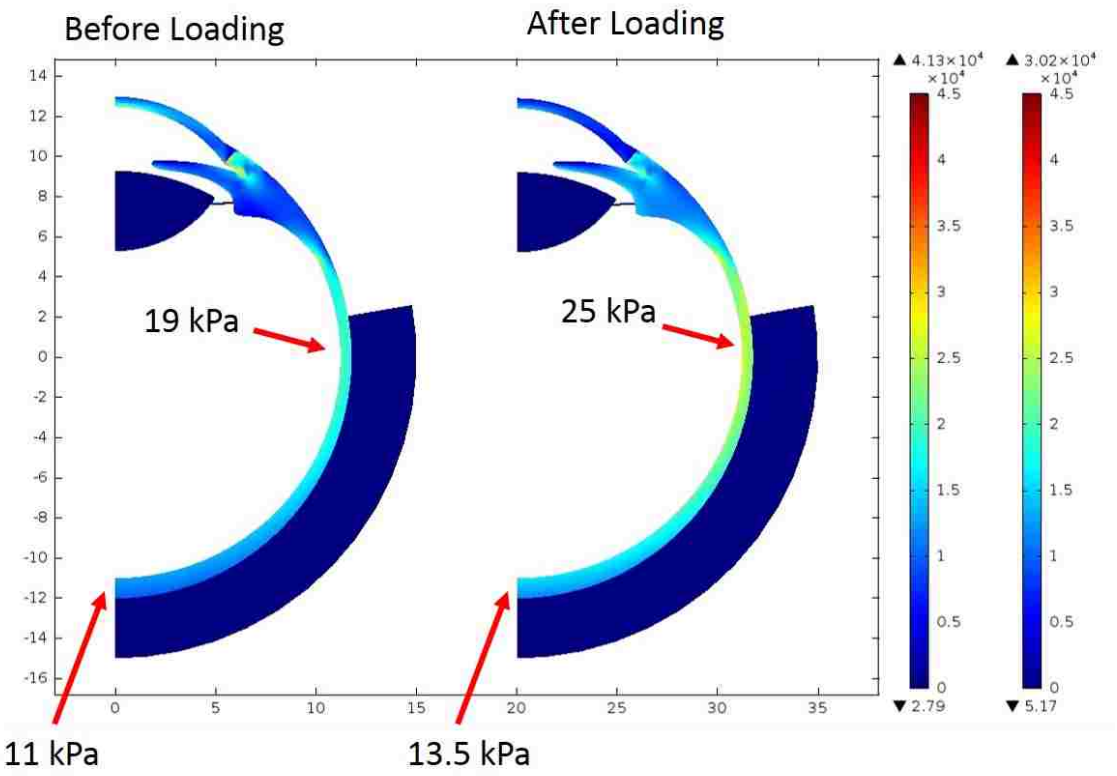

Figure 4.7: *Simulated stress (in Pa) in the eye both before (left) and after (right) loading occured*

The retina, which contains the vital ganglion cells, is located on the inner surface of the sclera. Before the external loading was applied, the sclera had a posterior stress value of approximately 11,000 Pa and an anterior stress value of approximately 19,000 Pa (caused by the initial IOP). After the external loading was applied, the sclera had a posterior stress value of approximately 13,500 Pa and an anterior stress value of approximately 25,000 Pa. This is a 22.7% increase in posterior sclera stress and a 31.6% increase in anterior sclera stress.

The retina is located on the interior boundary of the sclera. To form an understanding of how these changes in internal and external pressures effect the

stress in the retina, a plot of von Mises equivalent stress versus vertical location was created. The plot, seen in Figure 4.8, has the stress along the retina at time 0 and 3 for initial IOP values of 10, 15, 20, and 25 and an external load of 10.3 mmHg (0.2 psi) applied to the cornea and limbus.

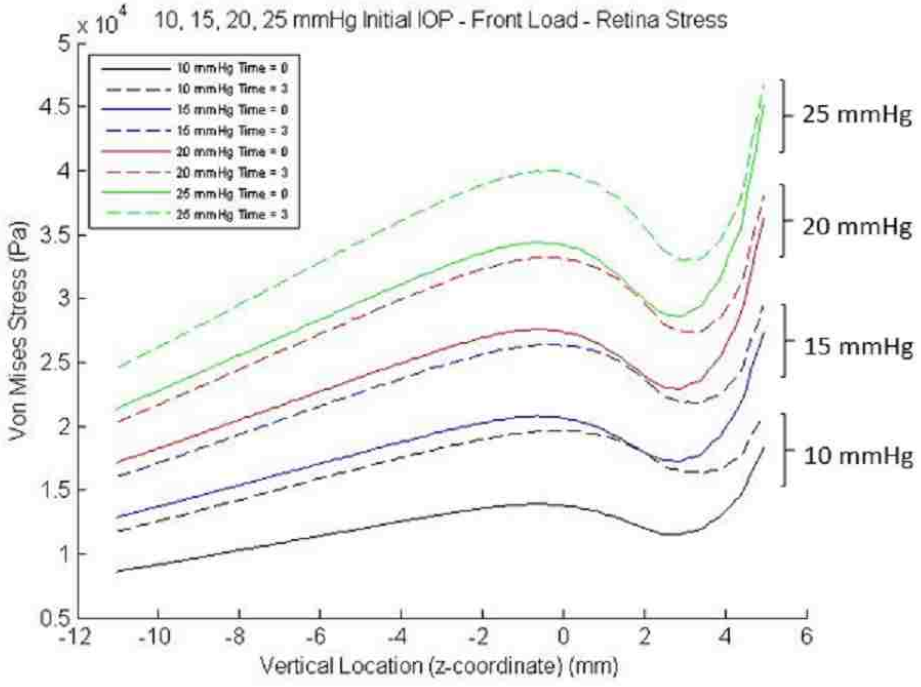

Figure 4.8: *Simulated stress (in Pa) in the retina for initial IOP of 10, 15, 20, 25 mmHg for an external load of 10.3 mmHg (0.2 psi) applied to the cornea and limbus (Time 0 = solid, Time 3 = dotted)*

The change in the retina stress from time 0 to time 3 can be seen in Figure 4.9. The maximum change in the retina stress due to a 10.3 mmHg external load to the cornea and limbus was located approximately 1.5 mm forward of the center point of the globe and has a value of roughly 6000 to 6200 Pa depending on the value of the initial IOP.

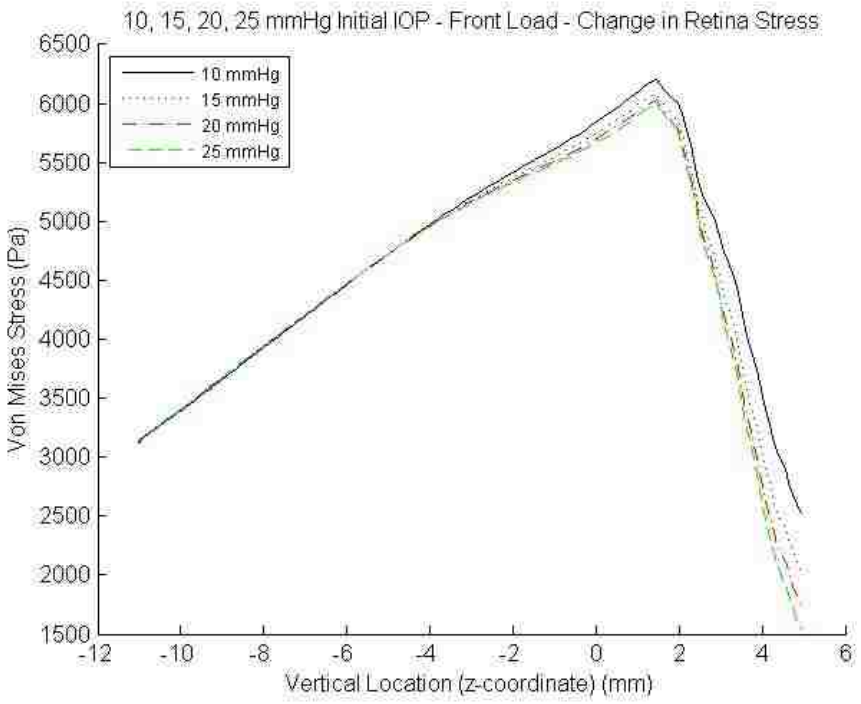

Figure 4.9: *Change in Simulated stress (in Pa) in the retina for initial IOP of 10, 15, 20, 25 mmHg for an external load of 10.3 mmHg (0.2 psi) applied to the cornea and limbus*

An additional case for external loading of the anterior sclera was also simulated. Depending on the non-supine position, it is possible that the majority of the external load may not be applied to the cornea and limbus only. The plot, seen in Figure 4.10, has the stress along the retina at time 0 and 3 for initial IOP values of 10, 15, 20, and 25 and an external load of 10.3 mmHg (0.2 psi) applied to the anterior sclera only.

The change in the retina stress from time 0 to time 3 for this case can be seen in Figure 4.11. The maximum change in the retina stress due to a 10.3 mmHg external load to the anterior sclera was located approximately 4 mm forward of the center point of the globe and has a value of roughly 1500 to 3000 Pa depending on

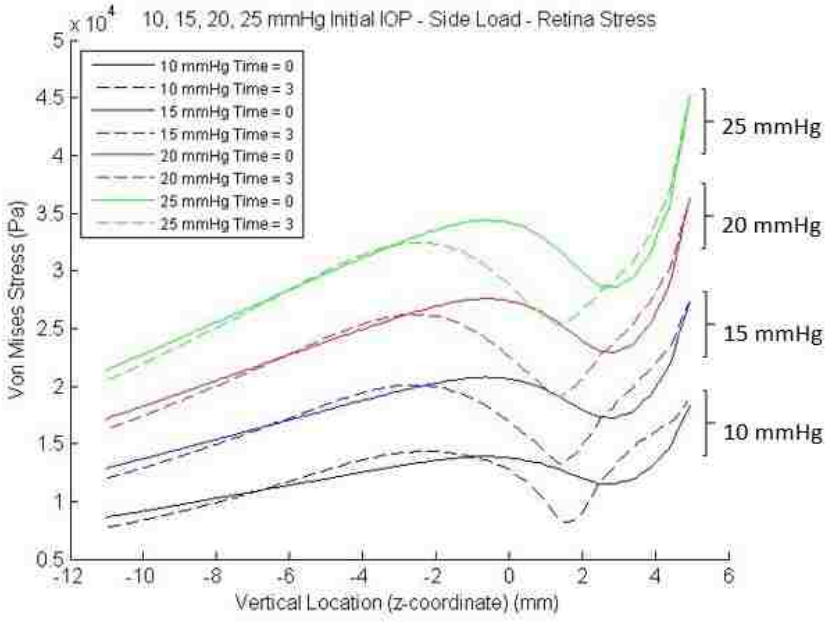

Figure 4.10: *Simulated stress (in Pa) in the retina for initial IOP of 10, 15, 20, 25 mmHg for an external load of 10.3 mmHg (0.2 psi) applied to the anterior sclera (Time 0 = solid, Time 3 = dotted)*

the value of the initial IOP. In this case, there was a significant decrease in retina stress, a change of roughly -4500 to -6500 Pa, between 0 and 2 mm forward from the center of the globe. It should be noted that this was the area in which the fatty tissue orbit was connected to the outer sclera and where the external load was applied to the anterior sclera.

It is also of interest to study the radial strain of the limbus for the cases presented above. This parameter will be helpful for comparison with and analysis of data presented in Chapter 6. Using the radial measurements of a point on the external surface of the limbus before and after applied loads, the limbus radial strain can be calculated. The data presented in Table 4.6 has radial strain of the limbus

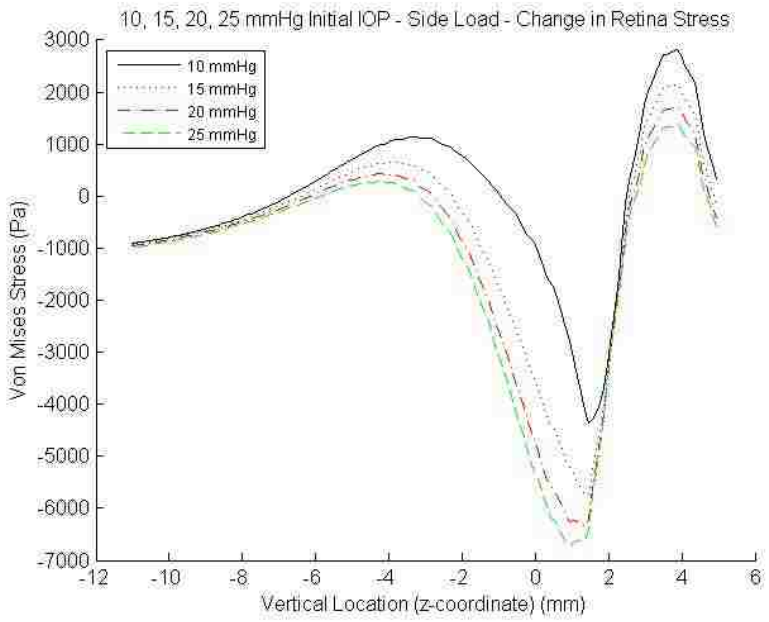

Figure 4.11: *Change in Simulated stress (in Pa) in the retina for initial IOP of 10, 15, 20, 25 mmHg for an external load of 10.3 mmHg (0.2 psi) applied to the anterior sclera*

for initial IOP values of 10, 15, 20, and 25 mmHg for the following cases: 1) increase in IOP by the amount seen in Table 4.4 without applying an external load, 2) an external loading of 10.3 mmHg applied the cornea and limbus , and 3) an external loading of 10.3 mmHg applied the anterior sclera.

The results seen in Table 4.6 suggest that the limbus region moves toward the center line of the eye (negative strain) when the external loading is applied to the cornea and limbus. When the external loading is applied to the anterior sclera, the limbus region moves away from the center line of the eye (positive strain). However for the case of anterior sclera loading, the limbus exhibits less positive radial strain in comparison to when the change in IOP is applied without the impact of the external forces.

Table 4.6: Radial strain of the limbus for initial IOP values of 10, 15, 20, and 25 mmHg for an external loading of 10.3 mmHg on both the cornea-limbus and the anterior sclera

Initial IOP (mmHg)	Strain from ΔIOP only	Cornea-Limbus loading strain	Anterior sclera loading strain
10	0.0014	-0.0011	0.00054
15	0.0015	-0.0012	0.00058
20	0.0016	-0.0013	0.00062
25	0.0016	-0.0014	0.00067

4.5 **Deformation Modeling**

4.5.1 Outflow Constriction

A 3-dimensional solid mechanics model of the eye was constructed in order to investigate the impact of the various loading on the deformation of the ocular shell. This geometric model can be seen in Figure 4.12. As mentioned in Chapter 2, much of the outflow fluid passes through a tube-like structure known as the Schlemm's canal. In order to investigate what might be happening to these outflow canals during the non-supine load, a geometric model of the shell of eye was constructed with cylindrical tubes penetrating through the limbus region. The Schlemm's canal tubes have a diameter of about 120 μm. In this case the diameter was modeled to be a perfect cylinder with a diameter of exactly 100 μm. The material properties of the shell (which includes the sclera, limbus and cornea) are the same as those used in the axisymmetrical model.

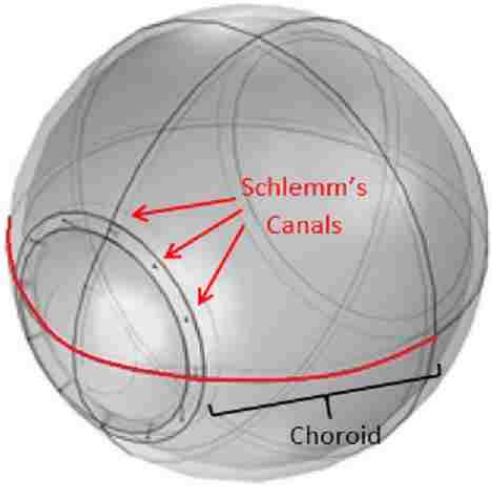

Figure 4.12: *3D ocular shell constructed for deformation modeling*

In order to investigate how much deformation was experienced by the outflow canals, the pressures on the various surfaces were applied as boundary loads. In this case the change in IOP from the steady-state value is applied as a boundary load across the entire inner surface of the eye. The external loading from the pillow is applied as a boundary load on the cornea and limbus as it was done in the axisymmetrical model. After solving for a solution, the cylindrical circumference was measured in both material and spacial reference frames representing before and after the deformation occurred. The result found that the loading causes a percent decrease in tube circumference of 0.73%. This amount of deformation corresponds to less than 1 μm change in diameter and it means that the loading does not cause outflow canal deformation large enough to effect the outflow of fluid from the eye.

4.5.2 Choroidal Expansion

The second aspect investigated was the phenomena known as choroidal expansion. In a paper written by one of the co-investigators in this project, Dr. Harry Quigley, MD, he discussed how expansion of one of the layers of the sclera known as the choroid is tied to increases in IOP. Dr. Quigley discusses how a choroidal expansion as small as 50 μm would be tied to a significant increase in IOP [29]. To investigate if such a phenomena would occur in this situation, this value was analyzed using the 3-dimensional deformation model.

The choroid is one of the many layers located within the sclera. In order to determine the amount of choroidal expansion occurring, a plot of the total displacement of an arc along the anterior surface of the glode was created. This arch can be seen highlighted in red in Figure 4.12. Figure 4.13 shows the total deformation versus the horizontal location of the points along this arc.

The region of the arc that contains the sclera is represented by the portion of the plot below the dotted red line in Figure 4.13. The portion of the plot above the dotted red line represents the limbus and cornea and does not contain any of the choroid. It is clear that the total displacement in any region of the anterior sclera is no more than roughly 31 μm at any point in the sclera. Since the choroid is part of the sclera, it is also known that the choroid does not experience expansion greater than that value. This choroidal expansion value is 62% of the mark of 50 μm set by Dr. Quigley.

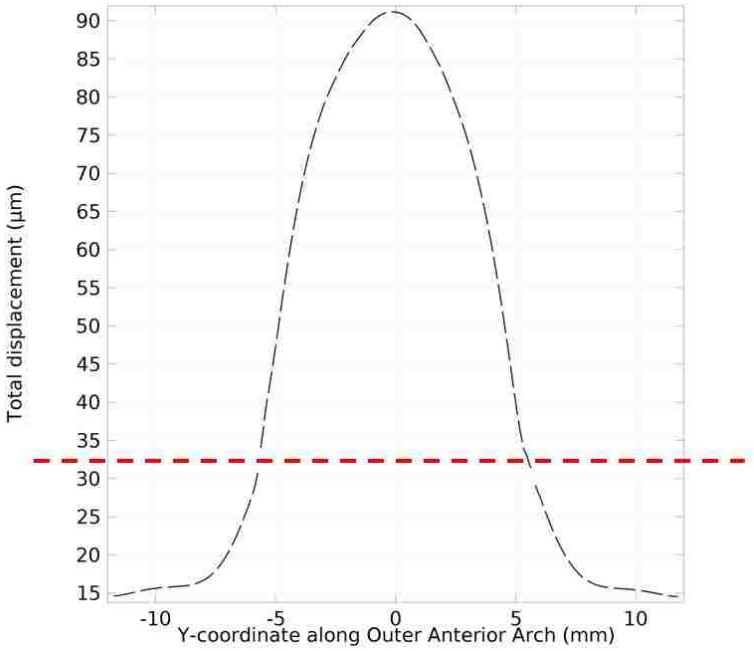

Figure 4.13: *Total deformation along exterior arch on anterior surface of the eye*

Chapter 5: **MATLAB Simulations**

5.1 Reason for using MATLAB

The second half of the simulations consist of an iterative MATLAB code that takes the result of the FSI simulations and illustrates the impact of this initial pressure increase over time. To obtain a complete picture of what is occurring to the eye during non-supine sleeping, the study of the IOP must continue beyond the quasi-static assumptions made for the FSI simulations. In those initial simulations, the eye was considered to be a completely closed pressure vessel with no ability to regulate the pressure of fluid inside. The iterative code simulates the response of the eye beyond this initial loading induced pressure change using pressure-volume relationships common to this field that are described in Chapter 2. It is left as future work to integrate appropriate pressure-volume relationships into a multiphysics finite element model.

5.2 Methodology

The code used to iterate the pressure values through time is based on the pressure volume relationships as presented in Chapter 2. The paper written by Van

der Werff et al. [20] highlights the various pressure volume relationships derived for the human eye. To build an iterative code, the pressure volume relationship can be coupled with the knowledge of the ocular fluid flux. These two fundamental relationships can be used to iterate the response of the IOP over time.

5.2.1 Flow Rates

One of the main purposes of the ocular fluids is to circulate proper nutrients to the inner components of the eye. This circulation requires a constant flux of fluid to and from different regions of the eye. As mentioned in Chapter 2, both the aqueous humor and vitreous humor have methods of circulating fluid. The vitreous humor fluid flux is independent of IOP however this is not the case for the aqueous humor fluid flux. The aqueous humor has a constant inflow rate of 2.5 $\mu L/min$ which helps the eye always remain in a rigid and pressurized state. The outflow of the aqueous humor is dynamic and always depends on the current conditions of the eye. The outflow relationship can be seen as Equation 2.1.

By knowing the rate at which aqueous humor is both entering and exiting the eye, the change in ocular fluid volume at any given point in time can be calculated. The iterative code takes these rates and multiplies them by a small increment of time and this results in the amount of fluid volume that has passed through that region during that time increment. The difference in the fluid volume entering and leaving the eye during one time increment represents the total change in fluid volume for that increment. This calculation can be repeated for every subsequent time interval.

Due to the fact that the outflow rate is dependent on the IOP, IVP and outflow facility, the change in ocular volume varies depending on the current condition of the eye. Knowing the incremental change in ocular fluid volume can be used to calculate the change in ocular pressure.

5.2.2 Pressure vs. Volume Relationship

The various pressure volume relationships for the eye were introduced in Chapter 2. There have been many different versions of this relationship developed over time. In order to represent the full scope of possible responses for this research, both the Friedenwald and the Woo pressure volume relationships were chosen to be highlighted (Equations 2.15 and 2.18). The Friedenwald equation represents the ocular response that returns to steady-state in the quickest manner. It is important to point out that according to Figure 2.5, the Holland relationship would represent the response with the quickest return to steady-state. However the Holland relationship is only valid for high IOP values which is not always the case. The reason this relationship is not always valid is due to the difference term between the pressure and constant c found in Equation 2.17 for the Holland relationship. For that reason, the Friedenwald relationship was chosen as the relationship representing the quickest response. On the other hand, the Woo relationship represents the relationship that returns to steady-state in the slowest manner. By analyzing the ocular response using both of these relationships, a range containing all of the possible pressure responses can be obtained.

Using the inflow and outflow equations as previously mentioned, the change in volume can be calculated for every iteration. Then by utilizing one of the pressure volume relationships (both Friedenwald and Woo for this research), this change in volume can be used to calculate the change in IOP. As the new IOP value is determined from the pressure volume relationship, the rate of outflow is then changed due to its dependence on the current IOP. These empirical formulas interact in such a way to produce the plot seen in Figure 5.1. This figure represents the response of the eye due to a sudden impulsive increase to IOP using the various pressure volume relationships introduced in Van der Werff et al. [20]. The Friedenwald and Woo relationships are highlighted with an F and a W respectively.

In order to further validate the choice of pressure volume relationship, a comparison of the Friedenwald equation simulation of change in pressure with time was made to the data presented in Figure 3 of Ernest et al. [21]. The results of this comparison can be seen in Figure 5.2.

The data presented in the Ernest et al. [21] consisted of IOP measurements every 5 minutes for a total of 35 minutes following the removal of Honan pressure reducing device. As expected, following the removal of the device, the IOP is initially much lower than the steady-state value (7 mmHg versus 16.5 mmHg). Due to the decreased outflow rate related to a lower IOP value, over time the eye begins to refill the ocular fluid that was evacuated at a higher than normal rate while the device was applied. As the ocular fluid volume increases, the IOP does as well until steady-state is reached. This scenario is very similar to what is expected of the eye following a non-supine sleeping position and this is why this data fit is important.

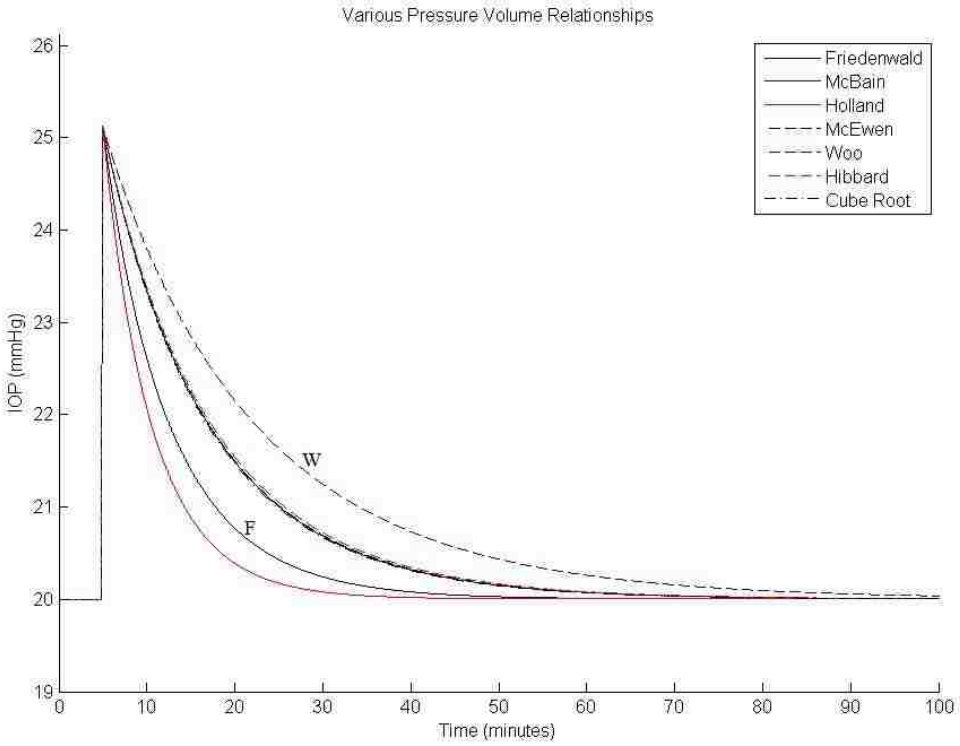

Figure 5.1: *Response of several pressure volume relationships to a sudden impulsive change to IOP*

In Figure 5.2, the red data points represent the data from the paper and the blue curve represents a second order polynomial fit to this data. The black curve represents how the iterative code would respond when using the Friedenwald relationship if the outflow facility had a value of 0.1667 $\mu L/min/mmHg$ and the constant uveoscleral outflow rate had a value of 1.24 $\mu L/min$ resulting in a return to a steady-state IOP of about 16.5 mmHg roughly 45 minutes after the loading is removed. When this fit was attempted with the Woo pressure volume relationship, the curve did not fit the data as well. This is further evidence that suggests that the Friedenwald relationship represents a more accurate relationship. However, both

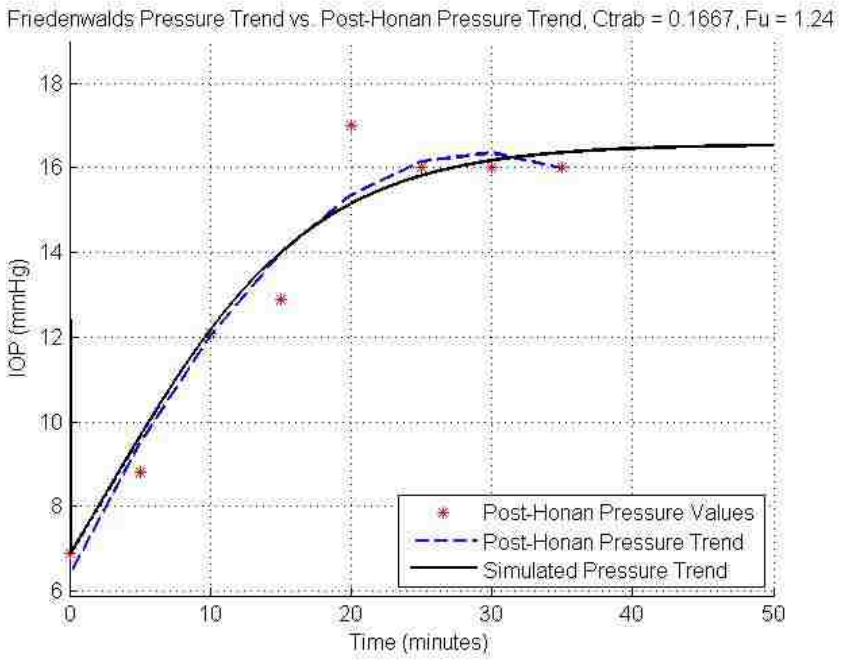

Figure 5.2: *Post-Honan pressure device data comparison - Shows how the simulated response matches measured changes in IOP over time*

relationships will still be considered in order to investigate the full range of pressure volume relationships in relation to this specific research problem.

5.2.3 Outflow

Every person has a unique steady-state IOP value and it is important to be able to modify the calculations to represent this natural variety. The steady-state IOP can be determined by altering the values of the flow facility through the trabecular meshwork. This flow facility corresponds to the term C_t in Equation 2.1 and it represents the ease at which the outflow can proceed through the outflow canals of the eye. The previous section discussed how an outflow facility of 0.1667

$\mu L/min/mmHg$ will yield a steady-state IOP of roughly 16.5 mmHg. Figure 5.3 depicts how a variety of steady state IOP values can be achieved using different outflow facility values.

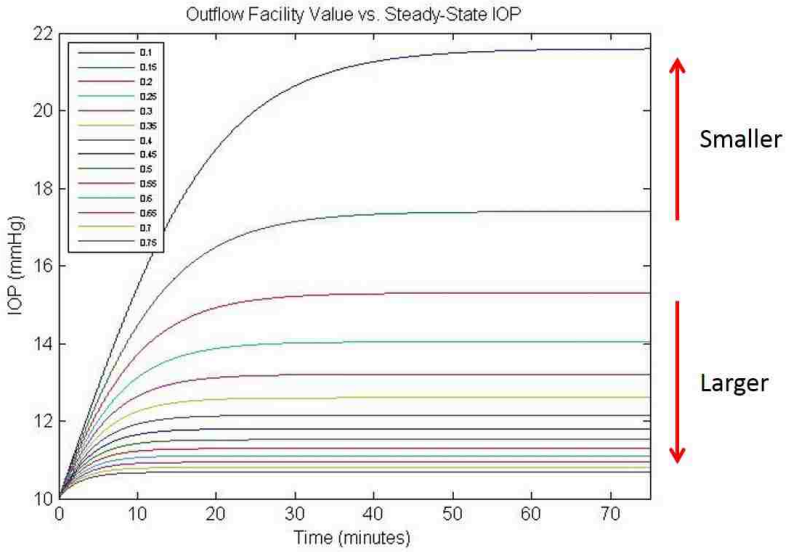

Figure 5.3: *Steady-State IOP values for various outflow facilities*

For an outflow facility of 0.1 $\mu L/min/mmHg$, the steady-state IOP would be roughly 22 mmHg. If the outflow facility was set to be as much as 0.75 $\mu L/min/mmHg$, then the steady-state IOP would be closer to 10.5 mmHg. These values bound the likely range of many normal steady-state IOPs. In this work, the uveoscleral outflow rate was assumed to have a constant value of 1.24 $\mu L/min$ for all of the cases.

5.2.4 Pressure Change Due to Loading

The one remaining component to incorporate into the iterative code is the way in which the external load pressure increase is included. When someone rolls onto their face while sleeping, the action occurs over a very short period of time. In the

FSI simulation, it was assumed that the eye goes from unloaded to fully loaded over a 0.5 second time span. This short of a time span is an insignificant amount relative to the length of time the eye would take to return back to steady-state (roughly 40 minutes using the Friedenwald pressure volume relationship). Therefore, the external loading pressure increase is considered as an instantaneous event that the eye then responds to. The code simply applies an IOP increase of 5.12 mmHg (the average pressure increase from the FSI simulations when using the original properties and a 10.3 mmHg external load) when the loading is set to occur. Similarly, when the loading is removed from the eye, an IOP decrease of the same amount is applied. The same amount of pressure change was removed upon unloading because it was assumed that the external loading transfers a certain amount of energy into the system that is then completely removed upon unloading.

5.3 The Iterative Code

At the start of the iterative code, several simulation parameters need to be set up. The iterative code will employ a small time step, Δt, to march the changes in IOP forward over the time range specified for the simulation. Both the time step and the time range need to be defined. The values used for the outflow capacity are chosen to represent the desired steady-state IOP for the patient in question. Additionally, the points in time when the external load application and removal will occur need to be entered so that the resulting pressure changes can be applied at

the appropriate moments in the time range. After also initializing the appropriate storage vectors, the iterative loop can begin.

The iterative code is built to calculate the current fluid flow rates, resulting change in fluid volume, and the change in pressure associated with that volume change for every successive iteration. This is done by utilizing a for-loop that spans the entire desired simulation time in increments of the Δt value set in the beginning of the code. As the code iterates through increments of time, the appropriate increase or decrease to the current value of IOP is applied when moments of loading and unloading occur respectively.

At this point, the code calculates what the aqueous humor outflow rate should be based on the set values for the outflow facility and the uveoscleral outflow rate and the current values of the IOP and IVP. The calculated outflow rate is used in combination with the constant inflow rate to determine the change in volume over the current Δt. The pressure volume relationship equations are then used to determine the new pressure based on the current pressure and the current change in fluid volume. The new pressure value is then set to update the current pressure value and the loop continues to its next iteration. This looping occurs until the end of the time range is met, and the desired pressure over time plot is obtained.

5.4 **Results**

In the pressure versus time plots shown here as Figures 5.4a to 5.6b, the non-supine loading was selected to occur at 5 minutes into the simulation and the

unloading at 30 minutes. The value of the pressure increase upon external loading was always set to be 5.1 mmHg because this was the average pressure increase for an external load of 10.3 mmHg across all initial IOP values from the FSI model when using the original material parameters as proposed be Lanchares et al. [1]. Initially, the simulations were done for only the case where the IOP was increased by the external loading on the eye. After further discussion with the collaborators at John Hopkin's Medical Center, it was proposed that in some cases, the IVP may also see an increase due to the external loading. The IVP (intravenous pressure) is the pressure in the veins and capillaries within and surrounding the sclera and limbus. It is likely that in certain loading positions, these blood vessels would also experience an increase in internal fluid pressure due to the same effect that is experienced by the IOP in the eye itself. Since not all patients exhibit a response indicative of an increase in IOP only, it was assumed that certain patients at certain moments experience a combination of IOP and IVP increases.

The first case that was simulated and presented here as Figures 5.4a and 5.4b, is the case for which the IOP value is the only variable that is initially increased and the IVP is assumed to be unaffected (as was originally suspected). As the iterations start, the IOP will establish a steady-state value corresponding to how the outflow parameters were set. At the moment when the external load is applied (in this case 5 minutes into the simulation), a pressure increase of 5.1 mmHg is applied to the current value of the IOP. This sudden impulsive shift takes the eye out of steady-state mode and into dynamic mode. During the dynamic mode, the eye adjusts the outflow rate in an attempt to regain the normal steady-state pressure. For both

the Friedenwald and Woo response curves, the response occurs as an exponentially decaying function until either steady-state is reached or the unloading occurs. At the moment when the external load is removed, a pressure decrease of 5.1 mmHg is applied to the current value of IOP. This action once again takes the eye out of steady-state mode and back into a dynamic mode. The response occurs as an inverse exponential decay just as the response to the post-Honan pressure reducing device did in Figure 5.2. This response continues until either steady-state is reached or another loading begins.

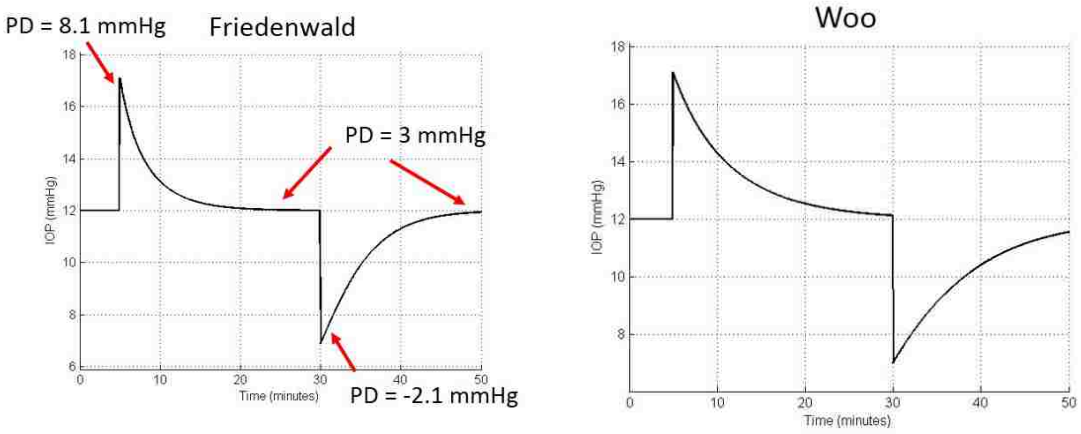

(a) *Friedenwald*

(b) *Woo*

Figure 5.4: IOP vs. Time simulation when a 5.1 mmHg initial pressue increase is applied to the IOP only

In this case, the IOP does not remain at a high level for a very long time. For the Friedenwald response, the IOP is +3 mmHg above steady-state for roughly 2 minutes and within +1 mmHg above steady-state after 5 minutes have elapsed. For the Woo response, the IOP is +3 mmHg above steady-state for roughly 4 minutes

and within +1 mmHg above steady-state after 10 minutes have elapsed. While neither of the plots show a sustained increase, the increase that does occur represents time spent with elevated IOP, and therefore elevated stress, which could be causing damage even over a short period of time. If one load/unload cycle occurred roughly once per hour throughout a nights sleep, a subject would spend approximately 40-80 minutes with pressures above +1 mmHg over steady-state values (assuming an 8 hours nights sleep).

Figure 5.4a introduces the the Pressure Drop (PD) notation useful in understanding the pressure vs. time plots. The pressure drop term is defined by Equation 5.1. This term is from the outflow formula defined by Equation 2.1 from Chapter 2. The pressure drop between the IOP and IVP is the main force controlling the rate of change of IOP through the cycles.

$$PD = IOP - IVP \tag{5.1}$$

Every eye has a specific pressure drop value which corresponds with a steady-state IOP and IVP (provided the outflow facility and uveoscleral outflow rate from Equation 2.1 remain constant). For the cases presented in this Chapter, the steady-state IOP is 12 mmHg and the steady-state IVP is 9 mmHg, therefore the equilibrium pressure drop is 3 mmHg. The pressure drop as a function of time, PD(t), in comparison to this equilibrium pressure drop will dictate the response of the eye and it follows the information presented in Table 5.1.

Table 5.1: Pressure Drop Relationship

For $PD_{eq} = 3mmHg$	Outflow is:	Volume is:	Pressure is:
$PD(t) < 3mmHg$	Less than inflow	Increasing	Increasing
$PD(t) = 3mmHg$	Equal to inflow	Constant	Constant
$PD(t) > 3mmHg$	Greater than inflow	Decreasing	Decreasing

The next case that was investigated, seen in Figure 5.5, is for an equal initial increase to both the IOP and the IVP. This case suggests that the loading from a non-supine sleeping position applies an external pressure to the blood vessel in and around the sclera in the same fashion it does to the eye itself. Since both the eye and the blood vessels are fluid filled hyperelastic chambers, it is assumed here that they would experience a similar increase in internal fluid pressure. Since Equation 2.1 for the outflow rate of the aqueous humor depends on the difference between the IOP and the IVP (the pressure drop), an increase to both of them by the exact same amount would results in no change to the outflow rate of aqueous humor. This means that both the inflow and outflow rates remain at their steady-state values and there is not change in fluid volume inside of the eye. This causes the pressure increase from the external load to be sustained for the entire length of the non-supine loading period. At the moment when the loading is removed, the pressure is decreased by the amount of the original increase and the eye immediately returns back to a steady-state. This results in a square wave response as seen in Figure 5.5. For the entire 25 minute non-supine period, the pressure remains at a value of +5 mmHg above the steady-state value.

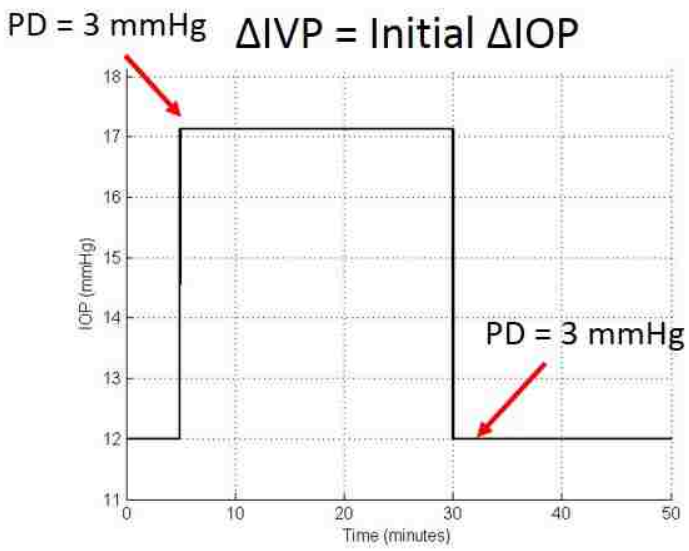

Figure 5.5: *IOP vs. Time when 5.1 mmHg initial pressure increase was applied to both IOP and IVP*

The case where both the IOP and the IVP are initially increased by the same amount have the same plot no matter what pressure volume relationship is used. This is because there is no change to the outflow rates at any point. Constant and equal inflow and outflow rates mean there is no change in volume and therefore no need for a specific pressure volume relationship.

The next case that was investigated, as seen in Figures 5.6a and 5.6b, is for an increase to the IVP only with no initial increase in IOP. It is proposed that this would occur in sleeping positions where the force of the sleeping surface is only applied to the regions immediately around the eye but not on the eye itself. As a result, the eye would not experience any initial load based increase to IOP. However, it is possible that the IVP does experience an increase due to external pressure on the soft tissue in which the blood vessels pass through in proximity to the eye. If

this were the case, the difference between the IOP and the IVP would decrease which would result in a decrease to the aqueous humor outflow rate (due to the pressure drop term in Equation 2.1). With a constant aqueous humor inflow, but a decrease in outflow, the volume of the eye would begin to increase. This fluid flow imbalance would result in an increase in pressure following an inversely exponential decay similar to that seen after the loading is removed in the case of an increase to IOP only (Figures 5.4a and 5.4b after time = 30 minutes).

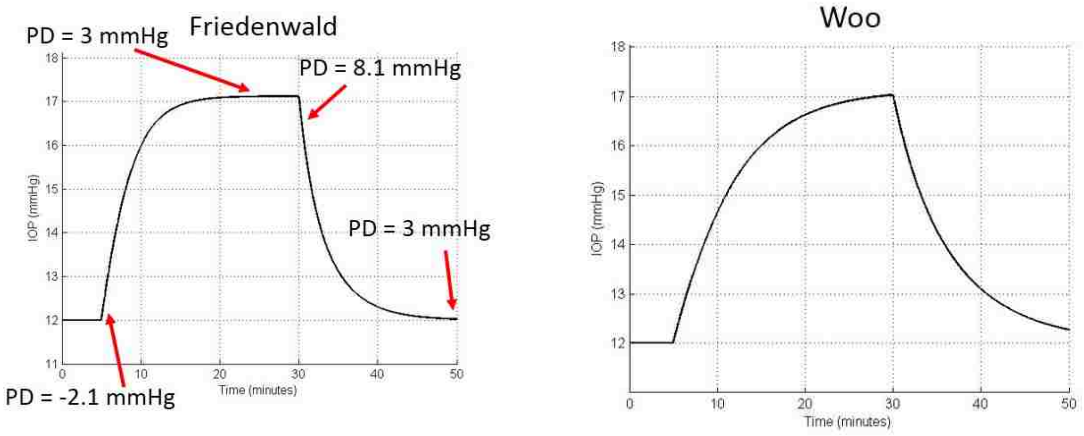

(a) *Friedenwald*

(b) *Woo*

Figure 5.6: IOP vs. Time when a 5.1 mmHg initial pressure increase is applied to the IVP only

Once again, this pressure over time plot represents a significant amount of time with elevated pressure conditions. As is evident with this case and the last, an increase to IVP can cause a potentially harmful sustained increase in IOP and ocular stress. Such an increase disrupts the normal outflow function of the aqueous humor and inhibits the eye from appropriately regulating the dangerous pressure.

Using the Woo relationship seen in Figure 5.6b, there is still an increase in pressure following an inverse exponential decay, however the increase occurs at a slower rate.

Two additional cases were simulated to illustrate the instances where the increase in pressure may have the full value in either the IOP or the IVP but a half value increase in the other. In Figures 5.7a and 5.7b is the response for the case of a full increase to the IOP (5.1 mmHg) and a half increase to the IVP (2.55 mmHg). This plot is very similar to that seen in Figures 5.4a and 5.4b, however the IOP does not return to the normal steady-state value during the loading due to the partial increase in the IVP. The IOP after the loading is removed still behaves the same but does not have as low of a minimum due to the higher steady state at the end of the loading region. Due to the higher steady-state value during the loading, this case has a higher average IOP under loading in comparison to the case where the IOP is increased alone. Once again, an increase to IVP results in some level of sustained increase to IOP and ocular stress.

In Figures 5.8a and 5.8b, is the response for the case of a full increase to the IVP (5.1 mmHg) and a half increase to the IOP (2.55 mmHg). These figures are very similar to those seen in Figures 5.6a and 5.6b. However the partial increase to IOP caused an initial step up by 2.55 mmHg that is absent in the case of an increase to the IVP alone. Similar to all of the previous cases where the IVP is increased, this case also exhibits a sustained increase in IOP and ocular stress.

In conclusion, the loading of the eye due to non-supine sleeping positions will likely cause an initial increase to loaded fluid filled regions by roughly 5.1 mmHg. This alteration from steady-state mode will cause the regulatory functions of the

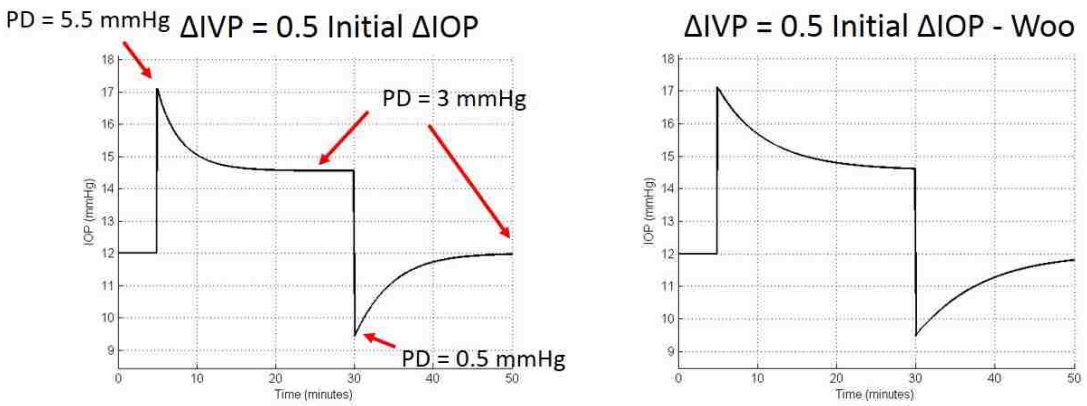

(a) *Friedenwald* (b) *Woo*

Figure 5.7: IOP vs. Time when a 5.1 mmHg initial pressure increase is applied to the IOP and 2.55 mmHg increase in pressure is applied to the IVP

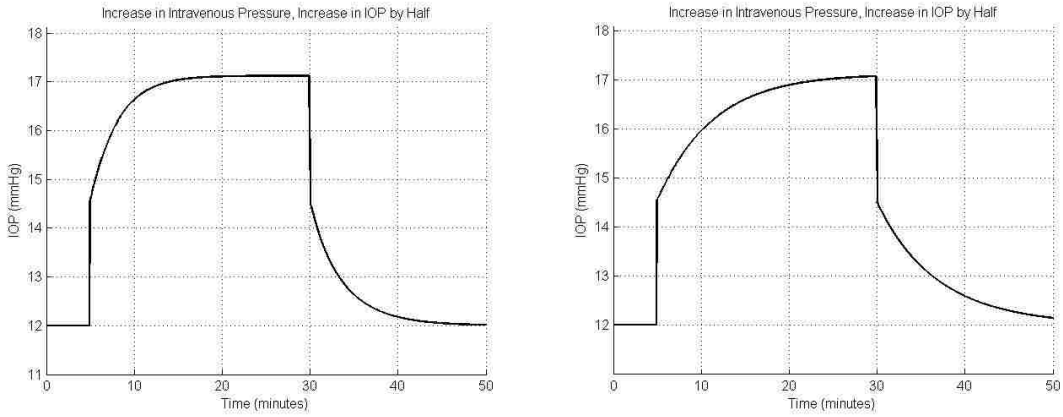

(a) *Friedenwald* (b) *Woo*

Figure 5.8: IOP vs. Time when a 5.1 mmHg increase in pressure is applied to the IVP and a 2.55 mmHg initial increase in pressure is applied to the IOP

eye to begin to react and adjust the pressure over time. In the case of an increase to IOP alone, elevated pressures are seen for a short amount of time, but the regulatory system is able to return the eye to relatively normal conditions in a swift manner. In the cases where the IVP experiences an increase in fluid pressure, the result is a

sustained increase in IOP. A sustained increase in IOP means a longer duration of exposure to potential damage causing stress levels.

Chapter 6: **Simulations vs. Triggerfish Data**

6.1 Introduction to Triggerfish Results

The SENSIMED Triggerfish® contact lens is a device developed by SENSIMED AG of Switzerland. The objective of this device is to measure the ocular strain associated with changes in ocular volume. A picture of what this device looks like can be seen in Figure 6.1.

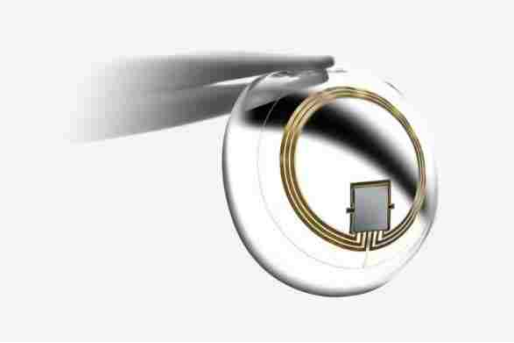

Figure 6.1: *SENSIMED Triggerfish® Contact Lens [30]*

As discussed earlier, the ocular volume and the IOP are directly linked through empirical formulas. The Triggerfish sensor gathers ocular strain data over 30 second bursts every 5 minutes at a rate of 10 hertz. A further description of the technology itself can be found in Appendix A of this document. For the purpose of this research, these specialty contact lenses are used to gather dynamic pressure information from

patients in both supine and non-supine positions. The need for this contact lens arises from the fact that typical IOP measuring techniques involve direct contact with the eye by a physician and a measuring apparatus. The Triggerfish contact lens is considered non-invasive because it can gather strain information from which IOP can be inferred while the patient's eye is located in a manner that cannot be reached by a physician using conventional means. Triggerfish lenses were designed primarily for study of pressure changes that are not influenced by external loads to the eye. Thus, while not designed for use in this application, these lenses do provide useful data on strains induced by non-supine sleeping positions. The extent to which IOP can be inferred from the lens output is still under study. Preliminary results suggest that in some individuals, the Triggerfish strain output tracks pressure change predictions from the simulations presented in Chapters 4 and 5. These cases will be discussed in this chapter.

The Triggerfish contact lenses were used on patients under the supervision of medical professionals at Johns Hopkins Medical Institute in Baltimore, Maryland. The patients underwent simulated sleep study procedures intended to mimic the actions of an individual naturally sleeping in non-supine positions. Over the course of several months (February to August), 32 study subjects have undergone this simulated sleep procedure.

Among the subjects participating in the study were 21 patients with glaucoma and 11 controls who did not have glaucoma. Of the glaucoma patients, roughly half exhibited noticeable changes in the Triggerfish lens output when they were in a non-supine sleeping position. The other subjects exhibited little or no change, possibly

because their facial geometry prevented significant load from coming in contact with their eye when in the non-supine position. Of the 11 responses that were significant, trends matching many of the scenarios presented in Chapter 5 were observed and will be discussed in this chapter.

6.2 Triggerfish Upward Bias

Some of the patients data has clearly shown an upward trend from the start to the finish of the sleep study session. It is thought that this gradual trend over several hours of data gathering is a type of creep occasionally seen with this technology [31]. The data shown in Figure 6.2 illustrates this upward trend.

This upward trend is not thought to be associated with the actual pressure increase, and therefore the data in this case must be re-scaled to remove the upward bias. In Figure 6.3, the same data is re-plotted as the residual from the trend line. The y-axis of this plot now represents the specific data points numerical distance from the trend line shown in Figure 6.2. By viewing the data in residual form, the effect of the upward trend in the initial data can be nullified. While further investigation as to the source of the upward trend should be conducted, it is believed that the residual data more accurately represents the simulated sleep position induced dynamic pressure changes.

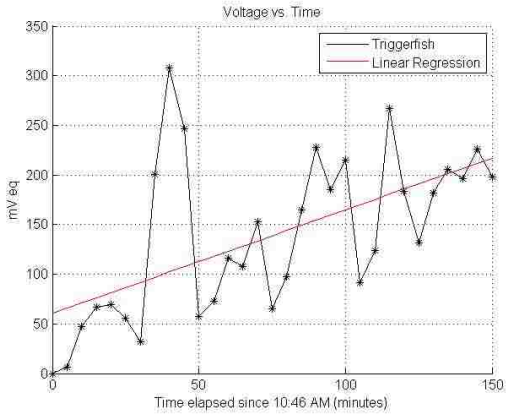

Figure 6.2: Trend Line

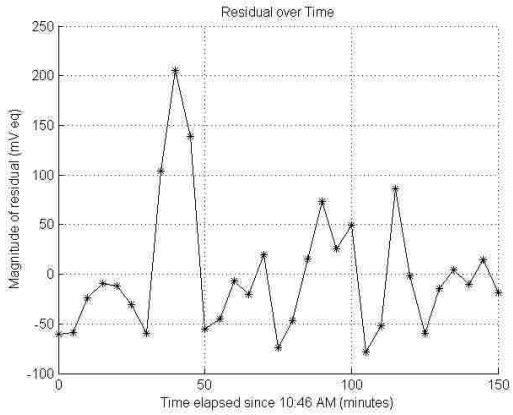

Figure 6.3: Data Residual

6.3 Simulated Triggerfish Data in MATLAB

In order to compare the continuous simulated IOP data from the iterative code to the actual Triggerfish data, it is helpful to generate simulated Triggerfish data. The simulated Triggerfish data uses bursts of data from the continuous simulated IOP that correspond to the bursts of the actual Triggerfish data. The actual sensor in the patients eye collects data every 5 minutes for a 30 second period at a rate of 10 Hz and then uses a software algorithm to determine the appropriate equivalent voltage average over that burst. The algorithm is meant to mitigate the effects of blinking and other disturbances not associated with IOP. Here, the simulated Triggerfish values are calculated by taking the statistical mean of the continuous simulated data corresponding to each 30 second burst. This allows for a direct comparison between experimental data and simulated IOP.

6.4 Scaling Triggerfish Data to IOP

The next step with analyzing the Triggerfish data is to determine how to scale the data from strain gauge units (mV eq.) to IOP (mmHg). The Triggerfish contact lens is detecting changes in strain associated with changes in ocular volume. It is known that the changes in volume are directly associated with changes in IOP, however the exact relationship between the changes in IOP and the values of strain picked up as changes in output voltage by the strain gauges on the Triggerfish lens, especially in the presence of an external load on the eye, is not known. A typical strain gauge functions by taking advantage of the properties of electrical resistivity. As a conducting material is elongated due to applied forces, the material becomes longer and thinner. Due to the relationship seen in Equation 6.1, the resistance will increase when this occurs. This resistivity change can be captured as a change in output voltage using a Wheatstone bridge resistor configuration.

$$R = \frac{\rho L}{A} \tag{6.1}$$

where R is the electrical resistance, ρ is the material resistivity, L is the material length and A is the material cross sectional area [32].

In order to interpret the changes in strain gauge output voltages as dynamic changes to the patient's IOP, the Triggerfish data must be scaled in some way. For this study, scaling was accomplished by assigning an IOP value to the minimum and maximum Triggerfish readings. Approach #1 for scaling the data is to set the maximum and minimum strain gauge voltage equal to the maximum and minimum

simulated pressure from the iterative code. In addition to scaling the maximum and minimum, the initial Triggerfish data point was also scaled to the initial simulation IOP. This method results in the scaling as seen in Figure 6.4.

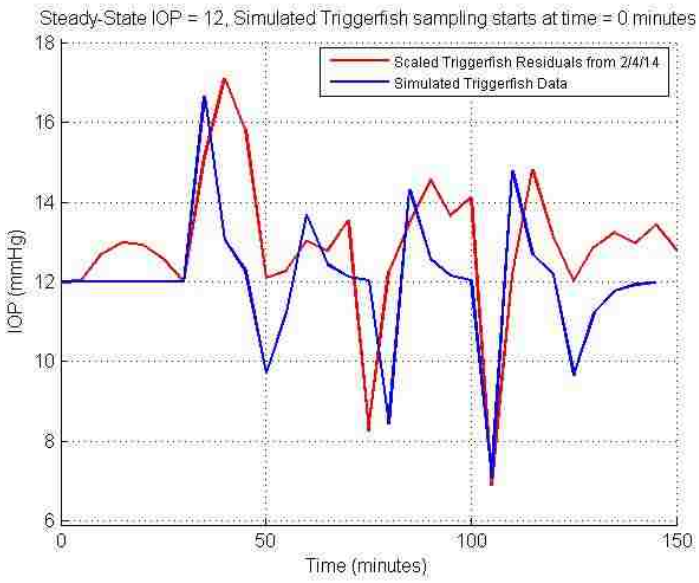

Figure 6.4: *Scaling if minimum, maximum and initial values are matched*

In Figure 6.4, the red line represents the scaled Triggerfish residual data and the blue line represents the simulated Triggerfish data from the code. While scaling approach #1 does appear to effectively match many of the regions to what is expected from the simulation, it tends to extremely over exaggerate the valleys in comparison to what is seen in Figure 6.3.

Instead of scaling approach #1 from Figure 6.4, an alternate approach, #2, was used for some of the data sets. Firstly, scaling approach #2 matches the maximum values from both the Triggerfish residual data and the simulated IOP. Next, the scaling matches the average Triggerfish residual data to the steady-state IOP value

from the simulated data. Finally, the minimum of the Triggerfish residual data was matched to the average continuous simulated data over the 5 minute time span in which that measurement would have taken place. The resulting scaling fit can be seen in Figure 6.5.

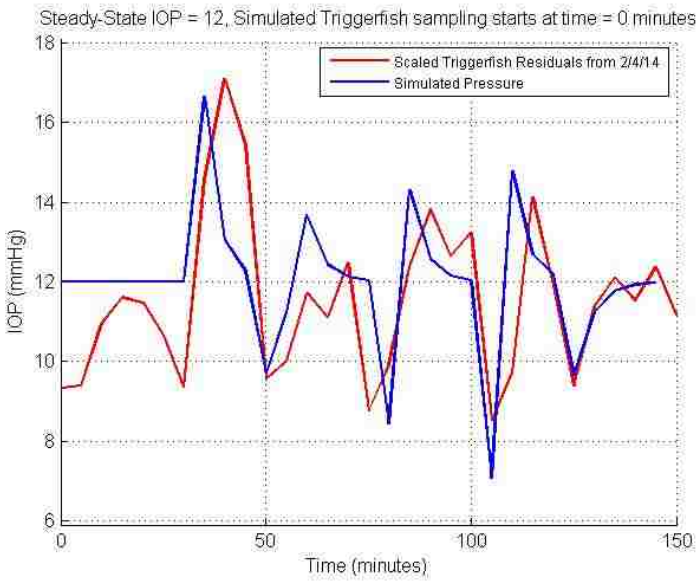

Figure 6.5: *Scaling if maximums are matched, average is set to initial and minimum is set to time interval average*

Scaling approach #2 seemed to fix the issues associated with approach #1. The valleys are no longer extremely exaggerated as in the case of Figure 6.4. In Figure 6.5 the relative height of the peaks and valleys are much closer to those seen in Figure 6.3.

A third scaling approach was developed that provided a more suitable fit for certain patient's data. Scaling approach #3 sets the initial and maximum values of the residual Triggerfish data equal to the initial maximum values of the continuously

simulated data. Additionally, the minimum residual Triggerfish data point was scaled by using a ratio between the initial, minimum and maximum normalized residual values. Both scaling approach #2 and #3 were used for the data presented in this chapter.

6.5 **Comparison**

6.5.1 Initial Configuration Session

The first Triggerfish session to have exhibited results similar to those of the simulations presented in Chapter 5 was the initial session conducted to help determine what the sleep study procedure should be going forward. This data is the same data used in Figures 6.2 to 6.5 to highlight specific aspects of the Triggerfish data analysis and it can be found again here as Figure 6.6.

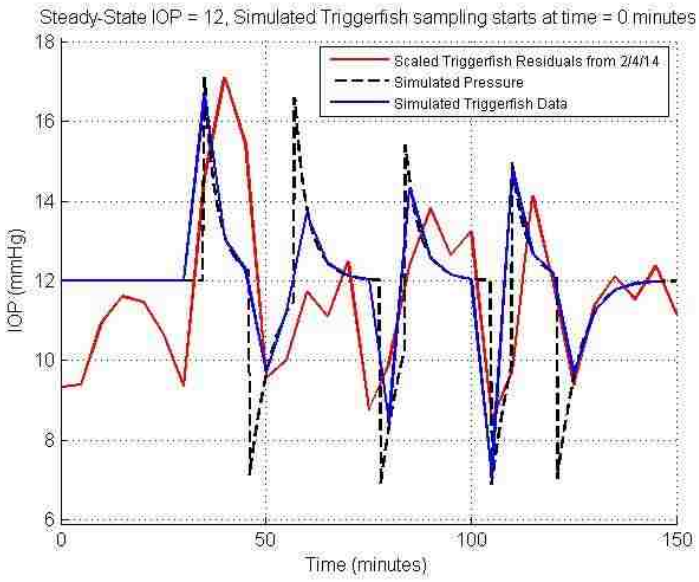

Figure 6.6: *Initial comparison between Triggerfish and simulated data*

Figure 6.6 contains three different plotted lines: 1) The scaled Triggerfish data from the sensor using scaling approach #2 (red), 2) the continuous simulated IOP from the iterative code (black) and 3) the simulated Triggerfish data from the continuous simulated IOP (blue). In this case, the iterative code used to produce the continuous simulated IOP simulates the scenario of an initial increase to the IOP only using the Friedenwald pressure volume relationship. The resulting IOP curve is similar to that seen in 5.4a. This can be seen more clearly with the continuous simulated IOP curve alone as seen in Figure 6.7.

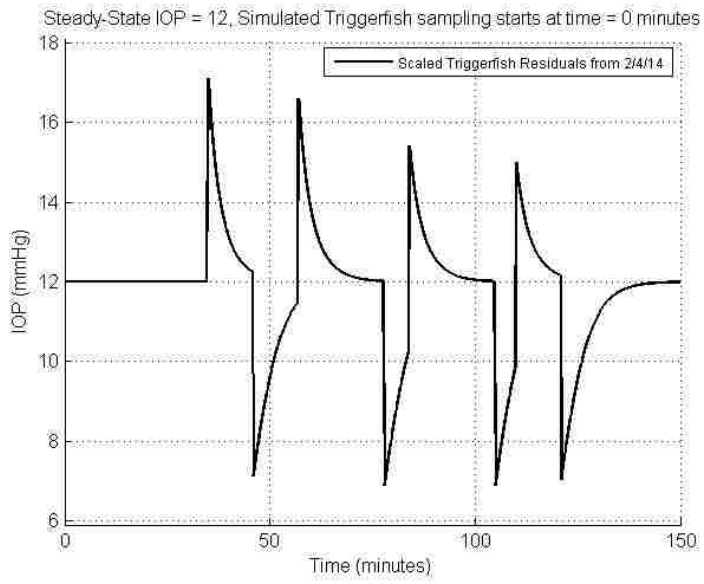

Figure 6.7: *Continuous simulated IOP plot for initial case*

During this study session, there were four non-supine portions and four supine portions. This session was conducted before the patient trials had begun and it had a purpose of helping to determine what the sleep study procedure should be for the actual patient trials. In Figure 6.7 the non-supine loadings are clearly evident

by the positive spikes in the IOP. Since this was modeled as an initial increase to IOP only, the pressure begins to drop immediately following an exponential decay pattern similar to the response seen in Figure 5.4a. The large sudden decreases in IOP correspond to the moments when the loading was removed. The reason that some of the IOP peaks are shorter than others is because the IOP had not yet returned to steady-state prior to that loading. This is the case with short supine portions that do not allow enough time for complete steady-state recovery.

An interesting point to note is the similarities between the relative peak heights of the various cycles in Figure 6.6. In the case for both the actual scaled Triggerfish residual data and the simulated Triggerfish data the first peak was the highest, followed by the fourth peak, then by the third peak and finally by the second peak. The determining factor for the height of the Triggerfish peak depends on when the sampling occurred. If sampling happens just as the loading is starting, the high pressure region will be captured, similar to peak #1. If the sampling occurs later on in a particular load cycle, the pressure will be farther along in it's recovery and the Triggerfish average will be lower, such as in peak #2. The simulated Triggerfish data was able to reproduce the pattern seen in the actual Triggerfish data as seen in Figure 6.6.

6.5.2 Patient TF003AGA

The next case of interest was an actual study case and it has the patient identifier of TF003AGA (used to keep patient information concealed). The data for this patient can be seen in Figure 6.8.

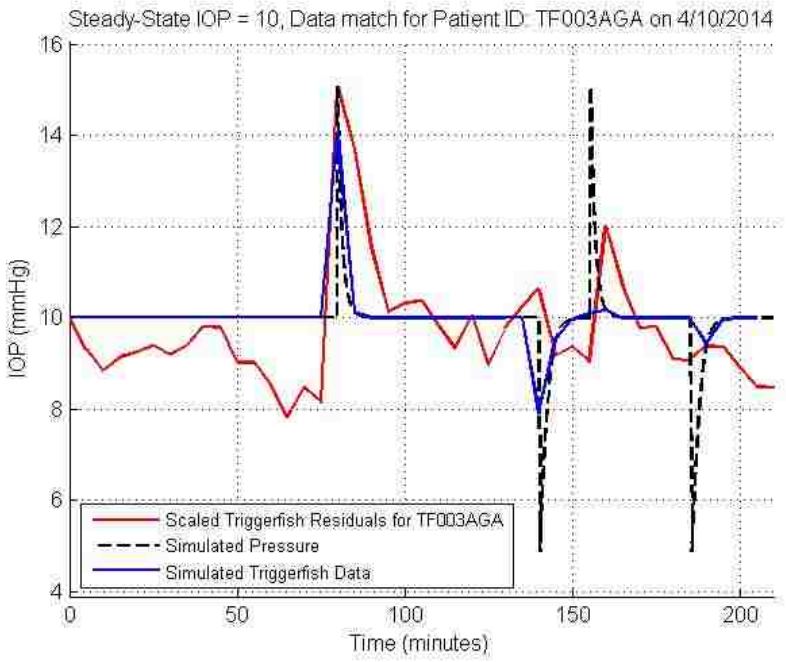

Figure 6.8: *Data comparison for patient TF003AGA*

This case uses scaling approach #3 which can be seen as the red line in Figure 6.8. This is another example of a patient whose data exhibited the patterns associated with an initial increase in IOP only using the Friedenwald pressure volume relationship. This is always indicated by the initial spike at the beginning of the non-supine loading followed by a relatively fast return to near steady-state values. The procedure for the sleep study ended up including two non-supine sleeping position portions each followed by a supine position portion. A detailed description of

the sleep study procedure can be found in Appendix A. Here both of the non-supine spikes were captured similarly to the case seen in Figure 6.6. There is an apparent lack of IOP drop when the face down loading is removed. It is unsure why this would be the case and it is a subject for future study.

6.5.3 Patient TF006UBE

The next case is that of patient TF006UBE. In this case, the patient's data showed two different phenomena: 1) An increase in IVP only and 2) an initial increase in IOP only. The plot showing the scaled residual Triggerfish data and the simulated data can be seen in Figure 6.9.

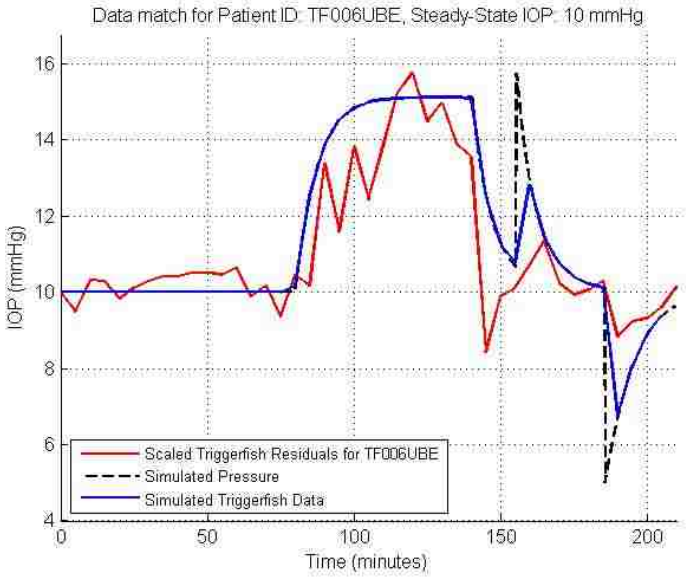

Figure 6.9: *Data comparison for patient TF006UBE*

This case also uses scaling approach #3 which can be seen as the red line in Figure 6.9. In this case using the Woo pressure volume relationship (Equation

2.18) had a slightly better fit and that relationship is what is represented in Figure 6.9. The first non-supine portion of the study seem to show a response very similar to that seen in 5.6b. The IOP during this portion increased following an inverse exponential decay similar to the simulations when only the IVP was increased. The second non-supine portion did not seem to exhibit much of a reaction at all, however here it was thought to slightly exhibit an increase in IOP only pattern. It is unknown exactly why some of the patient's data do not exhibit the expected trends. A brief discussion of this can be found in Chapter 7.

6.5.4 Patient TF019JHU

The next and final case of interest to be discussed here is that of patient TF019JHU. The data for this patient can be seen in Figure 6.10.

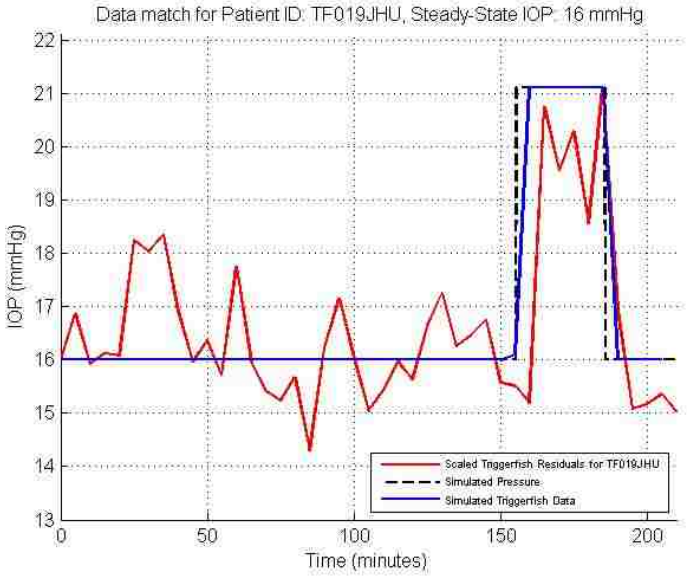

Figure 6.10: *Data comparison for patient TF019JHU*

This case did not have as successful of a fit as other cases but it did seem to exhibit the phenomenon of an increase to both the IOP and IVP at the same time. The second non-supine period seen in Figure 6.10 clearly shows a sustained value that can be interpreted as a sustained increase in IOP. As shown in Figure 5.5, an increase to both IOP and IVP by the same amount results in a square wave-like increase in IOP as seen here. The problem with this data fit occurred with the first non-supine portion. This portion did not seem to have any significant difference from the warm up period before the non-supine position was initiated. The specific reason why this happened is unknown but a simple guess is that the non-supine position was such that it did not apply a significant load anywhere near or on the eye. As mentioned previously, a discussion of alternate reasons for variations in results can be found in Chapter 7.

Chapter 7: **Discussions**

7.1 **Summary of Mechanics**

The following is a summary of the research done for this project. The project was initially separated into two main categories: 1) Fluid-Structure FEA Simulations to analyze the initial changes in IOP, stress, strain and deformation of the eye, and 2) iterative codes to calculate the changes in IOP over time. The reason for the segmentation of the simulations was to simplify the FEA complexity as well as to use well known empirical formulas to increase the similarities to known real world behavior.

The FSI simulations found that a facial pressure of 10.3 mmHg (0.2 psi) due to contact with a sleeping surface would cause an initial increase in IOP of roughly 5.1 mmHg (0.1 psi) and in increase in scleral stress of 20-30%. Using the known relationships for the inflow and outflow of aqueous humor out of the eye, and the known pressure volume relationships, IOP changes over time can be analyzed. Applying the initial increase in fluid pressure to the IOP only, the IOP over time experiences an increase for a 5-10 minute time period following loading, after which the IOP settles back to near steady-state values. When the IVP is also increased, IOP levels either

remain elevated (in the case of both the IOP and IVP being increased initially) or slowly build up to an elevated state (in the case of an increase in IVP only).

7.2 Implications of Comparison to Triggerfish Data

The results section of Chapter 6 clearly indicates that several patients' data exhibit patterns that are consistent with what was expected from the modeling. While only a portion of the patient data was presented in this paper, roughly one third of the patients that have undergone the simulated sleep study procedure have had data that resembles the types of curves seen presented here. This raises some major questions as to why only a portion of the test subjects would have data that resembles expected patterns.

One hypothesis that may explain why this might be occurring is related to ocular stiffness. According to the medical staff at Johns Hopkins Medical Center, it has been noted that subjects with higher ocular stiffness tend to also be patients with higher IOP values. While this is a theory that is still under investigation, it is thought that the ocular stiffness may also relate to the dynamics of the IOP changes in a situations with frequent fluctuations such as this. In order to investigate the effects of a stiffer eye, a simulation was performed that added fibrous properties to the sclera (which was not present in the original material definition). The result of this can be seen in Figure 4.6. With stiffer ocular properties, the pressure increase was 5.91 mmHg which is 15% increase over the original pressure increase of 5.13 mmHg. This is also combined with the results from the balloon experiment detailed

in Chapter 3. The results of this experiment can be seen in Figure 3.3. In the experiment, it was shown that applying a load of 10.3 mmHg (0.2 psi) to a standard rubber balloon pressurized with water (to approximately 10 mmHg, the highest possible with this balloon) leads to an increase in fluid pressure of only about 2 mmHg. An ordinary balloon is significantly less stiff than the walls of a human eye. These results do coincide with the previous hypothesis that less stiff, more elastic eyes will experience a smaller increase in fluid pressure whereas a stiffer eye would experience a larger increase in fluid pressure. With these results, it is reasonable to conclude that the reasons for certain patient data displaying dynamic activity while others do not may be related to their ocular stiffness.

As discussed in Chapter 5, each simulated case poses a different level of likelihood of ocular damage. With glaucoma, it is sought to avoid any sort of pressure increase as these increases are tied directly to increased ocular stress and vision loss. With the case of an initial increase in only the IOP due to non-supine sleeping position loading, the IOP only maintained a significant increase over a 5-10 minute span of time. During the cases where the IVP was set to increase, the increase in IOP was maintained during the duration of the loading. This is because the change in IVP directly impacts the regulatory mechanics of the eye. Since the eye depends on the pressure gradient from the intraocular fluids to the intra-venous fluids, a change to the IVP disrupts how these mechanisms can function. As a result, a higher, more dangerous steady-state IOP is formed during non-supine sleeping position induced loading. This sustained increase in IOP creates sustained periods of high ocular stress.

Based on the work done for this research, to reduce the risk of periods of time during which IOP, stress and strain of the eye are elevated as a results of external load on the eye, non-supine sleeping positions should be avoided. As this is often difficult to control, one method of achieving the same result, i.e. of avoiding periods of elevation in IOP, stress or strain would be to wear a load transferring device while sleeping. Such a device would distribute facial loading to the bony structure sufficiently far enough away from the eye. Any technique that sufficiently transfers the facial loading away from the region immediately on and around the eye would remove the risk of increasing IOP, stress and strain due to this phenomena.

Chapter 8: **Conclusions and Recommendations**

8.1 **Conclusions**

Chapter 3 investigated the load applied to the eye when in a non-supine sleeping position. It was discovered that the average load experienced by the eye is approximately 9.26 mmHg (0.179 psi) which is close to the predicted value of 9.92 mmHg (0.192 psi). This chapter also investigated the increase in internal pressure of a fluid filled balloon in response to an external loading. This experiment found that an external load of roughly 10 mmHg on a balloon with an initial pressure of 10 mmHg experienced a 2 mmHg increase in internal pressure.

The COMSOL Multiphysics software was used to build an axisymmetrical model of the eye to investigate the quasi-static change in stress, strain, deformation and IOP upon loading. The FSI simulation showed that an external loading of 10.3 mmHg (0.2 psi) will cause an increase in IOP of roughly 5.1 mmHg. The simulation also shows an increase in ocular wall stress of 20-30% with a 6 kPa increase in retina stress in certain locations when under such loading.

The iterative code is used to investigate the change in IOP following the initial external loading associated with non-supine sleeping positions. There are several scenarios presented in Chapter 5 corresponding to various ocular responses to ex-

ternal loads. The case for an initial increase in IOP only yields elevated IOP for roughly 3-10 minutes before returning to near steady-state values. An initial increase to both IOP and IVP results in a sustained increase in IOP of +5 mmHg. And an increase to the IVP alone results in a gradually escalating IOP.

The portion of the research involving the patients wearing the Triggerfish lenses resulted in 11 of 32 patients exhibiting significant changes in ocular strain when in non-supine sleeping positions, all of whom are diagnosed with glaucoma. Many of these 11 patients exhibit similar patterns to those introduced in Chapter 5. The variation of the results between patients may be linked to the ocular stiffness of each individual.

8.2 Future Research

From this point there are several areas that could be the focus of future research endeavors. One of these is further investigation into the variations in ocular stiffness between individuals. Since it has been hypothesized that the ocular stiffness has a large impact on the expected results, being able to effectively characterize the ocular stiffness of any one individual would help determine their expected response to loading induced by non-supine sleeping position. It has also been discussed that perhaps ocular pulsation is linked to ocular stiffness. One student working on this project has started analysis of the Triggerfish data to examine ocular pulse amplitude and rate.

With the suggestion that ocular stiffness and ocular pulsation are linked, that too is a region for further investigation. As for an engineering research subject, the modeling of the ocular pulsation as a result of varying ocular stiffness could be done. The key to both of these future areas is the development of material theories that accurately characterize the variations of ocular stiffness among individuals.

As mentioned in this thesis, originally the goal was to have a single simulation that linked both the external loading and the dynamic fluid flow situation all together. Difficulties with integrating the analytical relationships for fluid flow and pressure volume relationships redirected the research toward a two phase simulation. The first phase investigated the effects of the external load on the initial IOP, stress, strain and deformation of the eye and the second phase investigated the resulting changes in IOP over time due to fluid exchange. Future research could consist of utilizing alternative approaches and softwares to link the two systems together to be able to study the variation in the effects of the external load on IOP as fluid flow conditions change.

Work that is already under investigation by other researchers at the University of Maryland is the implication of facial structure on the resulting increase in IOP. To do this, researchers are using software that can construct 3-dimensional computer models of individual's faces from stationary photographs. This 3-dimensional model then allows for facial feature measuring that can quantify the relative protrusion of the eye with respect to various facial features. Perhaps a link between ocular protrusion and vulnerability to non-supine sleeping position loading damage can be uncovered.

Another possible area for further investigation of this topic could be micro-scale modeling the fluid outlet regions of the eye in extreme detail. This would include modeling the intricacies of the trabecular meshwork, Schlemm's canal and the collecting channels that make up the outflow structure. By modeling the biological and physical phenomena that occur on a microscopic scale, a more accurate characterization of the variability of aqueous humor outflow could be obtained. Additionally, a model of the episcleral veins could be constructed. Using such a model would help to understand the variations in IVP during facial loading.

A final suggestion for future investigation would be for a more accurate ocular orbit and muscle attachment model to be developed. This research took an idealized approach to modeling the orbit as a layer of fatty tissue with a fixed outer boundary. Modeling the eye's six muscle attachments as well as incorporating some of the cavities present in the orbit may help develop a more accurate model of the stress in the eye wall that directly causes the damage associated with glaucoma.

Chapter A: Triggerfish

A.1 Introduction to Triggerfish Technology

The SENSIMED Triggerfish® was introduced in Chapter 6 during the discussion of the patient data and its comparison to the work done for this research. Here in the appendices, a more in depth discussion of the Triggerfish technology will be conducted. As mentioned previously, the Triggerfish contact lens works by having embedded strain gauges within layers of a silicone contact lens. A typical strain gauge set up will utilize a Wheatstone Bridge resistor configuration to capture the effects of the deformation on the electrical voltage. A Wheatstone Bridge utilizes four resistors in a specific configuration and measures the voltage across the bridge relative to the supply voltage. In a typical case, three of the four resistors will have a known resistance and the fourth resistor will be a variable or "active" resistor. Active resistors are metallic strips whose resistance changes due to the relationship in Equation 6.1. As the resistance changes, the output voltage will vary. The varying output voltage is directly associated with extensional deformation of the active resistor which is why it is known as a strain gauge.

In the case of the Triggerfish, the configuration contains two active and two passive strain gauges to make up the four resistors of the Wheatstone Bridge. The

inclusion of the passive strain gauges (as opposed to resistors with known constant electrical resistance) allow for thermal compensation. The passive gauges are made of numerous rectilinear sections arranged in a radial pattern within the silicone lens. Due to the radial positioning, the gauges are not subjected to the spherical deformation associated with the pressure variations. However, these gauges would still pick up the effects associated with temperature changes [33]. Having these passive gauges allows for the removal of the temperature effects from the output of the active strain gauges.

The second difference between the set up used here and a traditional Wheatstone Bridge configuration is the utilization of two active resistors as opposed to a single one. Including an additional active resistor doubles the sensitivity of the measurements [33]. An increase in sensitivity is important when working with the very small changes in ocular strain associated with pressure changes and ocular pulsation.

The Triggerfish contact lens must also have a means of communicating the output voltage values with the data storage system. Since the lens and the sensor are located on the anterior surface of the subjects eye, the sensor must be completely wireless (to allow for blinks and overall patient comfort). As a result, the Triggerfish lens utilizes wireless data and power transmission. In order to do this, the lens must also be fitted with an antenna and a low-power transponder [33]. The power transmission and communication with the lens is done through an external loop antenna that is secured to the face of the patient, concentric with the lens in the patient's eye. The external antenna has a wired connection to the data recorder

located in an external pouch worn by the patient. After the recorder has been initialized, data will be gathered every 5 minutes for a burst period of 30 seconds at a rate of 10 Hz for an overall period of up to 24 hours. The reason that the data cannot be collected continuously is due to the caution that must be taken when dealing with wireless power transmission in close proximity to the brain. The picture in Figure A.1 is a close up picture of the various components embedded within the silicone lens.

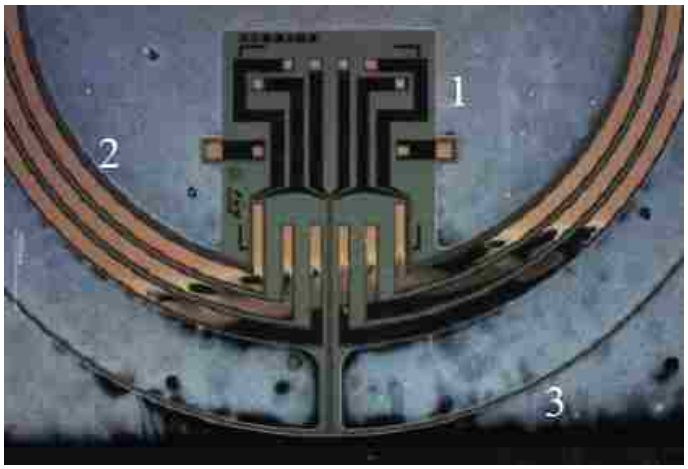

Figure A.1: *The strain gauges on the SENSIMED Triggerfish® Contact Lens [34]*

In Figure A.1, the rectilinear passive strain gauges (1), the circular active strain gauges (2) and the wireless antenna (3) are clearly visible.

A.2 Study at Johns Hopkins Medical Center

In order to test what is happening to the eye during non-supine sleeping positions, an environment must be set up that allows for this to happen. The original plan was to collaborate with The Sleep Disorder Center at the Johns Hopkins

Bayview Campus in Baltimore, Maryland. The sleep center has facilities set up to accommodate sleeping patients and monitor the conditions of their sleep. In this version of the research, patients with natural tendencies to sleep in non-supine positions would be gathered (both glaucoma and non-glaucoma individuals). They would be asked to spend the night at the sleep center and sleep how they found comfortable. Being individuals who naturally preferred non-supine sleeping positions, it is likely that at points during the night they would be in such a position. With video recordings of the patients, the moments corresponding to non-supine sleeping positions could be correlated to the Triggerfish data and the relationships could be determined.

However, issues arose that prevented using the sleep center in this research project. Following this, the idea of a simulated sleep study became the solution. A simulated sleep study is meant to mimic a real world sleeping situation without requiring patients to spend the night. To do so, the patients would be instructed to lay in certain positions at certain points in time following a specific procedure built to obtain Triggerfish readings at specific points.

A.3 Simulated Sleep Study Procedure

The Triggerfish contact lenses must be allowed to have a warm up period when they are first inserted into the patient's eye to ensure that the sensor is performing properly for the procedure. It is encouraged that the warm up period last for at least an hour so that the lens can find a definite position on the eye. The manufacturer

specifically mentions that the data from the first hour is less reliable because of this. Therefore all of the experimental procedures (minus the first few, which were conducted before the warm up necessity was realized) have a one hour warm up period following the syncing of the data recorder.

An iCare® Tonometer [35] was used to measure the IOP in the sitting and lying position both before and after the simulated sleep study. To help validate the readings from the Triggerfish lens, part of the simulated sleep study procedure includes a sitting and lying portion that can be compared to the readings on the tonometer. To do so, there is a sitting and lying portion immediately following the end of the warm up period and also at the end of the entire procedure just prior to the removal of the lens. This allows for some real world pressure measurement comparisons with the Triggerfish data.

The goal of the simulated sleep procedure is to investigate the ocular response to facial loading caused by non-supine sleeping positions. To investigate this, the procedure seen in Table A.1 was proposed.

The entire procedure takes roughly 3.5 hours to complete and it includes nine different portions. Starting with a warm up portion lasting an hour to make sure that the sensor warms up and finds a definite position. Following the warm up is a sitting portion lasting 7.5 minutes and a lying portion lasting 12 minutes that can be used to compare to the initial iCare measurements. Then a 60 minute non-supine sleeping position portion begins followed by a 15 minute supine portion. That cycle is repeated again but with shorter times (30 minutes non-supine followed by 10 minutes supine). Finally, the end of the study features a 7.5 minute lying and a

Table A.1: Simulated Sleep Study Procedure

Starting Time (min)	Action	Duration (min)	# of Samplings	Sampling at (min)
0	Warm Up	60	12	0,5,10,15,20,25,30,35,40,45,50,55
60	Sitting	7.5	2	60,65
67.5	Lying	12	2	70,75
79.5	Face Down	60	12	80,85,90,95,100,105,110,115,120,125,130,135
139.5	Face Up	15	3	140,145,150
154.5	Face Down	30	6	155,160,165,170,175,180
184.5	Face Up	10	2	185,190
194.5	Lying	7.5	2	195,200
202	Sitting	10	2	205,210
212	End Study			

10 minute sitting portion again to compare to the final iCare measurements. The duration for the sitting and lying portions was selected in order to ensure that every study portion contained at least two samplings. The non-supine sleeping position portions have a longer duration in order to study the ocular response over time. The timings also mimic those which a person might naturally undergo when sleeping. Overall, this procedure should be adequate for gaining an overview of what might be occurring during non-supine sleeping positions.

A.4 Overall Results

There were a total of 32 patients to undergo the simulated sleep study at JHMC. These 32 patients consisted of 21 individuals who have been diagnosed with glaucoma and 11 individuals who are healthy controls. Of the patients with glaucoma, 11 of them exhibited significant dynamic activity in between the supine

and non-supine positions. The data that corresponds to these patients can be seen collectively in Figure A.2.

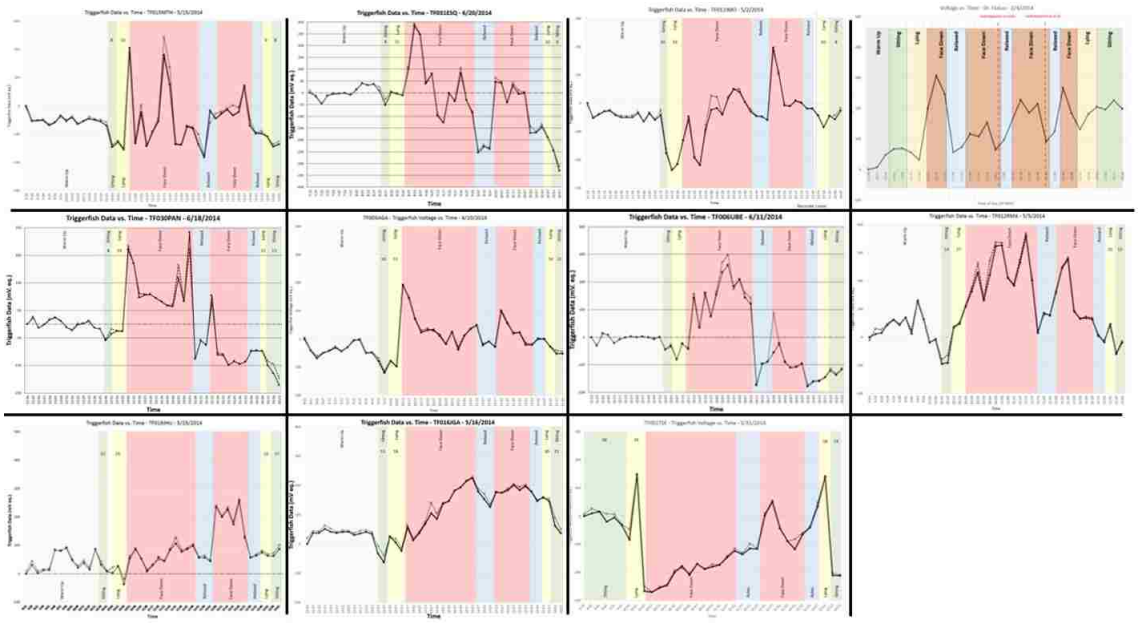

Figure A.2: *This set of patients exhibited significant dynamic activity going from supine to non-supine sleeping positions*

When observing the data in Figure A.2, there is a noticeable difference between the strain gauge output values between the supine positions and non-supine positions. This noticeable difference is what is referred to here as significant dynamic activity or a patient that falls in a "not-flat" category. The rest of the glaucoma patients did not appear to exhibit much dynamic activity. The patients who fall in this category, referred to as "flat" patients, can be seen collectively in Figure A.3.

When observing the data for the flat patients in Figure A.3, there is a lack of any significant changes in strain gauge output between the various supine and non-supine sleeping positions. This behavior is similar to that which was seen with

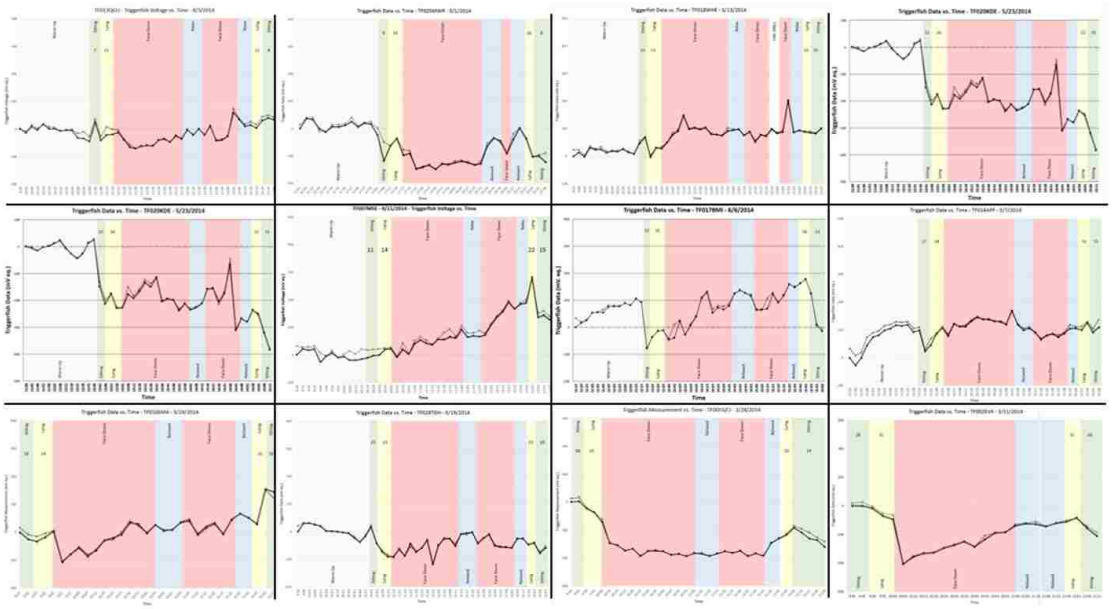

Figure A.3: *This set of patients did not exhibit significant dynamic activity going from supine to non-supine sleeping positions*

the healthy control patients. The collective results for the control patients can be seen in Figure A.4.

The behavior of the flat glaucoma patients and the control patients appears to be very similar. However, there is a distinct difference between these patients and the non-flat group of patients. This grouping was categorized by using the maximum strain gauge output value from either non-supine sleeping portions and the minimum output from the preceding action in the procedure and taking the difference between those two values. The results of this categorization can be seen in Figure A.5.

Patients whose difference falls above 250 mV eq. are definitively grouped in the non-flat category. The glaucoma patients found between 150 and 250 mV eq.

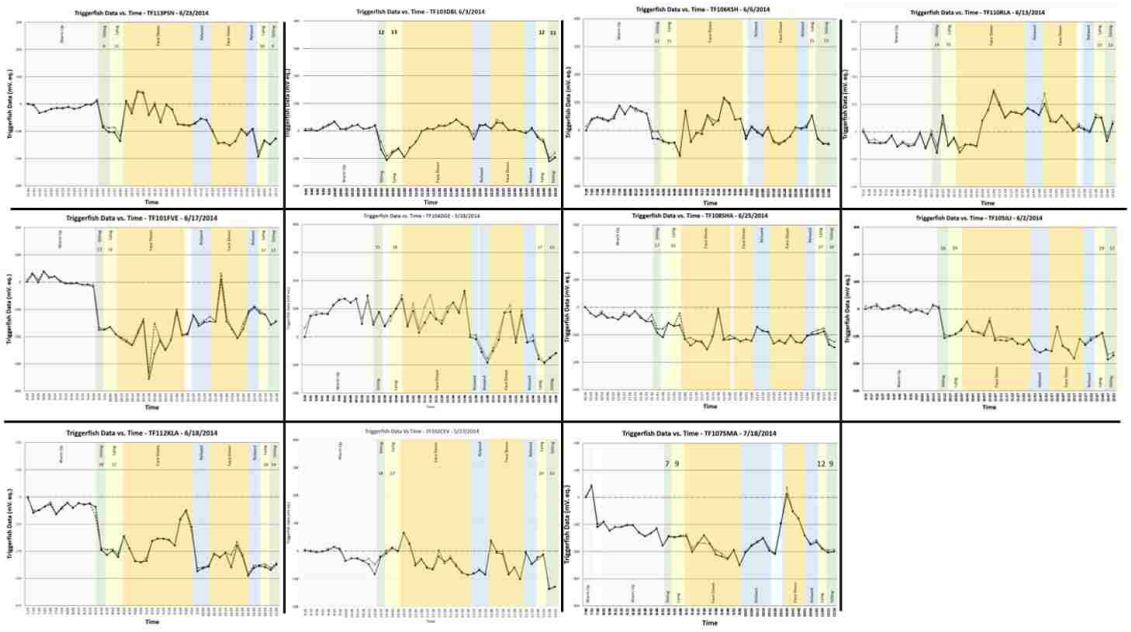

Figure A.4: *The control patient group did not exhibit significant dynamic activity going from supine to non-supine sleeping positions*

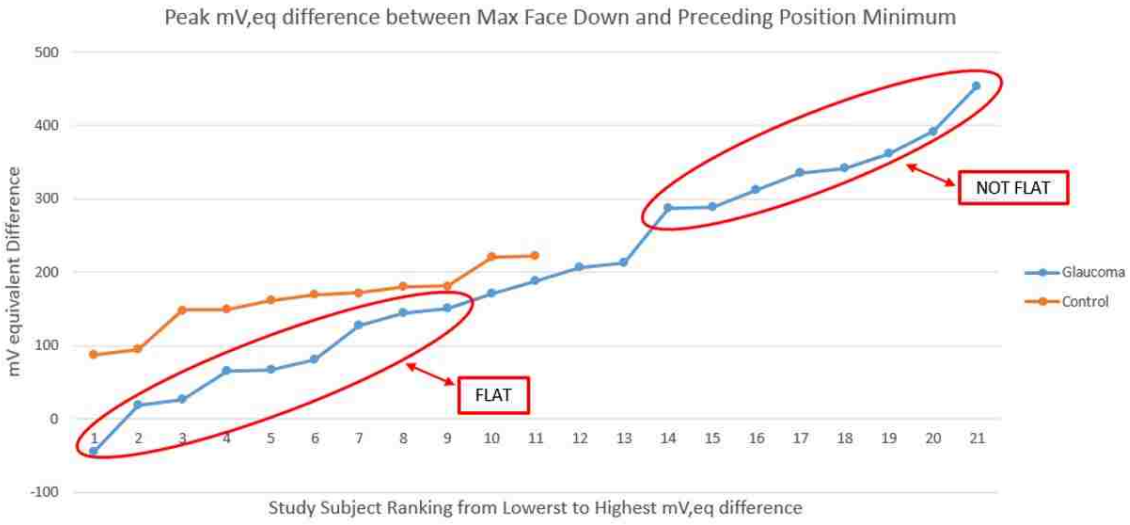

Figure A.5: *The difference between maximum non-supine strain gauge values and minimum preceding values*

were considered as "probably not-flat" however they had less dynamic activity in

comparison to the other non-flat patients. All of the control patients and the flat glaucoma patients show differences less than 250 mV eq.

A.5 Issues with Triggerfish

As previously mentioned, the Triggerfish contact lens allows for a unique approach to measuring the dynamics of IOP when a patients eye is unreachable by conventional means. When a patient is in a non-supine sleeping position with their eye pressed into a pillow, no standard tonometry methods can be used to measure IOP. The Triggerfish lens is situated on the eye itself with no physical contact with external systems. This allows for this dynamic IOP measuring to be done without disturbing the patient. In this respect, it is the perfect item to use for this research. However, there are also some challenges to deal with.

The main and most obvious issue is that the Triggerfish lens is only measuring strain. The strain is known to correspond to changes in ocular volume which is known to be tied to changes in IOP. That portion of the measurement is without flaw, but the issue is that the lens may also be picking up other strains that are not associated with changes in IOP. Since the lens is being directly loaded by an external force, the strains measured by the lens may be associated with the direct deformation of the lens and the eye and not changes in IOP. As seen in Table 4.6, the radial strain in the limbus varies from positive to negative depending on the location of the external loading. It is thought that the lens was specifically designed to work in situations where the only changes in ocular shape would be caused by

volume changes associated with pressure changes. Since that may not be the case here, there should be some skepticism as to the true source of the detected strains.

Another possible source of error is related to the wireless power transmission. Since Wheatstone Bridge strain gauge configurations return a voltage reading relative to the source voltage, any change to the source voltage would appear as a change in the strain gauge output voltage. Anything that might cause power signal attenuation will disturb the applied voltage and bias the sensor read out. It is possible that signal attenuation could occur with certain subject positions and external loads. While there is no alternative option for measuring changes in IOP for this research, these issues must be taken into consideration when analyzing the patient data.

Chapter B: COMSOL and MATLAB

B.1 COMSOL Details

In this section, the specific details of how the COMSOL Multiphysics FSI model was constructed are discussed. This description goes into the very particular details of how and where the parameters and variables were applied as well as the solver techniques needed to output a converged solution.

B.1.1 Parameters

Following the completion of the model geometry, the simulation parameters must be defined. As mentioned in Chapter 4, the external loading on the eye was applied using a 0.5 second ramp function. This function must be explicitly defined in the Global Definitions node of the model tree. Additionally, in order for this function to work properly, a time parameter must be initialized as zero. This makes it so the loading is only applied once the time marching portion of the simulation has begun and not at time equal to zero (this is important for generating the initial conditions of the simulation). Additional parameters that need to be defined are the hyperelastic material coefficients as described in Table 2.1. These parameters

are needed when Equations 2.13 and 2.14 are used in the simulation. It is simply easier to enter them as initial parameters and call upon them when needed. The pressure to be applied to the exterior of the eye representing the load associated with non-supine sleeping positions was entered as a parameter, as well as the value of the initial IOP in the current simulation.

A single parameter must be created for each of the fiber angles, β, of the sclera, cornea and limbus regions. In most of the simulations that were done, the fiber angle for the sclera, limbus and cornea were set as $32\,\mathrm{deg}$, $0\,\mathrm{deg}$ and $90\,\mathrm{deg}$ respectively. In reality, the fibers inside the wall are short collegen fibers spread all around. In this model, two layers of fibers in opposite directions create a multi-directional fiber effect. The angles used here were chosen based on the directions that would see the most loading. When this set of fiber orientations is generated on a 3-D model (as opposed to the axisymmetrical version of the model used in these simulations) the fibers look like those in Figure B.1. This provides a good visual aid to understand the structural support provided by the anisotropic portion of the material description.

B.1.2 Variables

Following the definition of numerical parameters, the equations must be fully defined within the software. Terms representing eqs. (2.8) to (2.11), (2.13) and (2.14) must be defined as variables in COMSOL. Starting with Equations 2.10 and 2.11, these vectors are entered in as a list of six components corresponding to the three

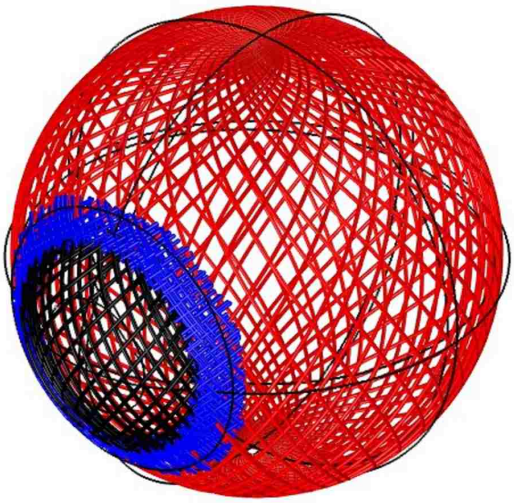

Figure B.1: *3-D Fiber Orientations*

components of each fiber direction vector. Table B.1 has the variable inputs as seen in the software. In this example, the variable is defined for the cornea (a separate variable for each hyperelastic region must be defined) and $betaF_c$ is a previously defined parameter representing the fiber angle for the corneal fibers. This would create the three components of the first fiber vector, $a_0 1C$, as $a01C1$, $a01C2$ and $a01C3$ and so on.

Table B.1: Fiber Angle Vectors

Name	Expression
a01C1	0
a01C2	$\cos(betaF_c)$
a01C3	$\sin(betaF_c)$
a02C1	0
a02C2	$\cos(betaF_c)$
a02C3	$-\sin(betaF_c)$

The fiber direction vectors need to be defined in this way so that the individual components can be used to define the invariants I_4 and I_6. Computing the tensor product in Equation 2.9 and the contraction in Equation 2.8 gives us an expression for invariants I_4 and I_6 in terms of fiber angle vector components and the right Cauchy-Green tensor components. The fourth invariant for some material j can be seen as Equation B.1 and the sixth invariant for some material j can be seen as Equation B.2.

$$\begin{aligned} I_{4j} =& a_{01j_1}^2 C_{11j} + a_{01j_2}^2 C_{22j} + a_{01j_3}^2 C_{33j} + 2a_{01j_1}a_{01k_2}C_{12j} \\ &+ 2a_{01j_1}a_{01k_3}C_{13j} + 2a_{01j_2}a_{01k_3}C_{23j} \end{aligned} \tag{B.1}$$

$$\begin{aligned} I_{6j} =& a_{02j_1}^2 C_{11j} + a_{02j_2}^2 C_{22j} + a_{02j_3}^2 C_{33j} + 2a_{02j_1}a_{02k_2}C_{12j} \\ &+ 2a_{02j_1}a_{02k_3}C_{13j} + 2a_{02j_2}a_{02k_3}C_{23j} \end{aligned} \tag{B.2}$$

The components of the right elastic Cauchy-Green tensor can be called on in COMSOL by inputting the variable *fsi.Clel11* where the prefix represents the physics module being used and the numbers represent the tensor component of interest. Similarly, the remaining principle invariants can be called upon by inputting the variable *fsi.I1Clel* again where the prefix represents the physics module being used and the one number represents the invariant of interest. The final variable needed to complete the strain energy density equations is the volume ratio (which is the determinant of the deformation gradient tensor) which can be called upon by inputting the variable *fsi.Jel* where once again the prefix represents the physics module in use [36]. Using all of these terms, the strain energy density functions of

Equations 2.13 and 2.14 can be input as variables themselves. The sclera, limbus and cornea will all need these variables defined separately corresponding to each individual fiber orientation and material parameters.

B.1.3 Materials

Inside this model, there are seven different material properties that need to be defined and assigned to their respective components. COMSOL Multiphysics allows for three types of materials to be assigned in an FSI model: linear elastic, hyperelastic and a fluid. The first step was to enter the values for the density, viscosity, modulus of elasticity and Poisson's ratio where applicable for the two fluid materials and the two linear elastic materials as they are seen in Table 4.1 and assign them to their appropriate geometric component seen in Figure 4.1. Now the hyperelastic material properties need to be assigned. This starts with adding three hyperelastic materials nodes to the model builder within the FSI node (one for each region of the ocular wall). Within a hyperelastic material node in the software, there is a pull down menu in the Hyperelastic Material sub-section that is for the material model type. Among the list are many of the famous published hyperelastic material theories and at the bottom is the option for User Defined, that is the option needed for the customized strain energy density functions used here. After checking off the option for nearly incompressible material, a total of three entry bars appear: 1) W_{siso}, 2) W_{svol} and 3) ρ. The first of which stands for the isochoric strain energy density and the second stands for the volumetric

strain energy density. Equations 2.14 and 2.13 should be entered respectively using the parameters and variables previously defined for each hyperelastic region. Each material definition also requires a density which can be found on Table 4.1. This can be done for all three ocular wall regions to finalize the definition of the material for every component inside of the model.

B.1.4 Studies

After the stationary study is added, the stationary solver option of fully coupled solver must be added. A fully coupled solver is one that solves both the fluid and the solid mechanics problems together rather then segregating them. The simulations have difficulty finding a converged solution if the solver is set to segregated. This can be added by opening up the various trees withing the study node and right clicking on the one labeled "Stationary Solver # ". From there a fully coupled solver can be added. One final note to add to the stationary study is that some of the simulations require the relative tolerance of the stationary solver to be increased to higher values. The purpose of the stationary study is to establish the initial IOP values and therefore altering the relative tolerance on this study does not have any negative impacts as long as the initial pressure is established relatively close to the value it is intended to be.

For the time dependent study, three settings need to be set. First are the values of the dependent variables. This can be found in the Step 1: Time Dependent node within the study node. From which the initial values of variables can be selected

from an earlier solution, in this case the stationary study used to establish the initial IOP should be selected. The second item to set is the time range for which the simulation will occur. This can also be found in the Step 1: Time Dependent node under study settings. From there, the time range and time marching increment can be set. This model uses a range of 0 to 3 seconds and a time marching increment of 0.1 second (input as range(0,0.1,3) into the "Times:" box). The third item to set is the same item as the stationary study, making sure the time dependent solver is using a fully coupled approach. I would like to thank Rui Zhu of Furtwangen University in Furtwangen, Germany for his assistance with adjusting the solver settings to produce a converged solution.

B.2 MATLAB Code

Included in this section of the appendix is the MATLAB code created to iterate through the pressure cycles. The code works by first initiating the necessary vectors and variables. Then the code begins an iterative loop that calculates the change in fluid flow rates, ocular volume and IOP for every sequential Δt value.

Eye Loading Pressure Simulator

```
clear; clc; close all

% THINGS YOU MAY WANT TO ALTER:

% Timing Variables
dt=0.01; % Time step in minutes (Do not make larger than 0.1 minutes)
t=0:dt:50; % Range of time in minutes (change end value to extend time)    *** CHA

Start_t=5; % Start time for first loading in minutes                       *** CHA

% First Loading Cycle:
Load_t1=25; % Length of time for each loading on first set of cycles         *** C
Unload_t1=5; % Length of time for each relaxation on first set of cycles    *** CH
Num_Load_1=1; % Number of loadings for first set of cycles                  *** CH

% Second Loading Cycle:
Load_t2=11; % Length of time for each loading on second cycle               *** CH
Unload_t2=11; % Length of time for each relaxation on second cycle          *** CH
Num_Load_2=0; % Number of loadings for second set of cycles                 *** CH

% Triggerfish sampling start time:
First_Measure=0; % Any time from 0 to 4.5 minutes                          *** CH


% FLOW FACILITY VALUES for Various steady state IOPs (12 mmHg set as standard):

% Loaded Outflow Contraint Factor:
CF=1; % Loaded outflow constraint factor (CF=1  represents no constriction) *** CH

%Ctrab_i=[0.1667 0.1667/CF]; % For Steady-State IOP = 16.5 mmHg             *** CH
%Ctrab_i=[0.25 0.25/CF]; % For Steady-State IOP = 14 mmHg                   *** CH
Ctrab_i=[0.42 0.42/CF]; % For Steady-State IOP = 12 mmHg                    *** CH

% Note: If you would like to use either of the first two flow facility,
% simply comment out all other Ctrabs and un-comment the one you're
% interested in


%*************************************************************************
% NO NEED TO ALTER BELOW THIS POINT

% Preset Variables
K=0.0215; % Pressure/Volume relation coefficient
Vin=2.5; % Constant inflow rate in cubic meters/min
IOP=12; % Starting IOP value in mmHg
Pe=9; % Venous Pressure in mmHg
Fu=1.24; % Outflow that is independent of pressure in microliters/min
IOP_inc=5.123; % Static IOP increase from sleep loading in mmHg

% Initializing variables and store vectors
```

```
Ctrab=Ctrab_i(1);
dV_store=zeros(length(t),1);
IOP_store=zeros(length(t),1);

Load_Length_1=Load_t1+Unload_t1;
Loading_1=zeros(Num_Load_1,1);
Unloading_1=zeros(Num_Load_1,1);

Load_Length_2=Load_t2+Unload_t2;
Loading_2=zeros(Num_Load_2,1);
Unloading_2=zeros(Num_Load_2,1);

% Building load and unload time vectors:
for n=1:Num_Load_1
    Loading_1(n,1)=Start_t+(n-1)*Load_Length_1;
    Unloading_1(n,1)=Loading_1(n,1)+Load_t1;
end

for n=1:Num_Load_2
    Loading_2(n,1)=(Unloading_1(Num_Load_1)+Unload_t2)+(n-1)*Load_Length_2;
    Unloading_2(n,1)=Loading_2(n,1)+Load_t2;
end

% Pressure simulation loop:
for i=1:length(t)
    for n=1:Num_Load_1 % First set of cycles
        if i==Loading_1(n)/dt
                IOP=IOP+IOP_inc; % Increase pressure at loading
                Ctrab=Ctrab_i(2);
        end
        if i==Unloading_1(n)/dt
                IOP=IOP-IOP_inc; % Decrease pressure at unloading
                Ctrab=Ctrab_i(1);
        end
    end

    for m=1:Num_Load_2 % Second set of cycles
        if i==Loading_2(m)/dt
                IOP=IOP+IOP_inc; % Increase pressure at loading
                Ctrab=Ctrab_i(2);
        end
        if i==Unloading_2(m)/dt
                IOP=IOP-IOP_inc; % Decrease pressure at unloading
                Ctrab=Ctrab_i(1);
        end
    end

    Vout=(Fu+Ctrab*(IOP-Pe)); % Total outflow in cubic meters / min
    dV=(Vin-Vout)*(dt); % Change in volume over one time span
    P=IOP*(10^(dV*K)); % New pressure based on change in volume
    IOP=P; % Set IOP to new pressure
    dV_store(i,1)=dV; % Store change in volume data
    IOP_store(i,1)=IOP; % Store change in IOP value
end
```

```
T=[First_Measure:5:max(t)]'; % Triggerfish sampling times
P=zeros(length(T)-1,1); % Initialize vector for Triggerfish pressure values

% Loop to calculate 30 second Triggerfish pressure readings
for c=1:length(T)-1
    a=(T(c)/dt)+1; % Start time for Triggerfish
    b=(T(c)+0.5)/dt; % 30 seconds later
    P(c,1)=mean(IOP_store(a:b)); % Average pressure over reading time
end

% Plotting:
hold on
plot(t(1:length(t)),IOP_store,'k','LineWidth',1.5) % Continuous
plot(T(1:length(T)-1),P,'b--','LineWidth',1) % Triggerfish
title(['Load/Unload Time #1 = ', num2str(Load_t1),'/', num2str(Unload_t1), ' min ,
xlabel('Time (minutes)')
ylabel('IOP (mmHg)')
grid on
axis([min(t) max(t) min(IOP_store)-1 max(IOP_store)+1])
legend('Continuous Simulated Data','Simulated Triggerfish Data')
set(legend,'FontSize',8);
```

Published with MATLAB® 7.14

Bibliography

[1] E. Lanchares, B. Calvo, J.A. Crisobal, and M. Doblare. Finite element simulation of arcuates for astigmatism correction. *Journal of Biomechanics*, 41:797–805, 2008.

[2] M. Asejczyk-Widlicka1, D. W. Srodka, H. Kasprzak, and D. R. Iskander. Influence of intraocular pressure on geometrical properties of a linear model of the eyeball: Effect of optical self-adjustment. *International Journal for Light and Electron Optics*, 115(11):517–524, 2004.

[3] H.A. Quigley. *Glaucoma: What Every Patient Should Know*. CreateSpace Independent Publishing Platform, 2012.

[4] L.A. Levin, S.F.E. Nilsson, J. Ver Hoeve, S. Wu, P.L. Kaufman, and A. Alm. *Adler's Physiology of the Eye, 11th Edition*. Elsevier, 2011.

[5] American Optometric Association. How your eyes work. http://www.aoa.org/patients-and-public/resources-for-teachers/how-your-eyes-work?sso=y. Online; Accessed 2014-07-21.

[6] A.J. Bron, R.C. Tripathi, and B.J. Tripathi. *Wolff's Anatomy of the Eye and Orbit*. Saunders, 1976.

[7] D. Smerdon. Anatomy of the eye and orbit. *Current Anaesthesia & Critical Care*, 11:286–292, 2000.

[8] D.L-Y. Woo, A.S. Kobayashi, W.A. Schlegel, and C. Lawrence. Nonlinear material properties of intact cornea and sclera. *Experimental Eye Research*, 14:29–39, 1972.

[9] E.D. Power. A nonlinear finite element model of the human eye to investigate ocular injuries from night vision goggles. Master's thesis, Virginia Polytechnic Institute and State University, Blacksburg, Virginia, 2001.

[10] C. MacLachlan and H.C. Howland. Normal values and standard deviations for pupil diameter and interpupillary distance in subjects aged 1 month to 19 years. *Opthalmic and Physiological Optics*, 22:175–182, 2002.

[11] G.A. Holzapfel. *Nonlinear Solid Mechanics: A Continuum Approach for Engineering*. Wiley, 2000.

[12] G.A. Holzapfel and H.W. Weizsacker. Biomedical behavior of the arterial wall and its numerical characterization. *Computers in Biology and Medicine*, 28:337–392, 1998.

[13] Y.C. Fung, K. Fronek, and P. Patitucci. Pseudoelasticity of arteries and of its mathematical expression the choice. *American Journal of Physiology*, 237(5), Nov 1979.

[14] G.A. Holzapfel and T.C. Gasser. A new constitutive framework for arterial wall mechanics and comparative study of material models. *Journal of Elasticity*, 61:1–48, 2000.

[15] V. Alastrue, B. Calvo, E. Pena, and M. Doblare. Biomechanical modeling of refractive corneal surgery. *Journal of Biomechanical Engineering*, 128:150–160, 2006.

[16] A. Pandolfi and F. Manganiello. A model for the human cornea: constitutive formulation and numerical analysis. *Biomechanics and Modeling in Mechanobiology*, 5:237–246, Nov 2006.

[17] J.C Gardiner and J.A Weiss. Subject-specific finite element analysis of the human medial collateral ligament during valgus knee loading. *Journal of Orthopaedic Research*, 21, 2003.

[18] D.A Hoeltzel, P. Altman, K. Buzard, and K. Choe. Strip exensiometry for comparison of mechanical response of bovine, rabbit and human corneas. *Journal of Biomedical Engineering*, 114:202–215, 1992.

[19] K.A. Buzard. Introduction to biomechanics of the cornea. *Journal of Refractive and Corneal Surgery*, 8:127–38, 1992.

[20] T.J. Van Der Werff and D. Phil. A new single-parameter ocular rigidity function. *American Journal of Opthalmology*, 92:391–395, 1981.

[21] T.J. Ernest, T.K. Goldstick, M.A. Stein, and J.D. Zheutlin. Ocular massage before cataract surgery. *Transactions of the American Ophthalmological Society*, 83:205–217, 1985.

[22] A. Villamarin, S. Roy, R. Hasballa, O. Vardoulis, P. Reymond, and N. Stergiopulos. 3d simulation of the aqueous flow in the human eye. *Medical Engineering & Physics*, 34:1462–1470, 2012.

[23] S.F.E. Nilsson. The uveoscleral outflow routes. *Eye*, 11:149–154, 1997.

[24] F.A. Irshad, M.S. Mayfield, D. Zurakowski, and R.S. Ayyala. Variation in schlemms canal diameter and location by ultrasound biomicroscopy. *Ophthalmology*, 117:916–920, 2010.

[25] R.N. Mudry and M.J. Wilcox. A finite element approach to predicting scleral response to mechanical stress. *Biomedical Sciences Instrumentation*, 44:329–335, 2008.

[26] Precision Polymer Engineering. Elastomer terminology. http://www.prepol.com/product-range/product-subpages/terminology. Online; Accessed 2014-07-24.

[27] S. Kumar, S. Acharya, R. Beuerman, and A. Palkama. Numerical solution of ocular fluid dynamics in a rabbit eye: Parametric effects. *Annals of Biomedical Engineering,*, 34:530–544, 2006.

[28] M. Giannaccini, M. Giannini, M.P. Cakatayud, Goya F.G., A. Cuschieri, L. Dente, and V. Raffa. Magnetic nanoparticles as intraocular drug delivery system to target retinal pigmented epithelium. *International Journal of Molecular Science*, 15:1590–1605, 2014.

[29] H.A. Quigley. What's the choroid got to do with angle closure? *Arch Opthalmol*, 127(5), May 2009.

[30] Sensimed. Sensimed triggerfish. http://www.sensimed.ch/en/products/sensimed-triggerfishr.html. Online; Accessed 2013-07-01.

[31] L. Beltran-Agullo, J. Cheng, Y. Buys, F. Jahan, J. Flanagan, C. Shapiro, N. Hossain, S. Simon-Zoula, and G. Trope. 24-hour iop monitoring with the sensimed triggerfish contact lens: effect of sleep position and assessment of upward drift. *Investigative Opthalmology & Visual Science*, 54, 2013.

[32] Georgia State University. Resistance. http://hyperphysics.phy-astr.gsu.edu/hbase/electric/resis.html. Online; Accessed 2014-07-14.

[33] J.M. Wismer. Intraocular pressure monitoring device, September 16 2010. US Patent App. 12/762,597. Patent Num. US20100234717 A1.

[34] R. Wilson. Contact lens has mems device to measure glaucoma. http://www.electronicsweekly.com/news/research/device-rd/contact-lens-has-mems-device-to-measure-glaucoma-2010-03/. Online; Accessed 2014-07-15.

[35] iCare. icare tonometer. http://www.icaretonometer.com/. Online; Accessed 2014-07-16.

[36] COMSOL Multiphysics. Arterial wall mechanics, 2013.